PARAMETERIZATION OF MOISTURE AND HEAT FLUXES ACROSS THE LAND SURFACE FOR USE IN ATMOSPHERIC GENERAL CIRCULATION MODELS

by
P. CHRISTOPHER D. MILLY
and
PETER S. EAGLESON

Ralph M. Parsons Laboratory
Hydrology and Water Resource Systems

Report Number 279

This material is based upon work supported by the National Science Foundation under Grant Numbers ATM-7812327 and ATM-8114723

June 1982

MIT

DEPARTMENT
OF
CIVIL
ENGINEERING

SCHOOL OF ENGINEERING
MASSACHUSETTS INSTITUTE OF TECHNOLOGY
Cambridge, Massachusetts 02139

R82-35

PARAMETERIZATION OF MOISTURE AND HEAT FLUXES ACROSS THE LAND SURFACE FOR USE IN ATMOSPHERIC GENERAL CIRCULATION MODELS

by

P. Christopher D. Milly

and

Peter S. Eagleson

Ralph M. Parsons Laboratory

Hydrology and Water Resource Systems

Report Number 279

This material is based upon work supported by the National Science Foundation under Grant Numbers ATM-7812327 and ATM-8114723

June 1982

PARAMETERIZATION OF MOISTURE AND HEAT FLUXES ACROSS THE LAND SURFACE FOR USE IN ATMOSPHERIC GENERAL CIRCULATION MODELS

Abstract

The response of a bare soil surface to atmospheric forcing -- rain, wind, sunshine, etc. -- may be expressed in terms of the resultant evaporation rate and sensible and radiant heat losses. Examining the earth-atmosphere interface in an idealized one-dimensional framework, we evaluate a hierarchy of mathematical models in terms of their ability to predict this land surface response. The evaluation is based on simulation, using typical climatologic and soil parameters. The reference model, against which the other models are tested, is based on a numerical solution of a very detailed description of heat and moisture movement in porous media. The alternative models are, to a greater or less extent, simpler both conceptually and computationally than the reference model. They include the following:

1. A family of models obtained by introducing various simplifying assumptions in the reference model. These concern the roles of water vapor, of soil moisture retention hysteresis, and of a few other minor effects.

2. A set of models constructed by linking the force-restore method of soil temperature prediction to each of three soil moisture parameterizations -- a two-node finite element model, a conceptualization used by climate modelers, and a nonlinear diffusion model.

Using the nominal soil and climatologic parameters, we determine the critical physical mechanisms affecting the surface fluxes of water and heat. We find that an isothermal moisture equation, with the hydraulic conductivity augmented by a vapor conductivity, and accounting for hysteresis, is sufficient. The nonlinear diffusion parameterization, which includes these effects, is extended to account for redistribution. In conjunction with the force-restore method, it successfully predicts evaporation under various climatic and soil conditions.

ACKNOWLEDGEMENTS

This work was performed with the support of the National Science Foundation under research grants numbers ATM-7812327 and ATM-8114723, and under its Graduate Fellowship program.

This document is essentially Part A of the doctoral thesis submitted by P. Christopher D. Milly to the Department of Civil Engineering at M.I.T. It completion was supervised by Dr. Peter S. Eagleson, Professor of Civil Engineering.

Dr. David Curtis of the National Weather Service provided a computer code for the surface boundary layer model.

TABLE OF CONTENTS

LIST OF FIGURES

LIST OF TABLES

NOTATION

NOTE: Most of the symbols used are listed here. Some minor symbols that are used infrequently are not listed. Occasionally, a single symbol takes two meanings when confusion seems unlikely.

Symbol	Description
A	albedo of land surface
A_o	time independent term in infiltration capacity
a'	$-\frac{1}{\psi}\frac{\partial \psi}{\partial T}\Big\vert_{\theta}$
C	volumetric heat capacity of soil
C_H	bulk transfer coefficient for heat
$(C_H)_N$	neutral value of C_H
C_M	bulk transfer (drag) coefficient for momentum
$(C_M)_N$	neutral value of C_M
C_W	bulk transfer coefficient for water vapor
$(C_W)_N$	neutral value of C_W
c_ℓ	specific heat of liquid water
c_p	specific heat of water vapor at constant pressure
D_a	molecular diffusivity of water vapor in air
D_{Tv}	thermal vapor diffusion coefficient
$D_{\psi v}$	isothermal vapor diffusion coefficient or vapor conductivity

Symbol	Description
E	evaporation rate
E_p	potential evaporation rate
F_e	cumulative depth of exfiltration since last storm
F'_e	apparent cumulative depth of exfiltration since last storm
F_i	cumulative depth of infiltration during storm
f_e	exfiltration rate
f^*_e	exfiltration capacity
f_i	infiltration rate
f^*_i	infiltration capacity
G	heat flux into the ground
g	acceleration of gravity
H	sensible heat flux into the atmosphere
$I_{\ell d}$	incoming (sky) longwave radiation flux
$I_{\ell u}$	outgoing (ground) longwave radiation flux
I_s	incoming solar radiation flux
I'_s	absorbed solar radiation flux
K	hydraulic conductivity
K_s	value of K when $T = T_o$ and $\theta = \theta_u$
K_{ei}	effective value of K for element i in the two-node model
k	von Karman constant
L	latent heat of vaporization of water
ℓ_1, ℓ_2	depths of cells in two-node model
N	proportion of sky observed by cloud

Symbol	Description
N_o	fair-weather value of N
NL	number of elements used in finite element model
n	porosity
P	precipitation rate
pF	$\log_{10}(-\psi)$
$\underset{\sim}{q}_h$, q_h	vector and vertical component of heat flux
$\underset{\sim}{q}_m$, q_m	vector and vertical component of total moisture flux
R	total runoff rate
R	redistribution parameter
R_g	groundwater runoff rate
R_s	surface runoff rate
R_v	gas constant for water vapor
Rn	net radiation received by surface
$(Ri)_B$	bulk Richardson number
S_e	desorptivity of soil mass
S_i	sorptivity of soil mass
T	temperature (Celsius)
T_a	air temperature
T_g	temperature of ground surface
T_o	an arbitrary reference temperature
T_1	surface temperature in force-restore model
T_2	deep soil temperature in force-restore model
TERR	maximum allowable temperature change per time step in finite element model
t	time

Symbol	Description
t_b	time between storms
t_r	storm duration
u_a	wind speed at screen height
W	different heat of wetting
XERR	maximum allowable change of θ per time step in finite element model
Z	storage cell depth in moisture parameterizations
Z_B	depth of deepest finite element node
ZRAT	ratio of top element size to average element size in the finite element model
z	vertical distance coordinate
z_a	screen height
z_o	surface roughness height
α	angle of the sun above the horizon
Δ_i	length of i'th element
ε	emissivity of the ground
ε_a	emissivity of the air
θ	volumetric liquid moisture content
θ_a	volumetric air content
θ_d	value of θ on main drying curve
θ_d^o	value of θ on first drying curve
θ_H	notation explicitly denoting hysteretic θ
θ_i	initial moisture content
θ_i	volumetric proportion of the i'th phase
θ_k	value of θ where liquid continuity fails

Symbol	Description
θ_u	value of θ upon re-wetting of a dry porous medium
θ_w	value of θ on main wetting curve
θ_1	surface moisture content in two-node model
θ_2	deeper moisture content in two-node model
$\overline{\theta}$	average moisture content in one-cell models
λ	effective thermal conductivity of soil
λ_a	thermal conductivity of air
λ_i	thermal conductivity of i'th soil constituent
ρ_a	density of air
ρ_ℓ	density of liquid water
ρ_v	density of water vapor or absolute humidity
ρ_{va}	ρ_v at screen height
ρ_{vg}	ρ_{vg} at ground surface
ρ_o	saturation value of ρ_v
σ	Stefan-Boltzmann constant
τ	surface shear stress
τ	period of one day
Ψ	value of ψ referenced to temperature T_o
ψ	matric potential
Ω	tortuosity of air phase of the porous medium

Chapter 1

INTRODUCTION

1.1 Objective

The goal of this research is to design and test a cost-effective parameterization of moisture and heat transfer between the atmosphere and the land surface for use in numerical global climate models. The parameterization is to be firmly based on the process physics and should be simple enough for use with an atmospheric general circulation model (GCM). Its development and validation is to be carried out using a detailed finite element model of the soil as a truth model. In recent years, many climate modelers have voiced the need for an improved land surface parameterization.

Cost-effectiveness, in the present context, implies ability to reproduce the release of heat and water from the land surface to the atmosphere by means of an algorithm having relatively modest computational requirements. Since a GCM may have hundreds of grid cells corresponding to the land surface, it is important that the surface state set be kept to a minimum and that the predictive equations for these states be numerically simple.

A physically-based approach is employed. As a consequence, the parameters and states appearing in the parameterization represent physically meaningful, measurable

quantities. This can facilitate parameter and state estimation by means of remote sensing, and it allows for utilization of available mapped information, e.g., from soil surveys.

The accuracy of the proposed parameterization is to be defined in terms of its ability to mimic the behavior of a highly-detailed simulation model of soil moisture and heat. As an experimental apparatus, the latter model allows us to simulate easily and quickly the response of any soil to any series of atmospheric forcing, thereby providing detailed data against which to test the parameterization.

In this analysis, only bare soil is considered. The resulting parameterization is at a level consistent with, and compatible with, existing parameterizations of the role of vegetation in water and energy exchange.

1.2 Background and Justification

The general circulation of the atmosphere is determined largely by the surface transfers of momentum, heat, and moisture. These transfers are intimately coupled one to another. Evapotranspiration from soil moisture is a major term in both the water and energy balances at the surface, returning 57 percent of continental precipitation to the atmosphere (Budyko et al., 1962) and consuming a large proportion of the radiation available at land surfaces

(Monin, 1972, p. 7). It follows that the rate of evapotranspiration may be limited by the availability of either water or heat at the surface.

Other major couplings may be identified. The available radiation is attenuated by the surface albedo, which is sensitive to soil moisture. Transport across the planetary boundary layer is dependent upon atmospheric stability, which is proportional to the vertical temperature gradient near the ground. The thermal properties of soil are sensitive to moisture content.

It is apparent that regional water balances (and surface heat balances) are linked to climate -- not passively, but actively. Due primarily to the great sensitivity of this coupling to soil moisture concentration, to surface temperature, and to the parameters of land surfaces, it is important to consider the spatial and temporal variations of these quantities in the formulation of transfer relations at the earth's surface. For example, Eagleson (1978) has shown the critical importance of soil type and vegetal density in determining the annual average state of soil moisture in a given climatic situation, and has demonstrated their control over the division of precipitation into its respective water balance components.

Several recent studies have demonstrated the sensitivity of weather and climate to land surface parameters

and states. Charney (1975) showed the potential role of albedo change in desertification. Reck (1978) found surface albedo to be one of the three largest sources of uncertainty in calculating the surface temperature using the Manabe-Wetherald radiative-convective atmospheric model. Surface albedo is strongly dependent on the soil moisture content of bare surfaces and on the extent and state of vegetal cover.

The influence of soil moisture on the atmosphere is not confined to the albedo effect. Charney et al. (1977) showed that local evaporation rates are as important as albedo in determining precipitation in semi-arid regions. Walker and Rowntree (1977) have illustrated the role of the soil moisture state in shaping weather patterns, using a numerical model with fixed surface albedo. Reck (1978) identified surface relative humidity as another major source of uncertainty in obtaining the surface temperature. Surface relative humidity is directly related to surface soil moisture content. Shukla and Mintz (1982) have demonstrated graphically the great sensitivity of the global distributions of rainfall, temperature, and air flow to the land surface evapotranspiriation.

The GCM's currently in use employ variants of the Budyko (1956) parameterization in which evaporation is linearly proportional to soil moisture concentration, up to a certain threshold value that is assumed constant everywhere.

These GCM's calculate the changes of moisture content using any of a variety of empirically-based runoff relations, which are also assumed independent of soil type and vegetal cover.

In the report of the 1974 Global Atmospheric Research Program (GARP) Climate Conference (GARP Publication No. 16), this method of modeling the land-atmosphere interaction is outlined and discussed critically. It is urged that the apparent sensitivity of climate models to the surface parameterization be studied using existing models. Assuming these tests to show that land surface characterization is a significant limitation to the accuracy of climate models, the GARP Climate Conference (1975, p. 51) recommends the following improvements as first priority:

> "more accurate and individual specification of the GCM grid-point values of: soil water capacity; the relation between actual and potential evaporation as a function of soil water content; albedo ..."

and

> "the introduction of a 'multiple bucket' concept at each grid point to take account of moisture storage and all depletion processes..."

This need has also been stressed recently by Gates (1975), who writes

> "A fourth problem area which appears to be critical for climate modeling is the treatment of the land surface. In comparison to the detailed attention given in GCM's to the representation of atmospheric and oceanic processes, the attention given to the earth's surface itself is almost cavalier. Yet it may well be that climatic changes on many time scales are primarily determined by such effects as surface albedo, the amount of

> moisture and heat retained in the soil, the surface roughness, and the character of the surface vegetation."

Finally, the Joint Organizing Committee (JOC) of GARP (1975) has singled out three elements of the hydrologic cycle that needs "efforts ... with regard to improving our knowledge of the hydrological cycle to be used for climate modeling." These three elements are snow cover, soil moisture, and runoff.

1.3 Outline of Research

The work documented in this report consists of the following four steps:

1. Assemble a numerical model -- the reference model -- based on the complete system of partial differential equations governing vertical heat and water (liquid and vapor) flow in the soil. Couple it to a parameterization of the surface boundary layer of the atmosphere. Assemble data sets describing two soils (a silt loam and a sand) and two climates (a hot, arid one and a cool, moist one).

2. Using the reference model with the various data sets, determine numerical convergence and stability criteria. Perform series of experiments to test the importance of several physical effects on model outputs and simplify the model accordingly.

3. Given the simplified physical description of the system resulting from the last step, propose one or more

parameterizations (computationally simplified models) that are consistent with, or derived from, that description.

4. Test the parameterization(s) against the reference model using the soil and climate data sets.

These steps are discussed in more detail in Section 2.2.

Chapter 2

DEFINITION OF THE SOIL SYSTEM

2.1 The Coupling between the Soil and the Atmosphere

For the sake of analysis, the soil and the atmosphere may be viewed as a coupled pair of systems (Figure 2.1). Both systems experience inputs, i.e., are acted upon or forced externally, and both respond by producing outputs. In the case of this simple coupling, one system's output is the other's input. (Of course, the atmosphere also interacts with the oceans, the sun, and outer space, but these physical entities can arbitrarily be incorporated into what we have called the atmosphere system.)

The output of a system (e.g., the soil system) is fully determined at any time by the forcing, the system state, and the system parameters. Parameters are independent of the forcing, while the states are not.

In order to study the behavior of the soil, we wish to decouple it conceptually from the atmosphere. We shall define precisely which physical properties are the input (forcing), the output (response), the states, and the parameters of the soil system. These definitions are somewhat arbitrary, being influenced both by our choice for the location of the soil system boundary and by the purpose of

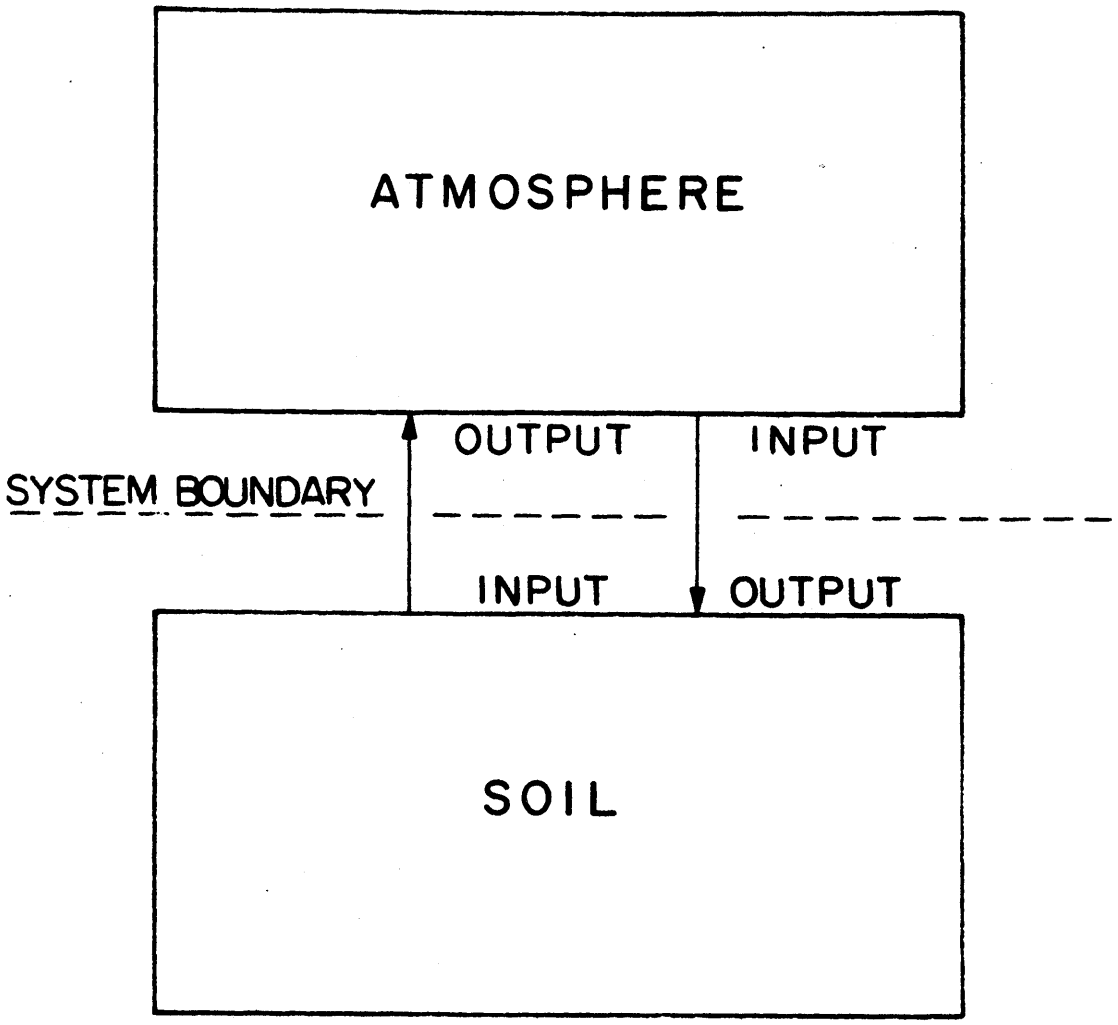

Figure 2.1

THE COUPLING BETWEEN SOIL AND ATMOSPHERE

our model.

Since we wish to study only the soil system, we must ignore the feedback of soil outputs through the atmosphere system and back to the soil. As an example, consider the option of defining the boundary between the "soil" and "atmosphere" (Figure 2.1) to be their actual interface, the surface of the ground. Suppose further that the atmospheric vapor pressure and temperature at this interface are defined to be two of the inputs to the soil. If this selection is made, it can be shown to follow that the injection of sensible heat and water vapor into the atmosphere is determined by the soil system and forces the atmosphere as an input. Now, due to the nature of the planetary boundary layer of the atmosphere, the vapor pressure and temperature at the surface are very strongly correlated with these upward fluxes, i.e., the importance of feedback is excessive.

In order to eliminate most of this feedback effect from the modelling problem, it would be desirable to define the system boundary in Figure 2.1 to be the top of the planetary boundary layer. The planetary boundary layer, which can be considered the layer of immediate influence of the earth's surface, varies in thickness (especially diurnally) from tens to thousands of meters. If we were to employ the top of the planetary boundary layer as

the boundary of our "soil" system, we would need to simulate the extremely complex dynamics of that critical part of the atmosphere. This is an area of ongoing research and is beyond the scope of our study.

In this analysis, we choose a compromise between these two alternatives. The boundary of the "soil" system is placed within the surface boundary layer (SBL) of the atmosphere at a height on the order of a couple meters above ground level. One advantage of this choice is that much of the turbulent diffusion resistance of the planetary boundary layer is located very near the surface, where the intensity of the turbulence is low. Atmospheric conditions two meters above the surface are therefore much more similar to those at the top of the planetary boundary layer than they would be if the turbulence were homogeneous. The error induced by neglecting feedbacks, mentioned earlier, is thus reduced significantly, though not entirely to zero, by this scheme. A second advantage of this approach is that the transfer relations for the SBL are very simple bulk transport equations, since this is a constant (i.e., no divergence) flux layer. A final advantage is the ready availability of data describing the state of the atmosphere at this height.

A system diagram of the coupled soil/SBL system and its interaction with the atmosphere is shown in Figure 2.2. The soil receives forcing directly from the atmosphere

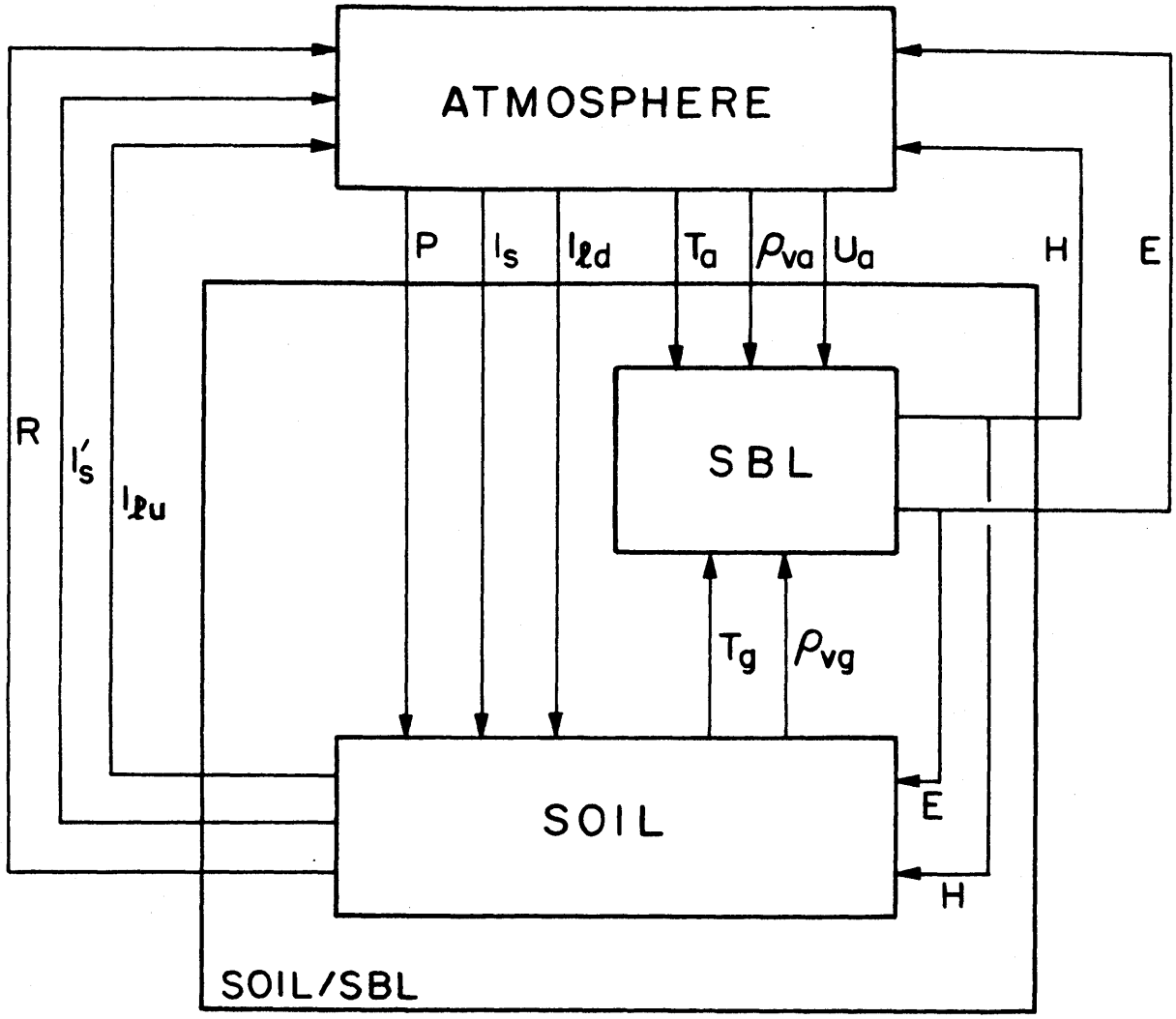

Figure 2.2

DETAILS OF THE INTERACTION OF THE SOIL/SBL SYSTEM WITH THE ATMOSPHERE

in the form of shortwave radiation (I_s), longwave atmospheric radiation ($I_{\ell d}$), and precipitation (P). Other forcing of the soil/SBL system consists of the air temperature (T_a), vapor density (ρ_{va}), and windspeed (u_a) at the so-called screen height. Together with the soil surface temperature (T_g) and vapor density (ρ_{vg}), these three quantities determine the rate of extraction of water (E) and sensible heat (H) from the soil by the action of the SBL. These outputs of the SBL system, E and H, are forcing for both the soil and the atmosphere. The other outputs of the soil/SBL system are the back longwave radiation ($I_{\ell u}$), the reflected solar radiation (I_s'), and the total runoff (R), or yield, of surface and ground water to the surface drainage network and thence, eventually, to the ocean or atmosphere. Of these, the reflected shortwave radiation is lost to space and is unimportant for weather or climate, while the runoff is of secondary importance and acts on a longer time scale, possibly affecting oceanic salinity and circulation. For climatic applications, we may usually be confident that correct prediction of evaporation will result in correct prediction of runoff on these longer time scales, since the storage capacity of the soil is finite. This argument may fail where the water table is very deep, allowing significant increases in stored groundwater. The analysis of long-term interactions of groundwater and

climate are beyond the scope of this work.

For the purposes of climate dynamics, we shall be more interested in the soil/SBL outputs E, H, and $I_{\ell u}$ that result from the atmospheric forcing. Among these, correct predictions of H and $I_{\ell u}$ rely on accurate simulation of surface temperature. Since H is more sensitive than $I_{\ell u}$ to surface temperature, we may concentrate on reproducing H and E, confident that $I_{\ell u}$ will follow.

2.2 Elaboration of Goal and Methodology

The goal of this research is to identify simple mathematical models of the soil system, as represented in Figure 2.2, and to evaluate their performance by comparing computed outputs to those obtained using a detailed numerical model of the system. The analysis consists of the following steps, already outlined in the first chapter, discussed here in the light of Figure 2.2:

1. Construct a detailed numerical model - the reference model - of a one-dimensional soil system. The model should accept E, P, H, I_s and $I_{\ell d}$ as part of its boundary conditions. Computed distributions of soil moisture and temperature yield the values of surface vapor density, ρ_{vg}, and surface temperature, T_g, as well as the upward longwave radiation from

the soil, $I_{\ell u}$, and the runoff, R. Construct a simple model of the SBL that yields E and H as functions of vapor and temperature differences across the layer and of the wind-speed.

Identify and quantify parameter sets describing (1) idealized periodic atmospheric forcing of the soil/SBL system, (2) the SBL, and (3) the soil.

2. Run experiments with the numerical model and the specified parameter sets. Using the parameter sets, determine convergence and stability criteria for the numerical model coupled to the SBL parameterization.

Through further experiments, analyze the influence of various physical effects on system outputs under realistic forcing. Control simulations are run with the full set of governing equations for the soil. Corresponding simulations are run with the same SBL model and atmospheric forcing, but with various simplifications or reductions of the physical description of the soil. These reductions are the following:

- Neglect soil water in the vapor phase
- Neglect the heat of wetting

- Neglect the temperature dependences of moisture retention and of hydraulic conductivity
- Replace the hysteretic moisture retention function with an approximate reversible one.

Compare computed evaporation, sensible heat flux, and net radiation for the reference model and the simplifications thereof. Calculate mean errors and root-mean-square errors of each flux and evaluate the validity, with possible limitations, of each simplification. Determine how much of the reference model structure, and hence how much of the process physics, is essential to the satisfactory prediction of the surface fluxes.

3. Given the findings of Step 2, formulate mathematically a few dynamic lumped-parameter models of the soil system. Like the reference model, they must specify ρ_{vg}, T_g, and $I_{\ell u}$ as responses to forcing by P, E, H, I_s, and $I_{\ell d}$ (Figure 2.2).
4. Using the same (periodic) forcing parameter sets and SBL parameterization as in the previous experiments, calculate the hourly response of the parameterizations. Compare

the output to that of the reference model. Calculate mean errors and root-mean-square errors and evaluate the performance of the parameterizations.

Repeat this step using more realistic random forcing based on actual data for the same sites.

In summary, the goal of this work is to simulate the behavior of the soil/SBL system pictured in Figure 2.2, using successively simpler, physically-based models to represent the soil component of the system. The criterion for evaluation of the models is their fidelity in reproducing the outputs of the most detailed model.

The remainder of this chapter is devoted essentially to Step 1 above. It consists of

(1) the definition of the reference model of the soil component and two soil parameter sets,

(2) the definition of the SBL parameterization to be used throughout the analysis, and

(3) the definition of two parameter sets that will also be used throughout the analysis to generate the deterministic periodic atmospheric forcing sequences.

2.3 The Reference Model of the Soil System

2.3.1 Governing Partial Differential Equations

What we shall refer to as the reference model is the system description of the soil based on the partial differential equations of mass and energy conservation in a partially-saturated, hysteretic porous medium under the following assumptions:

1. The air phase is static with pressure everywhere equal to atmospheric.
2. The soil is non-deformable and isotropic.
3. Moisture does not freeze.
4. There is local hydraulic and thermal equilibrium among the solid particles, the air, and the water.
5. There is no uptake of water by plants.

Under these conditions, the mass and heat conservation equations are (Milly and Eagleson, 1980)

$$\left[\left(1 - \frac{\rho_v}{\rho_\ell}\right) \left.\frac{\partial\theta}{\partial\psi}\right|_T + \frac{\theta_a}{\rho_\ell} \left.\frac{\partial\rho_v}{\partial\psi}\right|_T\right] \frac{\partial\psi}{\partial t}$$

$$+ \left[\left(1 - \frac{\rho_v}{\rho_\ell}\right) \left.\frac{\partial\theta}{\partial T}\right|_\psi + \frac{\theta_a}{\rho_\ell} \left.\frac{\partial\rho_v}{\partial T}\right|_\psi\right] \frac{\partial T}{\partial t} = -\nabla\cdot(\underset{\sim}{q}_m/\rho_\ell) \tag{2.1}$$

and

$$\left\{C + (L + c_\ell T)\theta_a \left.\frac{\partial \rho_v}{\partial T}\right|_\psi + [\rho_\ell c_\ell T - \rho_\ell W - \rho_v(L + c_\ell T)] \left.\frac{\partial \theta}{\partial T}\right|_\psi \right\} \frac{\partial T}{\partial t}$$

$$+ \left\{(L + c_\ell T)\theta_a \left.\frac{\partial \rho_v}{\partial \psi}\right|_T + [\rho_\ell c_\ell T - \rho_\ell W - \rho_v(L + c_\ell T)] \left.\frac{\partial \theta}{\partial \psi}\right|_T \right\} \frac{\partial \psi}{\partial t}$$

$$= - \nabla \cdot \underset{\sim}{q}_h \qquad (2.2)$$

where the moisture and heat fluxes $\underset{\sim}{q}_m$ and $\underset{\sim}{q}_h$ are given by

$$\underset{\sim}{q}_m / \rho_\ell = -(K + D_{\psi v})\nabla\psi - D_{Tv} \nabla T - K\underset{\sim}{k} \qquad (2.3)$$

and

$$\underset{\sim}{q}_h = - \lambda \nabla T - \rho_\ell L D_{\psi v} \nabla\psi + c_\ell T \underset{\sim}{q}_m \qquad (2.4)$$

In (2.1) and (2.3), ψ is the matric potential of water, T is temperature (we use Celsius), θ is the volumetric fraction of liquid water and θ_a the fraction of air, ρ_ℓ is the constant density of liquid water, ρ_v is the density of water vapor in the air phase, t is time, ∇ is the divergence operator, and $\underset{\sim}{k}$ is the unit vector opposing gravity. K is the hydraulic conductivity for liquid flow and $D_{\psi v}$ is the conductivity for vapor flow due to head gradients. D_{Tv} is the diffusion coefficient for vapor transport due to temperature gradients.

In (2.2) and (2.4), C is the volumetric bulk heat capacity of the soil, L is the latent heat of vaporization of water, c_ℓ is the heat capacity of liquid water, W is the

differential heat of wetting, and λ is the effective thermal conductivity.

In the derivation of (2.2) and (2.4), the reference temperature for zero heat content is arbitrarily taken to be 0°C.

At a given point in the medium, all of the coefficients in (2.1) through (2.4) can be expressed as functions of time-invariant parameters and of the soil variables ψ and T, which therefore can be used to represent the state of the soil system. In addition, hysteretic soils require a third state variable - the wetting history - in order to complete the state set. This variable is the Ψ_o introduced in the next section. It arises there in the statement of the diagnostic relation for moisture retention.

2.3.2 Boundary Conditions

The boundary conditions on (2.1) and (2.2) for a one-dimensional vertical system are the following:

1. Surface Condition on Moisture. The atmospheric source/sink of moisture, P-E, is equal and opposite in sign to the surface moisture flux as long as the surface is not saturated,

$$-(q_m/\rho_\ell)_{z=0} = P-E \quad , \quad \left.\frac{d\theta}{d\Psi}\right|_{z=0} \neq 0 \qquad (2.5a)$$

Otherwise, the infiltration rate (negative moisture flux) equals the current infiltration capacity of the soil. The boundary condition can then be written

$$\psi\Big|_{z=0} = h \ , \quad \frac{d\theta}{d\Psi}\Big|_{z=0} = 0 \qquad (2.5b)$$

where h is the depth of ponded water on the surface. The rate of change of the new state h is given by the balance equation

$$\frac{dh}{dt} = P-E + (q_m/\rho_\ell)_{z=0} - R_s \qquad (2.6)$$

in which R_s, the surface runoff, is given by

$$R_s = \begin{cases} P-E + (q_m/\rho_\ell)_{z=0}, & h=h_{max} \text{ and } P-E + (q_m/\rho_\ell)_{z=0} > 0 \\ 0 & \text{otherwise} \end{cases} \qquad (2.7)$$

where h_{max} is the depth of the surface retention "reservoir." When (2.5a) is the active boundary condition, h is zero; otherwise the surface would be saturated. Then (2.7) says that R_s is zero and (2.6) says h remains zero. When the surface becomes saturated, (2.5b) applies. In that case, the fully determined solution of (2.1) and (2.3) yields a value for $(q_m/\rho_\ell)_{z=0}$ by means of (2.3). This value determines $\frac{dh}{dt}$ and R_s through (2.6) and (2.7).

2. Condition on Moisture at Depth. A second boundary condition on the moisture distribution must be applied at

the bottom of the column. For a relatively static water table, this condition could be expressed as

$$\psi\Big|_{z=-Z_w} = 0 \qquad (2.8)$$

where Z_w is the water table depth. If the water table is sufficiently deep, we can identify the lower end of our column as any depth (above the water table) below the point where matric head gradients induced by surface forcing become negligible. Then, using (2.3),

$$(q_m/\rho_\ell)_{z=-Z_B} = -K\Big|_{z=-Z_B} - (D_{Tv} + D_{Ta}) \frac{\partial T}{\partial z}\Big|_{z=-Z_B} \qquad (2.9)$$

In this work, we shall concentrate only on (2.9).

3. Surface Condition on Heat. Considering the possible presence of ponded water ($h \neq 0$), the heat balance of the surface can be written as

$$q_h\Big|_{z=0} = -(1-A)I_s - \varepsilon I_{\ell d} + I_{\ell u} + \rho_\ell [L + c_\ell T\Big|_{z=0}]E$$
$$- \rho_\ell c_\ell T_a P + H + \rho_\ell c_\ell T\Big|_{z=0} R_s + \rho_\ell c_\ell \frac{d}{dt}\left[h\, T\Big|_{z=0}\right] \qquad (2.10)$$

Equation (2.10) is the energy balance for the layer of water (potentially of zero thickness) in depression storage. Assuming that the water has the same temperature as the soil surface, this equation is derived by equating the change in

heat storage (the last term) to the net sum of all radiative, sensible, and latent heat fluxes. The soil heat flux (sensible plus latent) is given by $q_h\big|_{z=0}$. I_s is incoming solar radiation and A is the albedo of the surface. $I_{\ell d}$ is the downward longwave radiation from the sky. The longwave absorptivity of the surface is taken to be equal to its emissivity, ε (Deardorff, 1978). Back longwave radiation upward from the surface, $I_{\ell u}$, is given by

$$I_{\ell u} = \varepsilon\sigma(T\Big|_{z=0} + 273)^4 \qquad (2.11)$$

where σ is the Stefan-Boltzman constant. Both A and ε depend on the surface soil moisture content, as discussed in the following section. Latent and a little sensible heat are carried away by evaporation. Precipitation at air temperature delivers sensible heat, while runoff and turbulent diffusion in the atmosphere (H) carry it away. In the absence of precipitation, with h = 0, (2.10) is the familiar expression that net radiation minus heat flow into the ground is equal to the sum of latent and sensible heat diffusion away from the surface.

4. Conditions on Heat at Depth

Annual fluctuations of ground surface temperatures are attenuated with depth, but persist up to a depth of ten to twenty meters. If the bottom boundary of the system is deeper than this, then with both $\nabla\psi$ and ∇T equal to zero,

the heat flux out the bottom is

$$q_h\Big|_{z=-Z_B} = c_\ell (T\ q_m)_{z=-Z_B} \qquad (2.12)$$

which allows heat to exit the column only by advection in the water phase. We shall apply this condition at the bottom of our column, with Z_B equal to only five meters. For our relatively short-term analyses, the neglected fluxes across the bottom boundary are small enough to be unimportant.

2.3.3 Initial Conditions

To begin a simulation, the initial state of the system must be specified. Depth distributions of ψ, T, and the wetting history are needed. Given the time of the year, the air temperature data, and typical values of the soil thermal parameters for our scenarios, we estimated the soil temperature at a depth of one meter, which is just below the depth of the diurnal fluctuations. This value was then applied as the initial temperature over the entire column depth. This approximation results in some error in the rates of heat conduction at depths of more than a meter, but the magnitude of these deep fluxes is small anyway.

The initial moisture content is also assumed to be constant in depth. For preliminary analyses in Section 3.1, its value is chosen so that the corresponding hydraulic conductivity (and thus the groundwater recharge rate) is

	Soil Temperature	Matric Potential
sand/Winslow	24°C	-167 cm
silt loam/Winslow	24	-388
sand/Dulles	14	- 71
silt loam/Dulles	14	-129

Table 2.1

INITIAL CONDITIONS FOR THE FOUR SCENARIOS.

MATRIC POTENTIAL VALUES ARE USED ONLY IN SECTION 3.1.

REVISED VALUES ARE DETERMINED IN SECTION 3.2.

20% of the annual precipitation rate. This choice is arbitrary and the system response is quite sensitive to the initial value chosen. A more useful method for specifying an initial moisture content is introduced and applied in Section 3.2.

Specification of the wetting history is accomplished by assuming that the soil is on the main drying curve (Section 2.3.4.1) initially.

The initial conditions applied are listed in Table 2.1.

Together with the p.d.e.'s (2.1) and (2.2), the flux equations (2.3) and (2.4), and the diagnostic descriptions of the parameters to follow, the boundary conditions (2.5ab)/(2.6)/(2.7), (2.9), (2.10)/(2.11) and (2.12) allow us to determine the evolution of the system states, given any initial states, and to find the soil outputs. This set of equations is thus a complete description of the soil system drawn in Figure 2.2.

2.3.4 Soil Properties and Soil System Parameters

Variables appearing in the p.d.e.'s, flux equations, boundary conditions, and auxiliary equations of the previous section include the state variables, $\psi(z,t)$, $T(z,t)$, $h(t)$, and the input variables, P, E, I_s, $I_{\ell d}$, H, T_a. All other variables can be expressed as functions of the soil state.

In this section, we present these equations of state. As we shall see, the diagnostic relations introduce constants that reflect the physical nature of the soil system. These are the system parameters. We present typical values of these parameters for two hypothetical bare soil systems - a silt loam and a sand.

2.3.4.1 Parameters relating to moisture storage

Moisture is present in two forms - liquid and vapor. Vapor is stored in the air of the medium, whose volumetric fraction is

$$\theta_a = n - \theta \qquad (2.13)$$

where n is the porosity. The vapor density is (Edlefsen and Anderson, 1943, p. 145)

$$\rho_v = \rho_o(T) \exp[\psi g/R_v(T + 273)] \qquad (2.14)$$

in which ρ_o is the saturation vapor density, g is the acceleration of gravity, and R_v is the gas constant for water vapor.

The proportion of the medium occupied by liquid water is a hysteretic function of ψ and T, mainly the former. Using an approximation of a theory proposed by Mualem (1977), Milly and Eagleson (1980) have expressed θ for an isothermal system as a function of (1) the present value of ψ and (2) the last value of ψ at which a wetting

reversal occurred. They also generalized this theory to account for non-isothermality by introducing the variable

$$\Psi \equiv \psi e^{a'(T-T_o)} \tag{2.15}$$

where

$$a' \equiv -\frac{1}{\psi}\frac{\partial \psi}{\partial T}\bigg|_{\theta} \tag{2.16}$$

is assumed to be a constant. We take T_o arbitrarily to be the initial soil temperature of the time period of interest. There is considerable uncertainty as to the value of a' (see Milly and Eagleson, 1980, pp. 90-93); here we have adopted a value of $6.8 \times 10^{-3} {}^{\circ}K^{-1}$, which is over three times the value predicted by the surface tension model (Philip and de Vries, 1957).

In terms of Ψ, the moisture content is given by

$$\theta = \begin{cases} \theta_w(\Psi) + \theta_w(\Psi_o)\left[1 - \dfrac{\theta_w(\Psi)}{\theta_u}\right] & \dfrac{d\Psi}{dt} > 0 \\ \theta_w(\Psi)\left[1 + \dfrac{\theta_w(\Psi_o) - \theta_w(\Psi)}{\theta_u}\right] & \dfrac{d\Psi}{dt} < 0 \end{cases} \tag{2.17}$$

in which

$$\theta_w(\Psi_o) = \begin{cases} \theta_u[\theta_1 - \theta_w(\Psi_1)][\theta_u - \theta_w(\Psi_1)]^{-1} & \dfrac{d\Psi}{dt} > 0 \\ \theta_w(\Psi_1) + \theta_u[\theta_1 \theta_w(\Psi_1)^{-1} - 1] & \dfrac{d\Psi}{dt} < 0 \end{cases} \tag{2.18}$$

where θ_1 and Ψ_1 are the values of θ and Ψ when the most recent wetting reversal occurred. The parameter θ_u is the proportion of the medium occupied by water upon re-wetting to $\psi = 0$. It is less than the porosity due to air entrapment. The value of θ_u/n may be taken as 0.9 (Mualem, 1974). The function $\theta_w(\Psi)$ is identical to the main wetting curve at temperature T_o.

Two useful relations derived by Mualem (1977) for his model are the following (expressed here in terms of Ψ):

$$\theta_d(\Psi) = \left[2 - \frac{\theta_w(\Psi)}{\theta_u}\right] \theta_w(\Psi) \qquad (2.19)$$

$$\theta_d^o(\Psi) = \frac{n}{\theta_u} \theta_d(\Psi) \qquad (2.20)$$

in which $\theta_d(\Psi)$ is the main drying function and θ_d^o is the first drying (from total saturation) function.

We have converted moisture desorption data for Geary silt loam (Hanks and Bowers, 1962) and for Plainfield sand (Jury and Miller, 1974) to wetting data using (2.19) and fitted smooth curves to them. The resulting main wetting functions are expressed in the form

$$\theta_w(\Psi) = \min\left\{\theta_u,\ a\left(\frac{\Psi}{b}\right)^c + d[7 - \log(-\Psi)] + e\right\} \qquad (2.21)$$

The fitted parameters for the silt loam and the sand are listed in Table 2.2.

Parameter	Silt Loam	Sand
n	0.46	0.35
θ_u	0.414	0.315
K_s	10^{-4} cm s^{-1}	2×10^{-3} cm s^{-1}
a	0.210	0.171
b	-495.	-15.7
c	-0.147	-1.77
d	0.0	0.00343
e	-0.0489	0.0
θ_3	0.16	0.65
θ_4	0.33	0.0
θ_5	0.05	0.0
θ_k	0.11	0.025
S	10^5 cm^{-1}	10^2 cm^{-1}
A_d	0.20	0.35
A_w	0.10	0.25
h_{max}	0.5 cm	0.5 cm

Table 2.2

REPRESENTATIVE VALUES OF THE SOIL PARAMETERS

FOR A SILT LOAM AND A MEDIUM SAND

Main branches of the hysteretic retention functions are plotted in Figures 2.3 and 2.4. Figures 2.3a and 2.4a show the main wetting and drying curves and the first drying curve of the silt loam and the sand, respectively. There is a wide range of pF over which significant moisture release/storage occurs in the silt loam, in contrast to the storage of most water in the sand at pF between 1 and 2 (-100 cm $< \psi < -10$ cm). The main hysteresis loop is much more open for the silt loam than for the sand. The relatively small influence of temperature on moisture retention can be seen in Figs. 2.3b and 2.4b.

2.3.4.2 Parameters relating to moisture transport

The hydraulic conductivity may be expressed as (Milly and Eagleson, 1980)

$$K = K_s \, K_\theta(\theta) \, K_T(T) \qquad (2.22)$$

where K_s is the value of K at saturation and temperature T_o, $K_T(T)$ is a viscosity correction given by

$$K_T(T) = \frac{\mu(T_o)}{\mu(T)} \qquad (2.23)$$

where μ is viscosity, and the dependence upon θ is given by Mualem (1976) as

$$K_\theta(\theta) = S_e^{1/2}\left[\int_o^{S_e} \frac{dS}{\psi(S)}\right]^2 \left[\int_o^{1} \frac{dS}{\psi(S)}\right]^{-2} \qquad (2.24)$$

$$S_e = \frac{\theta - \theta_r}{\theta_u - \theta_r} \tag{2.25}$$

We take θ_r to be zero. With higher values, K_θ falls off more sharply at low θ and vapor conductivity dominates over an increasingly wide range of moisture contents. We found that even with $\theta_r = 0$, this range was overestimated relative to the experimental findings of Rose (1963).

The values of n and the approximate values of K_s for Geary silt loam and Plainfield sand are given in Table 2.2. Hysteresis of K with respect to θ will be neglected.

The vapor conductivity, $D_{\psi v}$, is given by (Milly and Eagleson, 1980)

$$D_{\psi v} = \rho_\ell^{-1} D_a \Omega \theta_a \left.\frac{\partial \rho_v}{\partial \psi}\right|_T \tag{2.26}$$

where D_a is the molecular diffusivity of water vapor in air (Kimball et al., 1976)

$$D_a = 0.229 \left(1 + \frac{T}{273}\right)^{1.75}, \quad cm^2\ s^{-1} \tag{2.27}$$

The parameter Ω represents the tortuosity of the air-filled pore domain. Its dependence on air content will be expressed for both soils as (Lai et al., 1976)

$$\Omega = \theta_a^{2/3} \tag{2.28}$$

The final factor in (2.26) can be computed from (2.14).

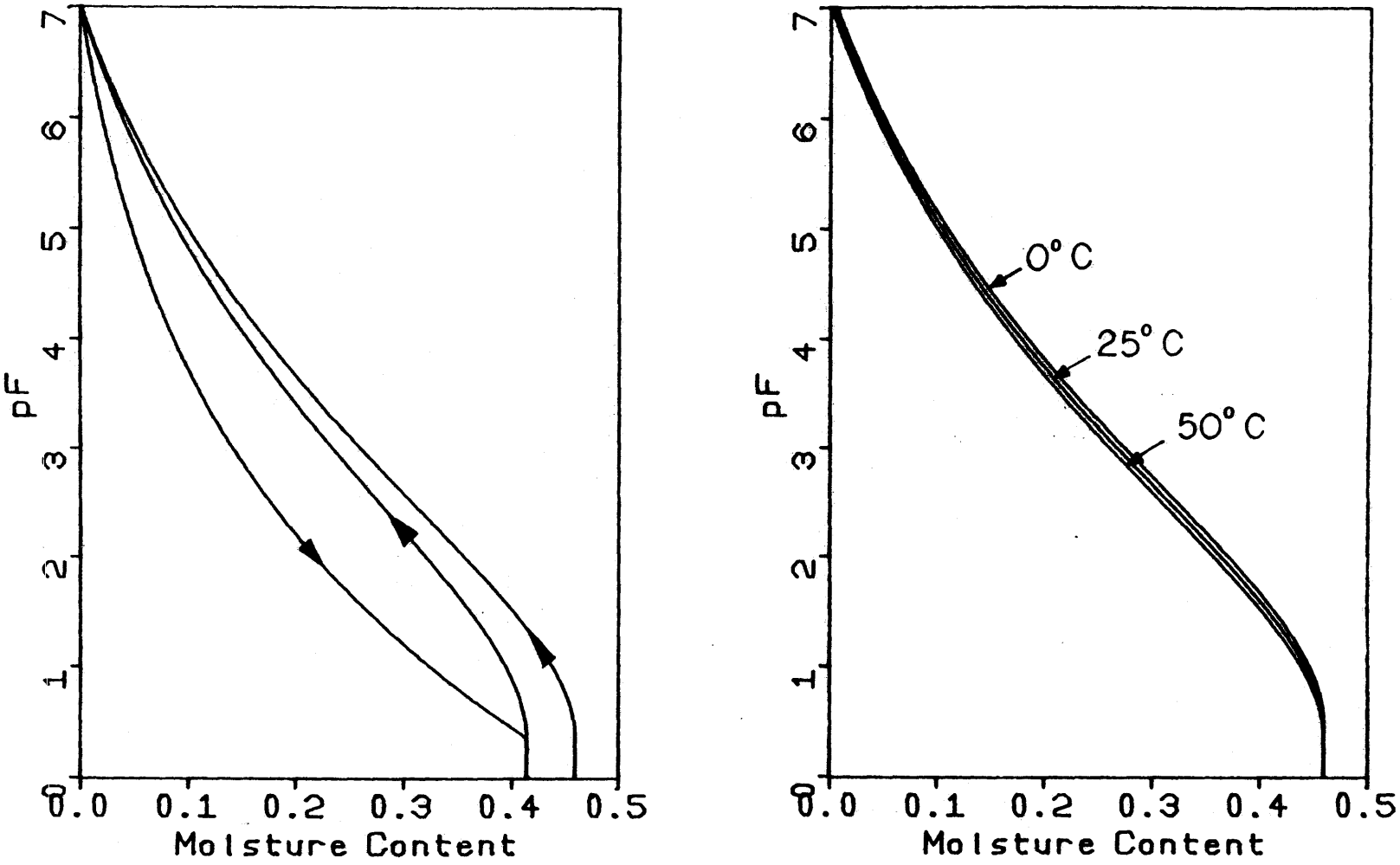

Figure 2.3

MOISTURE RETENTION IN THE SILT LOAM. Left: MAIN BRANCHES OF THE HYSTERETIC RETENTION FUNCTION. Right: DEPENDENCE OF THE FIRST DESORPTION CURVE ON TEMPERATURE.

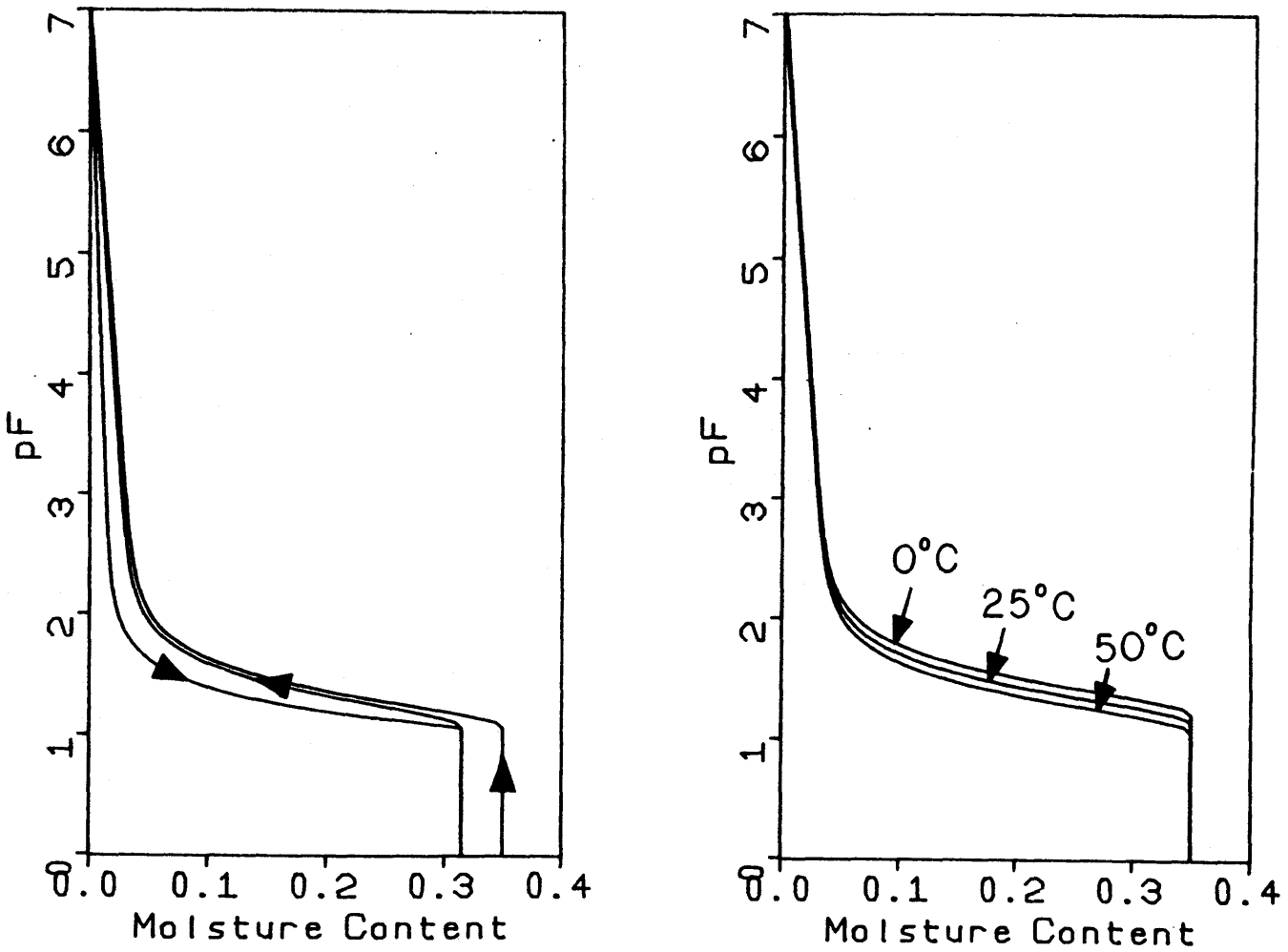

Figure 2.4

MOISTURE RETENTION IN THE SAND. Left: MAIN BRANCHES OF THE WETTING PROCESS AT FIXED TEMPERATURE. Right: DEPENDENCE OF THE FIRST DESORPTION CURVE ON TEMPERATURE.

The vapor conductivity is plotted with the liquid conductivity for both soils in Figure 2.5. For the purpose of these plots, θ and Ψ are assumed to be related by $\theta_d^o(\Psi)$ (Eq. 2.23). This procedure will also be used in the other plots of soil properties. The liquid conductivity of the sand is high for most θ, whereas that of the silt loam decreases steadily with θ. The range in each case is about ten orders of magnitude. There is a small temperature effect due to the viscosity. The vapor conductivity becomes dominant in the silt loam around $\theta = 0.10$ and in the sand around $\theta = 0.02$.

The diffusion coefficient for vapor transport due to temperature gradients is

$$D_{Tv} = \rho_\ell^{-1} D_a f \zeta \left.\frac{\partial \rho_v}{\partial T}\right|_\psi \qquad (2.29)$$

where (de Vries, 1958)

$$f = \begin{cases} n & \theta \leq \theta_k \\ \theta_a + \dfrac{\theta_a}{n-\theta_k}\,\theta & \theta_k < \theta \end{cases} \qquad (2.30)$$

in which θ_k is the moisture content at which liquid flow becomes negligible ($D_{\psi v}$ is an order of magnitude greater than K). This is estimated for both soils at 20°C from Figure 2.5. The values are given in Table 2.2. The parameter ζ is the ratio of the average temperature gradient in

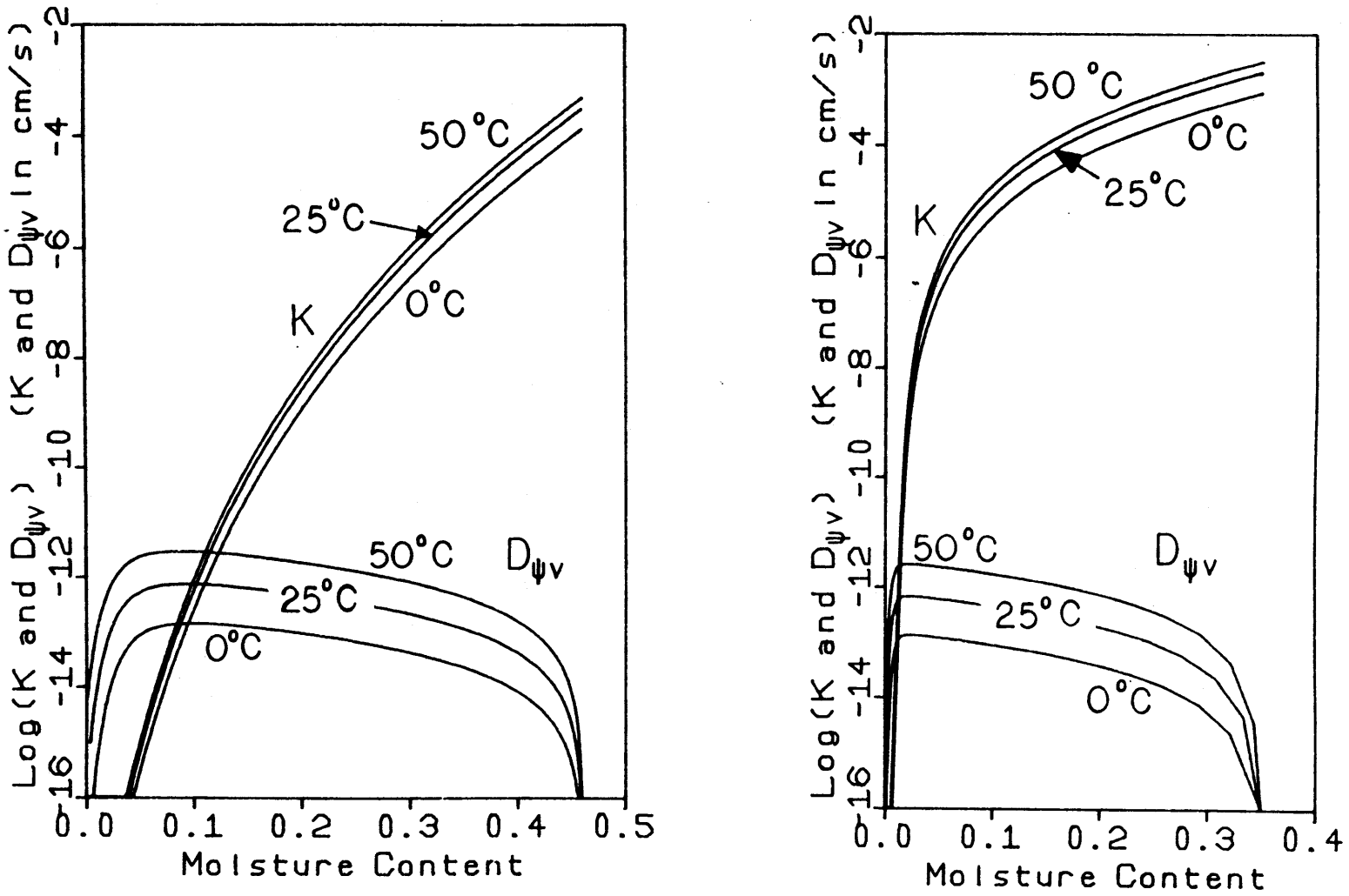

Figure 2.5

LIQUID HYDRAULIC CONDUCTIVITY, K, AND VAPOR CONDUCTIVITY, $D_{\psi v}$, AS FUNCTIONS OF θ AND T. Left: SILT LOAM. Right: SAND.

the air to the overall average (i.e., macroscopic) temperature gradient,

$$\zeta = \frac{(\nabla T)_a}{\nabla T} \tag{2.31}$$

This thermal gradient ratio is a function of the moisture content and the temperature. Its calculation is detailed in Section 2.3.4.4, in the discussion of the effective thermal conductivity. Figure 2.6 contains plots of D_{Tv}. We see that D_{Tv} is fairly sensitive to temperature and insensitive to θ, except near total dryness and saturation.

2.3.4.3 Parameters relating to heat storage

The volumetric heat capacity of a soil is a weighted average of the capacities of its components (de Vries, 1966),

$$C = \sum_{i=1}^{5} C_i \theta_i \tag{2.32}$$

where θ_i and C_i are the volumetric fraction and the volumetric heat capacity of the i'th soil constituent. The five components are (1) water, (2) air, (3) quartz particles, (4) other minerals, and (5) organic matter. The heat capacities suggested by de Vries (1966) are listed in Table 2.3. Reasonable volumetric fractions for a silt loam and a clean quartz sand are given in Table 2.2. The silt loam figures are based on those of Buckman and Brady (1969, p. 10) and

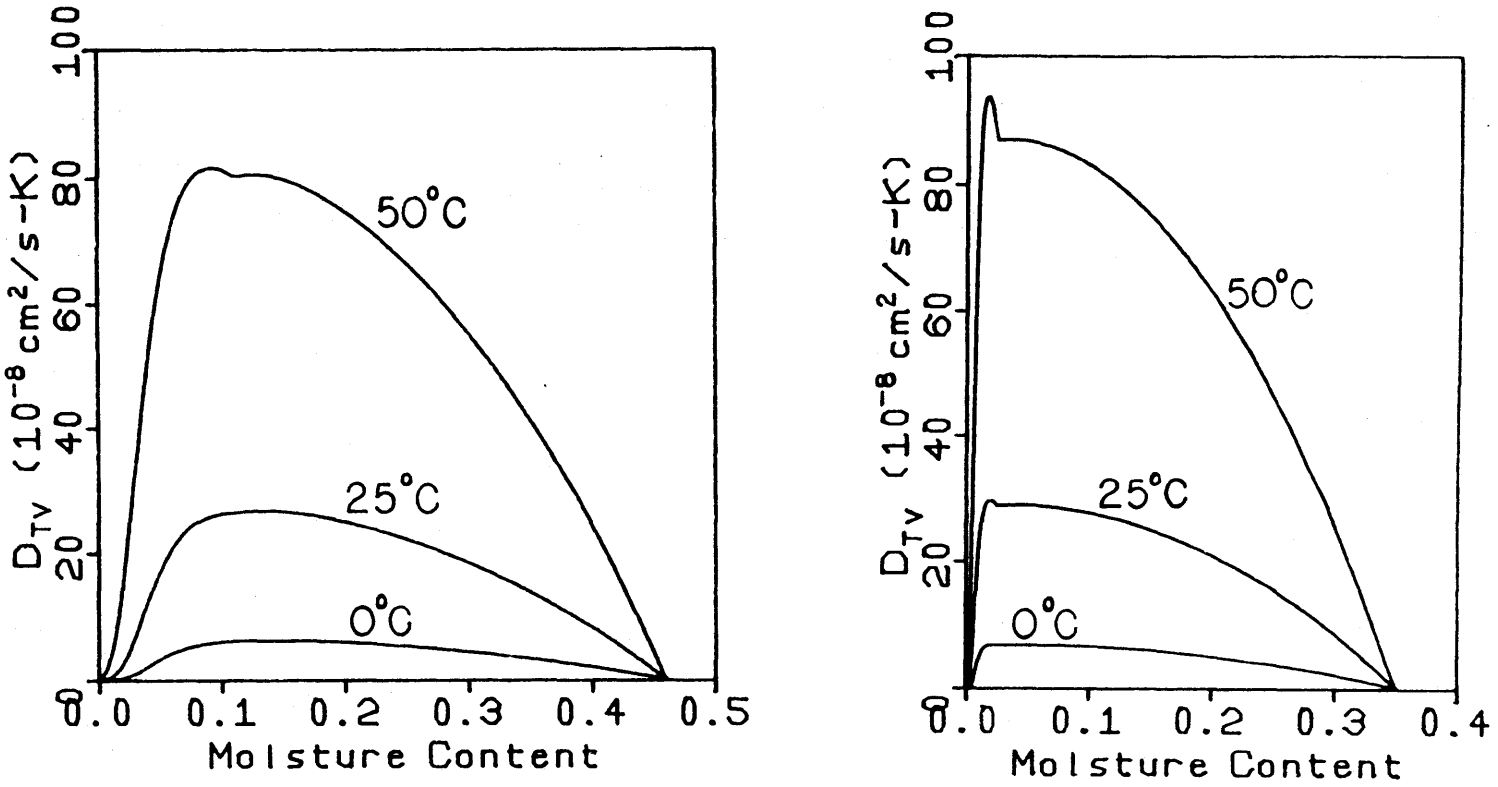

Figure 2.6

DIFFUSION COEFFICIENT OF VAPOR FLOW (D_{Tv}) DUE TO TEMPERATURE GRADIENTS.
Left: SILT LOAM. Right: SAND.

Constituent	i	C_i	λ_i	g_i
liquid water	1	1.0	1.37×10^{-3}	-
air	2	3×10^{-4}	$6 \times 10^{-5} + LD_a \left.\frac{\partial \rho_v}{\partial T}\right\|_\psi$	see text
quartz	3	0.46	2.1×10^{-2}	0.125
other minerals	4	0.46	7×10^{-3}	0.125
org. matter	5	0.6	6×10^{-4}	0.5

Table 2.3

PROPERTIES OF SOIL CONSTITUENTS.

C_i IN cal cm^{-3} $°K^{-1}$, λ_i IN cal cm^{-1} s^{-1} $°K^{-1}$.

Wierenga et al. (1969), adjusted for the porosity of our soil. The sand is assumed to contain only quartz.

The heat of wetting, W, is given by Groenevelt and Kay (1974) as

$$W = \frac{H_w}{\rho_\ell j \delta} \; -\xi/\delta \qquad (2.33)$$

where ξ is the water film thickness on the soil particles and the conversion factor j is 4.18×10^7 erg cal^{-1}. Values of H_w and δ are 10^3erg cm^{-2} and 10^{-7} cm, respectively. We can approximate ξ by θ/S, where S is specific surface, because

$$\xi = \text{film thickness} = \frac{\text{volume of water per unit bulk volume}}{\text{surface area per unit bulk volume}} \qquad (2.34)$$

Then (2.33) becomes

$$W = \frac{H_w}{\rho_\ell j \delta} \; e^{-\theta/\delta S} \qquad (2.35)$$

Values of S are given in Table 2.2.

2.3.4.4 Parameters relating to heat transport

The effective thermal conductivity of a moist soil is given by de Vries (1966) as

$$\lambda = \frac{\sum_{i=1}^{5} k_i \theta_i \lambda_i}{\sum_{i=1}^{5} k_i \theta_i} \qquad (2.36)$$

where λ_i is the thermal conductivity of the i'th constituent (Table 2.3), and k_i is the ratio of the average temperature gradient in the i'th constituent to the average temperature gradient of the bulk medium. A conceptual model yields

$$k_i = \frac{2}{3}\left[1 + \left(\frac{\lambda_i}{\lambda_1} - 1\right)g_i\right]^{-1} + \frac{1}{3}\left[1 + \left(\frac{\lambda_i}{\lambda_1} - 1\right)(1 - 2g_i)\right]^{-1} \tag{2.37}$$

where the liquid phase is considered continuous and g_i is the "shape factor" of the i'th constituent. For the solid particles, constant values as given in Table 2.2 are assumed. No value is needed for g_1, since its coefficient is zero. The value of g_2 is considered a function of moisture content as follows (Kimball et al., 1976):

$$g_2 = \begin{cases} .013 + \left(\dfrac{.022}{\theta_w(pF=4.2)} + \dfrac{.298}{n}\right)\theta & \theta < \theta_w(pF=4.2) \\ .035 + \dfrac{.298}{n}\,\theta & \theta_w(pF=4.2) < \theta \end{cases} \tag{2.38}$$

The effective thermal conductivity of the air-filled pores, enhanced by vapor distillation (de Vries, 1958), is given by

$$\lambda_2 = \lambda_a + D_a L \left.\frac{\partial \rho_v}{\partial T}\right|_\psi \tag{2.39}$$

where λ_a is the conductivity of the dry air alone.

Values of λ obtained using this model are good down to a moisture content approximately equal to θ_k, at

which the theory breaks down due to loss of continuity in the liquid phase. At total dryness, the same theory may be applied by substituting λ_2 for λ_1 in (2.37), i.e., by taking air as the continuous phase. In this case, a correction factor for λ of 1.25 is required. Between $\theta = 0$ and $\theta = \theta_k$, values of λ are usually estimated by an interpolation scheme. In our scheme, we first evaluate λ at θ_k in the usual manner, except that we use $\lambda_2 = \lambda_2(\theta) \neq \lambda_2(\theta_k)$ as given by (2.39), and then we use the known value of λ for $\theta = 0$ to find λ at θ by means of linear interpolation. This scheme happens to be convenient computationally and produces a more realistic $\lambda(\theta)$ curve than simple linear interpolation.

The computed thermal conductivity functions for our two soils are plotted in Figure 2.7. All curves are qualitatively similar, reflecting the rapid increase of λ with θ near dryness that results when contacts between soil grains - the bottlenecks of heat flow - are bridged by added moisture. The rate of increase in efficiency of heat conduction with θ decreases significantly once these gaps are closed. There is a moderate influence of temperature, which enters through (2.39). The thermal conductivity of the sand is roughly twice that of the silt loam at a given saturation.

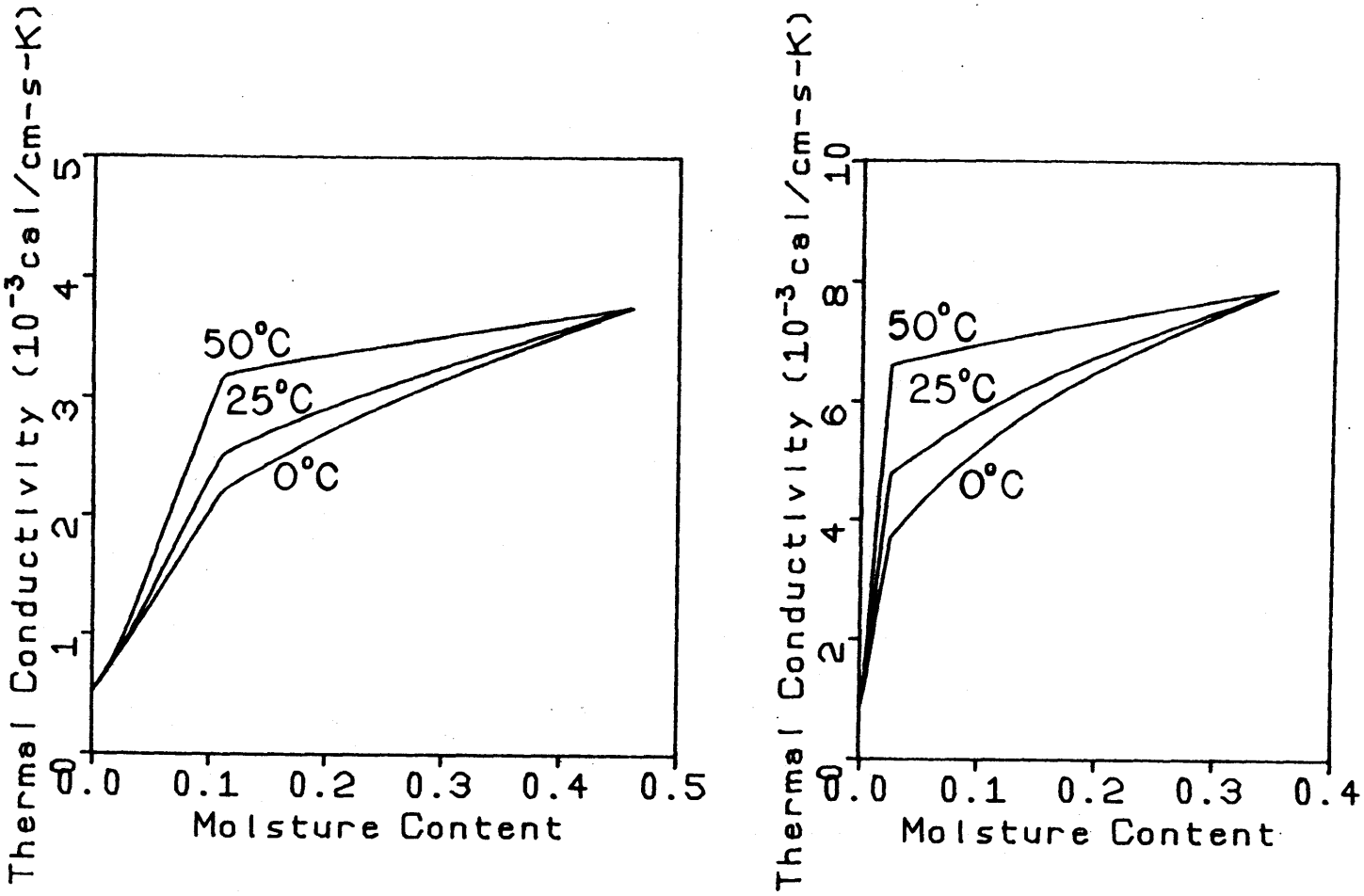

Figure 2.7

EFFECTIVE THERMAL CONDUCTIVITY AS A FUNCTION OF θ AND T.
Left: SILT LOAM. Right: SAND.

Given the ratios k_i, we may now compute ζ in (2.29) and (2.31). Calculating the bulk thermal gradient as the volumetrically weighted average of the gradients in the various soil components, we obtain (Philip & de Vries, 1957)

$$\zeta = \frac{(\nabla T)_a}{\sum_{i=1}^{5} (\nabla T)_i \, \theta_i} \tag{2.40}$$

where $(\nabla T)_a$ is the thermal gradient in the air and $(\nabla T)_i$ is the thermal gradient in the i'th constituent. Applying the definition of the k_i's, we transform this to

$$\zeta = \frac{k_2}{\sum k_i \theta_i} \tag{2.41}$$

This value of ζ is valid for θ down to θ_k. For $\theta = 0$, ζ may be calculated using air as the continuous phase, and ζ may be interpolated for θ between 0 and θ_k using the scheme discussed earlier.

2.3.4.5 Soil surface and deep soil parameters

In Sections 2.3.4.1 through 2.3.4.4, we have specified the variables in the partial differential equations as functions of state, defining the necessary soil parameters and assigning typical values to them. Here we treat the additional variables and parameters that arise in the boundary conditions. These are h_{max}, A, ε, and Z_B.

The maximum ponding depth h_{max} represents the sum of the storage capacity of surface depressions and the detention of surface runoff in transit. We shall assign it a value of 0.5 cm for both soil types.

The bare soil albedo, A, is known to be very sensitive to the surface moisture content. There is also a small dependence on the solar zenith angle, which we shall ignore. Sellers (1965) and Eagleson (1970) give data for wet and dry, sand and non-sand soils. The dry soil always has the higher albedo. The variation of A with moisture content was analyzed by Idso et al. (1975) for Avondale loam. They discovered a perfectly linear decrease of A for θ from 0 to about .20 and relatively little decrease for wetter soil. We shall assume a linear variation of albedo from the dry value to the wet value at half-saturation of the soil and above,

$$A = \begin{cases} A_d + (A_w - A_d)\,\dfrac{2\theta}{n} & 2\theta < n \\ A_w & 2\theta > n \end{cases} \qquad (2.42)$$

The wet (w) and dry (d) values, estimated for our hypothetical silt loam and sand from the sources mentioned above, are listed in Table 2.2.

Sellers (1965) suggests that the emissivity of a soil surface decreases slightly from wet to dry conditions. We shall employ a linear dependence on θ between dryness and full saturation, with $\varepsilon_d = 0.9$ and $\varepsilon_w = 0.95$,

independent of soil type.

The depth of the lower boundary of the soil system represented explicitly by the reference model will be assigned a nominal value of 5 meters. This value is sufficiently deep to be beyond the range of diurnal temperature variations and is probably usually greater than the depth of penetration of the storm/interstorm moisture waves.

Table 2.2 summarizes the parameter values for the two soils. Of the sixteen listed, twelve are independent, given the assumptions discussed in the previous sections. The value θ_u is a fixed fraction of n, and one of the five parameters of the main wetting curve is determined by the other four and by the condition that $\theta = 0$ at pF = 7. The parameter θ_5 is porosity minus θ_3 and θ_4. The θ_k value is estimated as described in Section 2.3.4.2. Further considerations could be applied to reduce the parameter set farther.

2.4 The Parameterization of Fluxes in the Surface Boundary Layer

As illustrated in Figure 2.2, we shall express the evaporation rate, E, and the atmospheric sensible heat flux, H, in terms of T_a, T_g, ρ_{va}, ρ_{vg}, and u_a. In order to do this, we borrow the relations used by Anderson (1976), which in turn are based heavily on Deardorff's (1968) application of the similarity theory of Monin and Obukhov

(1954).

The transfers of momentum, heat, and water in the atmospheric surface boundary layer (SBL) are given by

$$\tau = \rho_a C_M u_a^2 \tag{2.43}$$

$$H = -\rho_a c_p C_H u_a (T_a - T_g) \tag{2.44}$$

$$\rho_\ell E = - C_W u_a (\rho_{va} - \rho_{vg}) \tag{2.45}$$

where τ is the shear stress, ρ_a is the density of air, and C_M, C_H and C_W are bulk transfer coefficients.

Under conditions of <u>neutral stability</u>, these coefficients are given by

$$(C_M)_N = (C_H)_N = (C_W)_N = \frac{k^2}{(\ell n \frac{z_a}{z_o})^2} \tag{2.46}$$

where the N subscript denotes neutral conditions, k is von Karman's constant (=0.4), z_a is the screen height, and z_o is the surface roughness length.

Under <u>unstable</u> conditions, the bulk transfer coefficients are related to their neutral values through

$$\frac{C_M}{(C_M)_N} = \left\{ 1 - \frac{(C_M)_N^{1/2}}{k} \left[\ell n \left(\frac{1+x^2}{2} \right) + 2 \ell n \left(\frac{1+x}{2} \right) - 2 \tan^{-1}(x) + \frac{\pi}{2} \right] \right\}^{-2} \tag{2.47}$$

and

$$\frac{C_H}{(C_H)_N} = \frac{C_W}{(C_W)_N} = \left[\frac{C_M}{(C_M)_N}\right]^{1/2}\left[1 - \frac{2}{k}(C_M)_N^{1/2}\ \ell n\left(\frac{1+x^2}{2}\right)\right]^{-1} \tag{2.48}$$

in which x is a function of stability,

$$x = (1 - 16\ z_a/L)^{1/4} \tag{2.49}$$

where L is the Monin-Obukhov length. It is related to the bulk Richardson number,

$$(Ri)_B \equiv \frac{2g\ z_a(T_a - T_g)}{(T_a + T_g)\ u_a^2} \tag{2.50}$$

by the expression

$$\frac{z_a}{L} = \frac{k\ \dfrac{C_H}{(C_M)_N}}{(C_M)_N^{1/2}\left[\dfrac{C_M}{(C_M)_N}\right]^{3/2}}\ (Ri)_B \tag{2.51}$$

Knowing $(C_M)_N$ and $(Ri)_B$, we can solve (2.47), (2.48), (2.49) and (2.51) for C_M and $C_H = C_W$.

For <u>stable</u> conditions, assuming equality of the stability functions,

$$\frac{C_M}{(C_M)_N} = \frac{C_H}{(C_H)_N} = \frac{C_W}{(C_W)_N} = \begin{cases} \left(1 - \dfrac{(Ri)_B}{Ri_{cr}}\right)^2, & (Ri)_B < Ri_{cr} \\ 0, & (Ri)_B \geq Ri_{cr} \end{cases} \tag{2.52}$$

where Ri_{cr} is the critical Richardson number, above which there is no turbulence. We employ the value $Ri_{cr} = 0.2$.

In all of our simulations, we shall take z_a = 200 cm. Oke (1978) gives z_o for soils in the range 0.1 to 1 cm and for "desert" as 0.03 cm. Van Bavel (1966) gives 0.02 cm for a wet soil. We shall employ a fixed value of z_o = 0.1 cm for all computations. From (2.46), we then obtain

$$(C_M)_N = (C_H)_N = (C_W)_N = 0.00277 \qquad (2.53)$$

2.5 Deterministic Sequences of Atmospheric Forcing

As depicted in Figure 2.2 and demonstrated in the last two sections, the soil/SBL system is forced by six atmospheric variables - I_s, $I_{\ell d}$, P, T_a, u_a and ρ_{va}. In this work, these inputs are provided in two ways. The first is by defining a deterministic and periodic structure for these time series and fixing the parameters for two characteristic weather patterns - a relatively cool, moist one and a hot, arid one. This class of sequences is documented here. The parameters for the two deterministic patterns are nominal ones based on the data for a particular month of the year at each of two sites in the U.S. - the month of May at Dulles International Airport in northern Virginia and the month of July at the Municipal Airport in Winslow,

Arizona. Data is available in the "Local Climatological Data" and other publications of the Environmental Science Services Administration - Environmental Data Service of the U.S. Department of Commerce.

The random sequences are hourly interpolations of the 3-hourly meteorological data for Winslow in July 1968 and for Dulles in May 1972. These data are available as "Local Climatological Data." Average rainfall intensity is available there on an hourly basis for Winslow and 6-hourly for Dulles.

2.5.1 Reduction to Primary Forcing Variables

Of the six input variables, we shall express two - the radiation terms - as functions of fixed climatic parameters and the other four variables. The sequences of the other four variables will then be defined.

The intensity of shortwave radiation reaching the soil surface is given by (Eagleson, 1970; Curtis, 1982)

$$I_s = \begin{cases} W_{BO} \sin\alpha \, e^{-n' a_1 m}(1 - 0.65N^2) & \sin\alpha > 0 \\ 0 & \sin\alpha \leq 0 \end{cases} \qquad (2.54)$$

where W_{BO} is the solar constant (2 cal cm^{-2} min^{-1}), α is the angle of the sun above the horizon, a_1 is the molecular scattering coefficient, n' is a turbidity factor, m is the relative thickness of the atmosphere through which the light

travels, and N is the proportion of sky covered by clouds. The angle α can be expressed as

$$\sin \alpha = \sin \delta' \sin \phi + \cos \delta \cos \phi \cos\left[\frac{\pi}{12} (t - 12)\right] \quad (2.55)$$

where δ' is the solar declination, ϕ is latitude, and t is time in hours since midnight. The molecular scattering coefficient is

$$a_1 = 0.128 - 0.054 \log m \quad (2.56)$$

and

$$m = (\sin \alpha)^{-1} \quad (2.57)$$

Climate parameters for Dulles and Winslow are listed in Table 2.4. At Dulles the annual mean temperature, $\overline{T}$, is 12.1°C and the annual mean precipitation rate, $\overline{P}$, is 102 cm yr^{-1}. For Winslow, $\overline{T}$ = 12.9°C and $\overline{P}$ = 9.3 cm yr^{-1}. Dulles is located at about 39°N latitude and Winslow at 35°N. According to Eagleson (1970), values of the turbidity factor ordinarily range from 2 for clear mountain air to 4 to 5 for smoggy urban areas. We assign values of 2.5 at Winslow and 3.5 at Dulles. The solar declination averages about 19° in May and 21.5° in July.

The cloud cover ratio, N, required for use in (2.54), is taken as

Parameter	Dulles/May	Winslow/July
$\bar{T}$	12.1°C	12.9°C
$\bar{P}$	102 cm yr^{-1}	18.6 cm yr^{-1}
ϕ	38° 57'	35° 01'
δ'	19° 0'	21° 30'
n'	3.5	2.5
N_o	0.50	0.45
t_b	57 hours	94 hours
t_r	15 hours	2 hours
t_i	22 hours	20 hours
i	0.061 cm hr^{-1}	0.193 cm hr^{-1}
F(•)	SEE TEXT	
T_m	16.7°C	25.8°C
T_{di}	5.6°C	7.8°C
t_T	14.5 hours	15 hours
U_m	360 cm s^{-1}	360 cm s^{-1}
U_{di}	100 cm s^{-1}	180 cm s^{-1}
t_u	13 hours	18.5 hours
ρ_{va}	10^{-5} g cm^{-3}	7×10^{-6} g cm^{-3}

Table 2.4

REPRESENTATIVE VALUES OF THE FORCING PARAMETERS

FOR DULLES IN MAY AND WINSLOW IN JULY

$$N = \begin{cases} N_o & P = 0 \\ 1 & P > 0 \end{cases} \qquad (2.58)$$

i.e., total cover during rain events and a constant fair-weather value in between. Values of N_o for Dulles in May and Winslow in July, chosen to make the average cloudiness over the month equal its observed value, are 0.50 and 0.45, respectively.

The atmospheric longwave radiation incident upon the surface, $I_{\ell d}$, is expressed as (Curtis, 1982)

$$I_{\ell d} = \varepsilon_a \, \sigma(T_a + 273)^4 \, (1 + 0.17N^2) \qquad (2.59)$$

where the atmospheric emissivity is

$$\varepsilon_a = 9.37 \times 10^{-5} \, (T_a + 273)^2 \qquad (2.60)$$

By means of (2.54) through (2.60), we have reduced the variations of I_s and $I_{\ell d}$ to variations of P and T_a, which are two of our primary forcing variables.

2.5.2 Sequences of Primary Forcing Variables

We express the primary forcing variables as simple periodic functions of time. The period of P is the storm inter-arrival time, and the period of T_a and u_a is one day. The vapor density has a relatively small diurnal variation component and is thus considered constant here.

The precipitation rate is given by

$$P = \begin{cases} 0 & t_i - t_b + k(t_b + t_r) < t < t_i + k(t_b + t_r) \\ iF\left[\frac{t - t_i - k(t_b + t_r)}{t_r}\right] & t_i + k(t_b + t_r) < t < t_i + k(t_b + t_r) + t_r \end{cases} \tag{2.61}$$

where F gives the normalized storm intensity as a function of normalized time, i representing the average intensity of the entire storm, t_b the time between storms, t_r the storm duration, t_i the starting time of the first storm, and k is any integer. The average storm intensity is computed as the average storm depth divided by the average storm duration.

Values of the various parameters in (2.61) appear in Table 2.4. For Winslow, t_i is set as 20 hours and $t_r + t_b$ is made an integral number of days in order to reproduce the typical occurrence of rain in the evening. The estimates of t_b and t_r for Dulles are based on 6-hourly, rather than hourly, records, so they may be somewhat too large.

The function $F(\tau)$ is constant at unity for Winslow. For Dulles, it is

$$F(\tau) = \begin{cases} 0.25 & 0 < \tau < .4 \\ 2.0 & .4 < \tau < .8 \\ 0.5 & .8 < \tau < 1 \end{cases} \tag{2.62}$$

These hypothesized forms, the second taken from Eagleson and Shack (1966), appear generally consistent with the

observed data. For any given storm, of course, the temporal intensity variations are not so smooth. The large fluctuations in intensity that occur over relatively short time periods may be important for surface runoff production.

Monthly averages of the 3-hourly, diurnally-varying temperature and windspeed at each site are fitted to cosine curves,

$$T_a = T_m + T_{di} \cos \left[\frac{\pi}{12} (t - t_T) \right] \qquad (2.63)$$

$$u_a = u_m + u_{di} \cos \left[\frac{\pi}{12} (t - t_u) \right] \qquad (2.64)$$

where t_T and t_u are times in hours of the day at which T_a and u_a achieve their maxima. For both stations (Table 2.4), these occur between noon and early evening.

Values of ρ_{va}, assumed constant, are listed in Table 2.4.

Chapter 3

EXPERIMENTS WITH THE REFERENCE MODEL

3.1 Model Convergence

3.1.1 Introduction

The reference model equations are solved by means of a numerical (finite element) algorithm called SPLaSHWaTr (Simulation Program for Land Surface Heat and Water Transport), which is described elsewhere (Milly and Eagleson, 1980; Milly, 1982). Convergence is the uniform approach of the SPLaSHWaTr solution to the exact solution that results from successive refinement of the computational grid in space and time. The discretization in space and time is controlled by four parameters. In this section, we shall examine the sensitivity of the computed solutions to these parameters, determining the most economical set that will yield sufficient accuracy for our purposes.

Two parameters specify the spatial discretization. The first of these is NL, the number of elements. The second parameter, ZRAT, quantifies the concentration of the node points near the land surface. It is defined by

$$ZRAT = \frac{NL \cdot (\Delta Z)_o}{Z_B} \qquad (3.1)$$

where $(\Delta Z)_o$ is the length of the top element in the column and Z_B is the total column length. For ZRAT = 1, the top

element thus has length Z_B/NL. Smaller values of ZRAT indicate smaller elements near the surface. Given the values of NL and ZRAT, the node coordinates are calculated by a procedure that spaces them in a logarithmic fashion. Sample grids are shown in Figure 3.1.

The other two discretization parameters are employed in the specification of the time step duration. At the end of each time step, an upper limit on the new time step duration is computed by

$$\Delta t \leq \min \left[\frac{XERR}{\max_i \left| \frac{d\theta_i}{dt} \right|} , \frac{TERR}{\max_i \left| \frac{dT_i}{dt} \right|} \right] \qquad (3.2)$$

where θ_i and T_i denote moisture content and temperature at node i. The derivatives are estimated from the previous time step. Equation (3.2) says that the anticipated change in moisture content during the next time step shall not exceed XERR at any node. Similarly, TERR is the maximum allowable change in temperature.

The most accurate solutions would use large NL, small XERR and TERR, and, as we shall see, ZRAT considerably less than unity. On the other hand, the least expensive solutions would minimize NL and maximize XERR and TERR. In the following sections, we analyze this tradeoff for each of the four combinations of the two soils and the two forcing sequences described in Chapter 2.

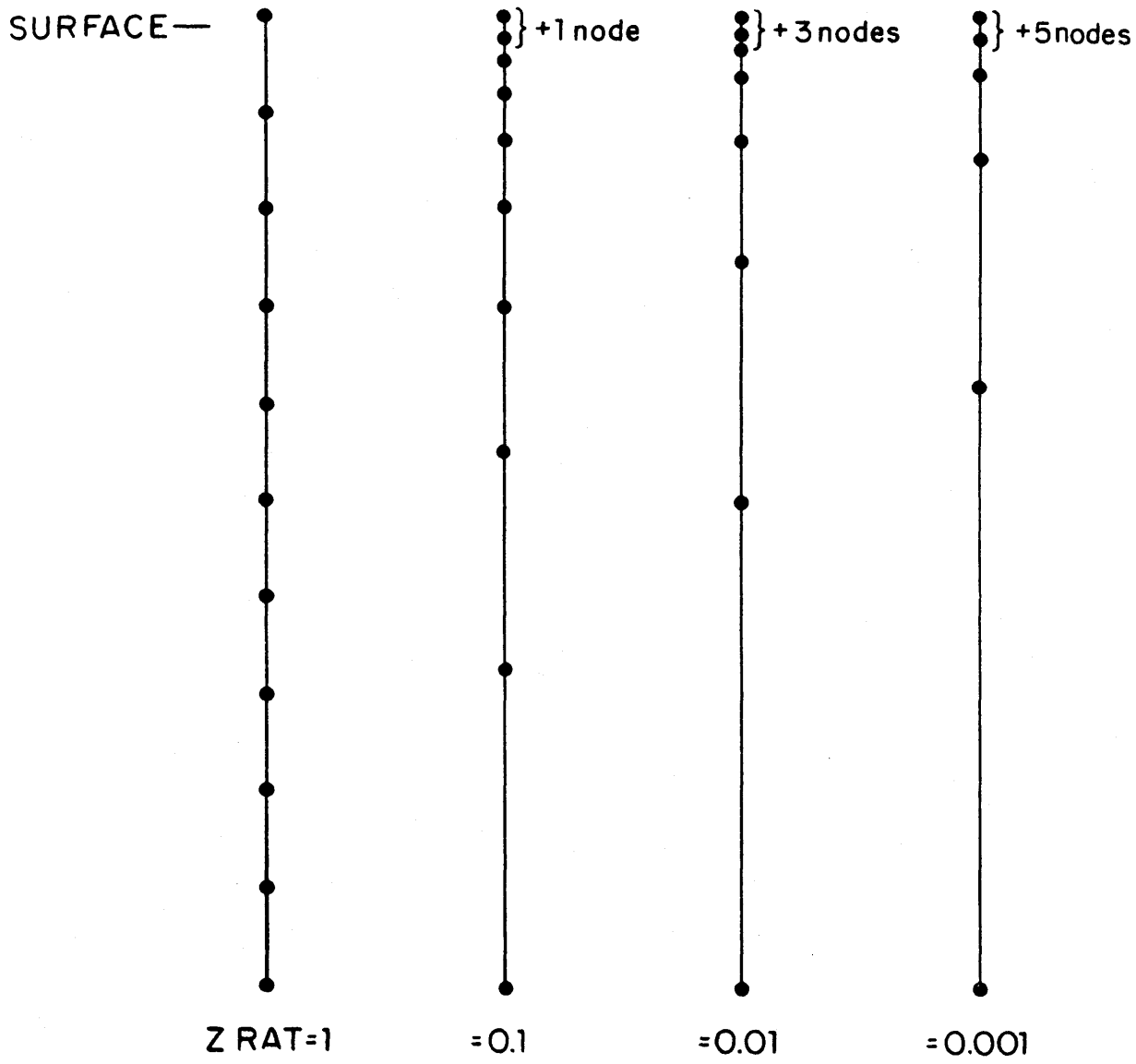

Figure 3.1

EXAMPLES OF SPATIAL DISCRETIZATION WITH TEN ELEMENTS.
THE NUMBER OF NODES NOT PLOTTED NEAR THE TOP IS INDICATED.

3.1.2 Spatial Discretization Parameters

We vary both NL (=5, 10, 20, 40) and ZRAT (=1, .1, .01, .001) in search of an optimal pair. The time step parameters are kept at very small values (XERR = 0.0005, TERR = 0.1). These values were determined to be more than sufficient for convergence in preliminary simulations.

Given that there are four different physical problems, each to be simulated with 16 different combinations of NL and ZRAT, it is desirable to isolate only a few critical pieces of the solution on which to base the convergence analysis. We shall employ the total changes in stored (1) water and (2) heat that are calculated (1) between the start of the simulation (t=0) and the first rainfall (t=20 hours at both Dulles and Winslow) and (2) from the start of the rainfall until shortly after it ends (t=36 hours for Dulles and t=24 hours for Winslow). The first time span is essentially one of storage depletion by evaporation while the second is one of recharge by infiltration. More detailed analyses of the fluxes and states of the system verified that these storage changes are sufficient indicators of convergence.

Table 3.1 summarizes the results for a sand with Winslow forcing. As an indicator of relative computational effort, the execution time is given for each simulation. The first column of results from Table 3.1 is plotted in

NL	ZRAT	MASS STORAGE CHANGE (cm) t=0 to t=24 hr	MASS STORAGE CHANGE (cm) t=20 to t=24 hr	HEAT STORAGE CHANGE $_2$ (cal/cm^2) t=0 to t=20 hr	HEAT STORAGE CHANGE $_2$ (cal/cm^2) t=20 to t=24 hr	EXECUTION TIME (min.)
5	1	-.774	.231	-68.4	-64.	0.9
5	0.1	-.526	.254	- 2.7	-42.9	1.9
5	0.01	-.402	.245	32.2	-50.7	2.9
5	0.001	-.486	.233	29.6	-61.4	2.6
10	1	-.753	.256	-54.2	-42.1	2.2
10	0.1	-.448	.252	16.4	-45.3	4.8
10	0.01	-.378	.245	37.0	-50.1	5.9
10	0.001	-.386	.244	36.9	-50.9	6.2
20	1	-.613	.250	-20.8	-48.2	5.4
20	0.1	-.401	.249	28.5	-47.5	10.6
20	0.01	-.366	.245	39.0	-50.2	12.0
20	0.001	-.368	.245	38.9	-50.5	12.5
40	1	-.516	.256	- 3.4	-41.7	13.5
40	0.1	-.379	.248	34.7	-48.8	22.3
40	0.01	-.363	.245	39.3	-50.1	24.5
40	0.001	-.363	.246	39.5	-50.3	25.6

Table 3.1

CONVERGENCE RESULTS WITH RESPECT TO NL

AND ZRAT FOR SAND/WINSLOW

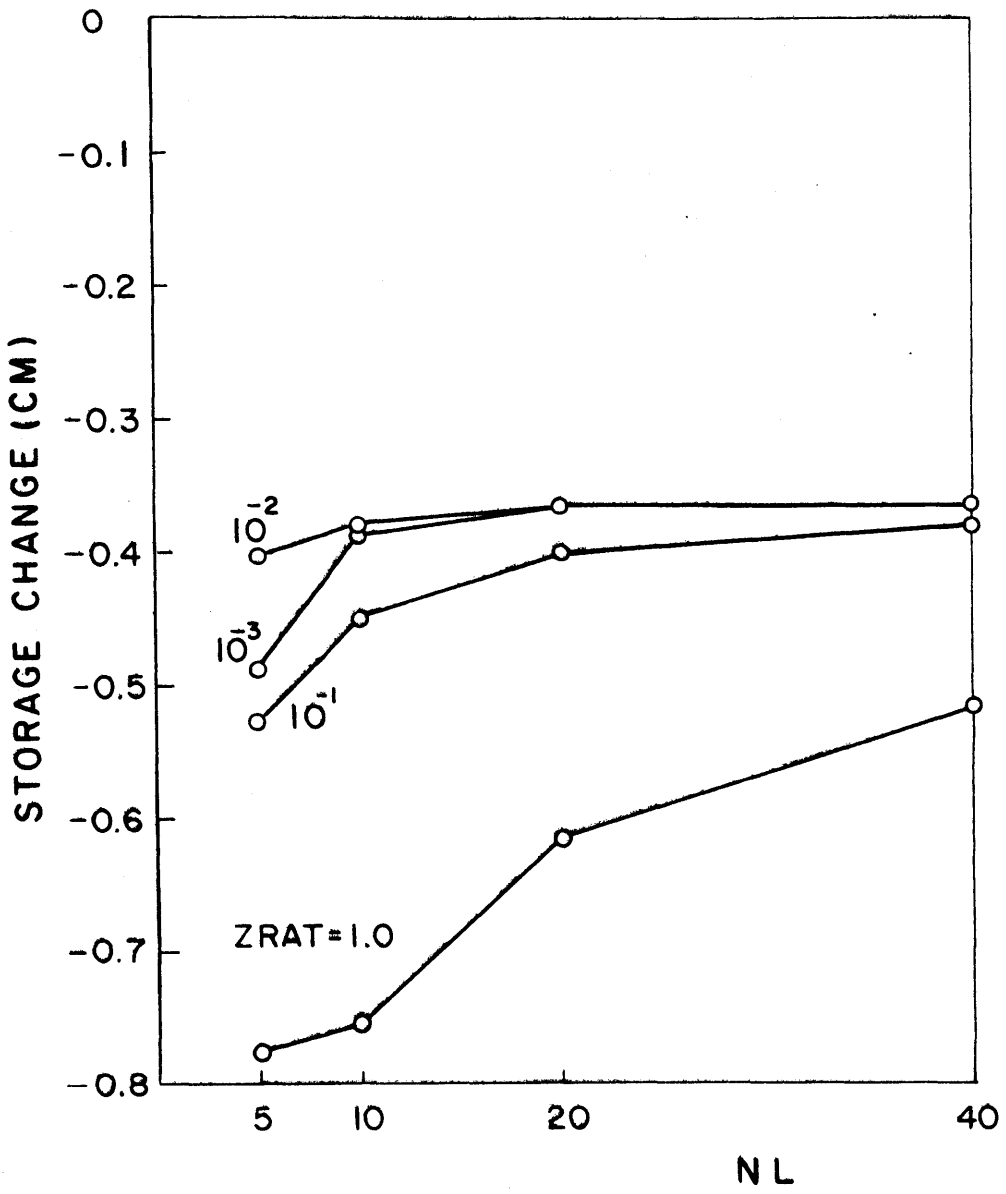

Figure 3.2

CONVERGENCE OF TOTAL STORAGE CHANGE AT t = 20 hr FOR SAND/WINSLOW AS FUNCTION OF NL AND ZRAT

Figure 3.2. From this figure and the other data in the table, several observations can be made. First, for fixed ZRAT, the solution approaches an asymptote uniformly as the number of elements increases. Second, for fixed NL, convergence is more closely approached for the smaller values of ZRAT. In particular, with ZRAT = 1 (which corresponds to constant node spacing), the solution is far from convergence. Third, Table 3.1 shows that convergence of the evaporation results (t=0 to t=20 hr) requires many more elements than does convergence of infiltration (t=20 to t=24 hr). The former requires accurate simulation of the surface temperature, while the latter does not. In fact, since the surface never becomes saturated during this particular rainfall, the infiltration rate is simply equal to the rainfall rate minus relatively small concurrent losses to evaporation.

Figure 3.3 depicts the tradeoff between total CPU time and mass storage change error at t=20 hours for the sand/Winslow example. The storage error is estimated by assuming that the value -.363 cm, achieved with 40 elements and ZRAT = 10^{-2} or 10^{-3}, is exact. At fixed NL, the increased cost of a small ZRAT is more than offset by improved predictions.

Tables 3.2, 3.3, and 3.4 list the corresponding results for the other soil/forcing combinations. The general behavior is similar, but some significant differences are

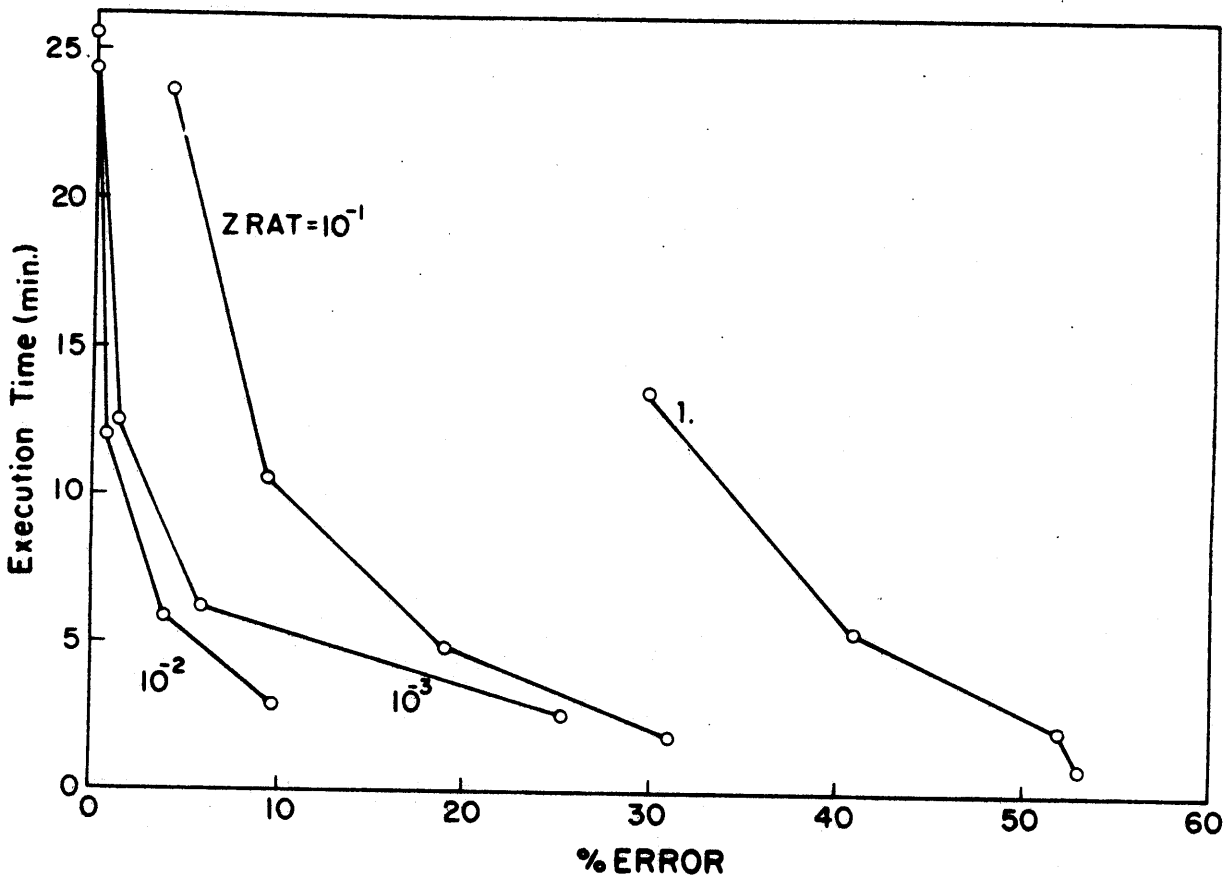

Figure 3.3

TIME-ERROR TRADEOFF CURVES FOR SAND/WINSLOW.

THE ABSCISSA IS NORMALIZED ERROR IN TOTAL MASS CHANGE

AT t = 20 hr.

NL	ZRAT	MASS STORAGE CHANGE (cm) t=0 to t=20 hr	MASS STORAGE CHANGE (cm) t=20 to t=24 hr	HEAT STORAGE CHANGE$_2$ (cal/cm^2) t=0 to t=20 hr	HEAT STORAGE CHANGE$_2$ (cal/cm^2) t=20 to t=24 hr	EXECUTION TIME (min.)
5	1	-.889	.186	-42.8	-101.	0.9
5	0.1	-.905	.271	-40.2	-26.3	2.2
5	0.01	-.812	.259	-19.7	-37.6	4.8
5	0.001	-.716	.250	10.5	-45.3	5.4
10	1	-.926	.241	-64.5	-54.	2.4
10	0.1	-.882	.273	-35.9	-26.1	5.9
10	0.01	-.669	.254	10.2	-42.1	10.7
10	0.001	-.638	.251	15.8	-44.7	12.8
20	1	-.928	.270	-58.7	-27.6	6.2
20	0.1	-.830	.268	-25.7	-29.6	16.3
20	0.01	-.623	.253	17.1	-43.0	22.4
20	0.001	-.616	.252	18.0	-43.5	29.3
40	1	-.912	.274	-44.5	-23.8	14.7
40	0.1	-.749	.261	- 6.6	-36.2	37.9
40	0.01	-.615	.253	18.2	-43.3	47.6
40	0.001	-.607	.252	19.2	-43.6	68.9

Table 3.2

CONVERGENCE RESULTS WITH RESPECT TO NL

AND ZRAT FOR SILT LOAM/WINSLOW

NL	ZRAT	MASS STORAGE CHANGE (cm) t=0 to t=20 hr	MASS STORAGE CHANGE (cm) t=20 to t=24 hr	HEAT STORAGE CHANGE (cal/cm^2) t=0 to t=20 hr	HEAT STORAGE CHANGE (cal/cm^2) t=20 to t=24 hr	EXECUTION TIME (min.)
5	1	-.398	.682	61.7	- 4.6	0.9
5	0.1	-.434	.683	21.8	13.9	1.8
5	0.01	-.432	.682	22.7	13.5	2.2
5	0.001	-.419	.673	33.9	0.8	2.1
10	1	-.434	.703	22.9	32.2	2.3
10	0.1	-.435	.681	20.8	12.2	3.9
10	0.01	-.434	.681	21.5	11.2	4.5
10	0.001	-.433	.681	22.1	11.2	4.6
20	1	-.441	.696	16.8	27.2	5.4
20	0.1	-.435	.681	20.6	11.6	8.4
20	0.01	-.434	.680	20.8	11.3	9.1
20	0.01	-.434	.680	21.0	11.3	9.2
40	1	-.437	.685	19.3	16.6	12.5
40	0.1	-.435	.681	20.6	11.4	17.5
40	0.01	-.435	.681	20.7	11.3	18.1
40	0.001	-.435	.681	20.7	11.3	18.3

Table 3.3

CONVERGENCE RESULTS WITH RESPECT TO NL

AND ZRAT FOR SAND/DULLES

NL	ZRAT	MASS STORAGE CHANGE (cm) t=0 to t=20 hr	MASS STORAGE CHANGE (cm) t=20 to t=24 hr	HEAT STORAGE CHANGE (cal/cm^2) t=0 to t=20 hr	HEAT STORAGE CHANGE (cal/cm^2) t=20 to t=24 hr	EXECUTION TIME (min.)
5	1	-.411	.615	130.	-41.6	0.8
5	0.1	-.525	.662	31.0	18.3	1.9
5	0.01	-.520	.657	34.1	14.0	2.3
5	0.001	-.504	.645	47.9	0.1	2.2
10	1	-.497	.672	54.7	23.3	2.4
10	0.1	-.526	.657	29.3	14.9	4.0
10	0.01	-.525	.656	30.4	12.7	4.6
10	0.001	-.523	.655	31.7	12.4	4.7
20	1	-.533	.687	25.1	42.6	6.0
20	0.1	-.526	.656	29.1	13.4	8.5
20	0.01	-.526	.656	29.4	12.8	9.3
20	0.001	-.525	.655	29.7	12.7	9.4
40	1	-.532	.669	25.6	26.4	13.4
40	0.1	-.526	.655	29.1	13.0	17.6
40	0.01	-.526	.655	29.2	12.8	18.6
40	0.001	-.526	.655	29.2	12.8	18.7

Table 3.4

CONVERGENCE RESULTS WITH RESPECT TO NL AND ZRAT

FOR SILT LOAM/DULLES

apparent. The silt loam and the sand at Dulles converge rapidly, ten elements being sufficient for fairly accurate predictions. The greater number of elements required at Winslow appears to be due to the necessity there for accurate simulation of the moisture field in addition to the temperature field. Whereas evaporation and heat storage changes at Dulles are governed by energy availability, the evaporative demand at Winslow is so great that the surface dries out and evaporation comes under the control of the soil moisture supply. Accurate simulation of moisture availability apparently requires more elements than for energy supply.

On the basis of the data presented here, we shall use 20 elements and ZRAT = 10^{-2} in the remainder of this report, unless otherwise noted.

3.1.3 Time Discretization Parameters

Using the fixed values of NL and ZRAT determined in the previous section, we vary XERR and TERR, looking for a satisfactory pair. Each problem is run for all combinations of XERR = .0005, .001, .002 with TERR = .1, .3, 1. and of XERR = .002, .004, .008 with TERR = 1., 3., 9.

The results for all four problems with certain pairs of XERR and TERR are summarized in Tables 3.5 through 3.8. The "balance errors" in those tables are the differences between computed net inputs and computed storage

XERR	TERR	MASS (cm) STORAGE CHANGE	MASS (cm) BALANCE ERROR	HEAT (cal/cm^2) STORAGE CHANGE	HEAT (cal/cm^2) BALANCE ERROR	EXECUTION TIME (min.)
.008	9	UNSTABLE				
.004	3	UNSTABLE				
.002	1	-.124	$-9x10^{-4}$	-11.4	$5x10^{-2}$	2.8
.001	.3	-.122	$6x10^{-5}$	-11.3	$3x10^{-2}$	5.4
.0005	.1	-.121	$2x10^{-6}$	-11.2	$1x10^{-2}$	12.0

Table 3.5

CONVERGENCE AND BALANCE DATA AS FUNCTIONS OF XERR AND TERR FOR SAND/WINSLOW. VALUES ARE FOR THE ENTIRE 24-HOUR SIMULATION.

XERR	TERR	MASS (cm) STORAGE CHANGE	MASS (cm) BALANCE ERROR	HEAT (cal/cm^2) STORAGE CHANGE	HEAT (cal/cm^2) BALANCE ERROR	EXECUTION TIME (min.)
.008	9	-.379	$-4x10^{-2}$	-18.1	$2x10^{-1}$	1.8
.004	3	-.371	$-5x10^{-3}$	-25.0	$3x10^{-2}$	2.9
.002	1	-.370	$-3x10^{-4}$	-25.7	$2x10^{-2}$	5.3
.001	.3	-.370	$-2x10^{-5}$	-25.9	$2x10^{-2}$	10.5
.0005	.1	-.370	$-6x10^{-7}$	-25.9	$9x10^{-3}$	21.9

Table 3.6

CONVERGENCE AND BALANCE DATA AS FUNCTIONS OF XERR AND TERR FOR SILT LOAM/WINSLOW. VALUES ARE FOR THE ENTIRE 24-HOUR SIMULATION.

		MASS (cm)		HEAT (cal/cm^2)		
XERR	TERR	STORAGE CHANGE	BALANCE ERROR	STORAGE CHANGE	BALANCE ERROR	EXECUTION TIME (min.)
.008	9	.242	$-2x10^{-2}$	34.8	$4x10^{-1}$	1.2
.004	3	.242	$5x10^{-4}$	31.3	$2x10^{-1}$	1.6
.002	1	.245	$3x10^{-4}$	31.8	$1x10^{-1}$	2.5
.001	.3	.246	$-3x10^{-5}$	32.1	$4x10^{-2}$	4.5
.0005	.9	.246	$-6x10^{-6}$	32.1	$2x10^{-2}$	9.1

Table 3.7

CONVERGENCE AND BALANCE DATA AS FUNCTIONS OF XERR AND TERR FOR SAND/DULLES. VALUES ARE FOR THE ENTIRE 36-HOUR SIMULATION.

		MASS (cm)		HEAT (cal/cm^2)		
XERR	TERR	STORAGE CHANGE	BALANCE ERROR	STORAGE CHANGE	BALANCE ERROR	EXECUTION TIME (min.)
.008	9	.134	$-3x10^{-2}$	46.6	$4x10^{-1}$	1.3
.004	3	.125	$4x10^{-3}$	41.0	$3x10^{-1}$	1.6
.002	1	.129	$1x10^{-3}$	41.9	$2x10^{-1}$	2.4
.001	.3	.129	$1x10^{-4}$	42.1	$8x10^{-2}$	4.4
.0005	.1	.130	$2x10^{-5}$	42.2	$3x10^{-2}$	9.3

Table 3.8

CONVERGENCE AND BALANCE DATA AS FUNCTIONS OF XERR AND TERR FOR SILT LOAM/DULLES. VALUES ARE FOR THE ENTIRE 36-HOUR SIMULATION.

changes. The sensitivity of the computed solution to XERR and TERR is very similar for all the problems. Convergence of storage changes within about 1% is achieved with XERR = 0.002 and TERR = 1.0. Mass and heat balance errors increase with the larger time steps. On the sand/Winslow problem (Table 3.5), the solution was unstable (error grew unbounded) for the larger time step parameters.

On the basis of computational cost, convergence, stability, and balance properties, the values XERR = .002 and TERR = 1. appear to be appropriate ones for use in our applications. They will be employed henceforth unless otherwise noted.

3.2 Identification of Consistent Initial Conditions

For the purpose of the convergence analyses in Section 3.1, we employed initial conditions on moisture that allowed a fixed proportion of the average annual precipitation to drain from the bottom of the soil column. That proportion was arbitrarily chosen to be 20%.

Consider now what happens if, for example, we overestimate the column drainage rate. Then the initial moisture content assigned will be excessive. The system will be in disequilibrium and will approach a long-term equilibrium through net storage losses to evaporation and drainage. Eventually, the soil will become drier, thereby

reducing the sum of average evaporation and drainage losses to the average rate of soil moisture replenishment by rainfall. This equilibration process may require several months.

Given our constraints on computational time and our primary interest in studying the soil moisture dynamics at time scales on the order of days, we shall first need to identify the initial moisture conditions that are consistent with the forcing. Otherwise, our system behavior may be dominated by transient adjustment to atmospheric conditions. Having determined these new initial conditions, we can then re-check the convergence results of Section 3.1.

Figure 3.4 illustrates the transient behavior caused by an inconsistent initial condition. The results of three simulations of the sand with Dulles forcing are presented there. The only difference among the simulations is the initial matric potential, which takes values of -100 (too dry), -70 (about right), and -60 (too wet). In each plot, the vertical line at the bottom identifies the initial condition. Near the surface, alternate precipitation and evaporation periods result in wide fluctuations of moisture content on short time scales. With the dry initial condition, a persistent wetting of the soil at about 1 meter depth is discernible. On the average, the surface is wetter than the initial condition, and this results in diffusion of moisture downward. The opposite effect is seen with the

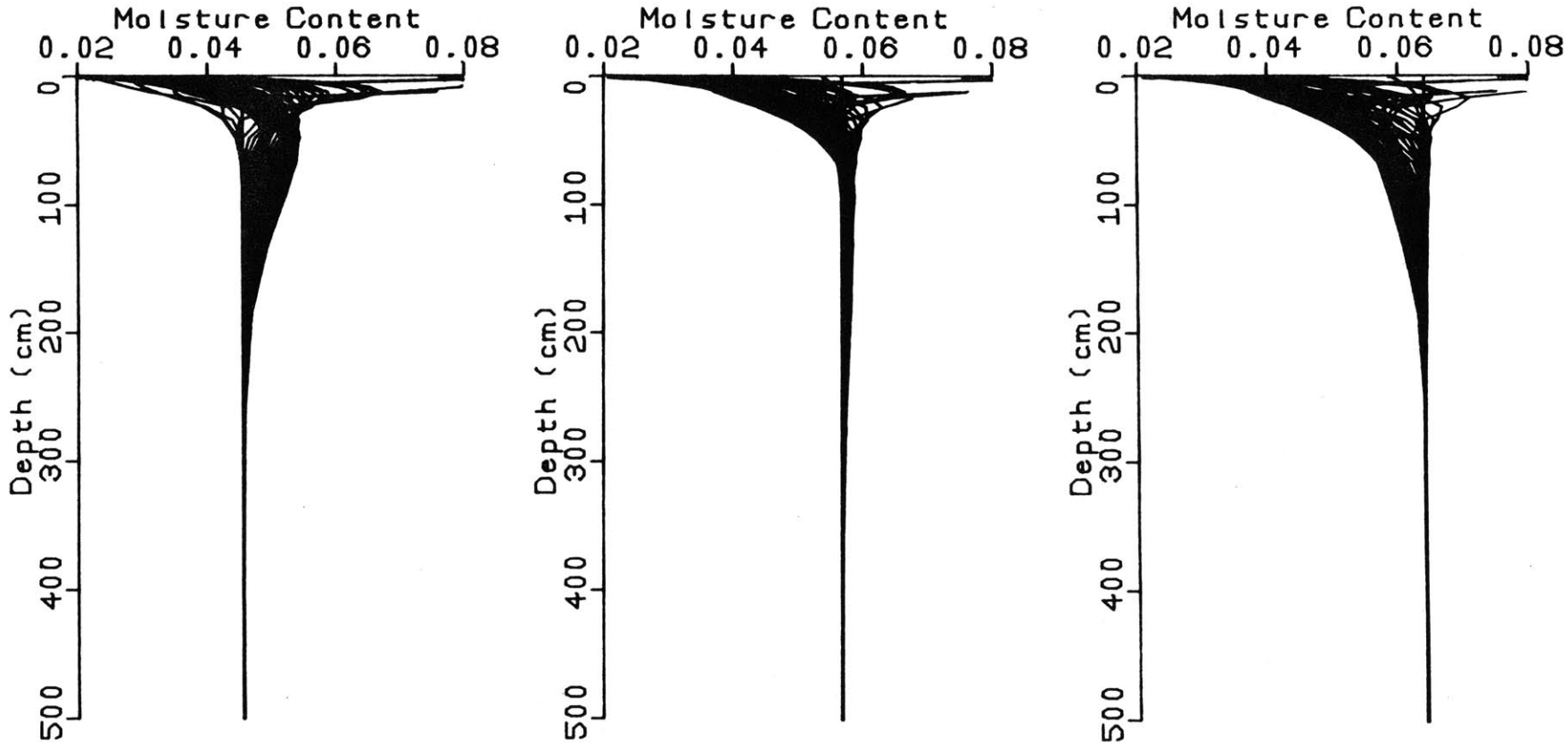

Figure 3.4

THE EFFECT OF INITIAL MOISTURE CONTENT ON DEEP MOISTURE STORAGE. THE DARKENED AREAS ARE THE LOCI OF MOISTURE CONTENTS CALCULATED DURING SIMULATIONS USING INITIAL MATRIC POTENTIALS OF -100 cm (left), -70 cm (center), AND -60 cm (right) FOR THE SAND AT DULLES.

wet initial condition, where total water stored ir the column decreases with time. The equilibrium initial condition shows negligible persistent diffusion of moisture between the surface and deeper levels.

A convenient way to quantify the results presented visually in Figure 3.4 is to tabulate the total water storage changes during a sequence of repeated periods of identical forcing. For the current problem, the period of the forcing is three days (Section 2.5.2). Thus, in Table 3.9 we record these storage changes for several periods and for each of the initial conditions of Figure 3.4. Initial system response displays a transient behavior representing adjustment of the near-surface moisture distribution. After two periods (six days), the storage rates stabilize. For an initial potential of -60 cm, the excess moisture is then lost at a rate of about (.74 cm/3 days) or .25 cm/d. With an excess moisture content of about 0.01 (Figure 3.4) and a total column depth of 500 cm, we can estimate an equilibration time of (0.01x500 cm)/(.25 cm/d) or 20 days. In fact, the required time will be longer, as the rate will decrease with time. The significant magnitude of this storage rate is apparent upon comparison with the rainfa l at Dulles in May, which averages about 0.3 cm/d. An ini ial matric head of -70 cm appears to meet our goal of elimin t-ing long-term storage effects in this example.

Initial Matric Head	Water Storage Change (cm) during Specified 3-day Period					
	1	2	3	4	5	6
-30	-15.0	-8.4	-4.2	*	*	*
-60	-.553	-.300	-.74	*	*	*
-70	-.406	.189	0	-0.14	*	*
-80	-.0805	.1704	.152	.138	.131	.124
-100	.0553	.302	.282	*	*	*

Table 3.9

PERSISTENT DRYING OR WETTING OF THE SAND AT DULLES RESULTING FROM DISEQUILIBRIUM INITIAL CONDITIONS. THE VALUE -70 IS IN APPROXIMATE EQUILIBRIUM, AS EVIDENCED BY THE SMALL STORAGE RATES AFTER THE INITIAL TRANSIENTS.

*Not computed.

An analysis similar to that represented by Figure 3.4 and Table 3.9 was performed for each of the other three simulation scenarios. The intial conditions determined are tabulated in Table 3.10.

Also listed in Table 3.10 are the corresponding moisture contents, the resultant rates of drainage to groundwater, and the calculated values of the Bowen ratio, which is defined by

$$\beta \equiv \frac{H}{LE} \qquad (3.3)$$

the ratio of sensible heat flux to latent heat flux. The tabulated values of β are based on fluxes averaged over one period of forcing, after the initial transient has disappeared. The values for Winslow are reasonable ones for a semi-arid location, where evaporation is almost equal to precipitation. Values for Dulles might be expected to lie between 0.4 and 0.8 (Oke, 1978, p. 59). It is possible that the somewhat excessive evaporation calculated for Dulles is due to the absence in the model of vegetation and its resistance to evapotranspiration.

The validity of the convergence results of Section 3.1 was verified with the new initial conditions by repeating selected simulations.

	Initial Matric Potential	Moisture Content	Drainage Rate	Bowen Ratio
Silt loam/Winslow	-10^6 cm	0.038	0. cm/yr	3.6
Sand/Winslow	-330	0.032	1.9	2.6
Silt loam/Dulles	-500	0.26	4.3	0.11
Sand/Dulles	-70	0.057	51.0	0.23

Table 3.10

EQUILIBRIUM VALUES OF THE INITIAL MATRIC POTENTIAL, WITH ASSOCIATED MOISTURE CONTENTS, DEEP PERCOLATION RATES, AND BOWEN RATIOS.

3.3 Model Simplifications and Their Effects on Surface Fluxes

3.3.1 Introduction

In this section, we analyze the significance of various physical modes of moisture and heat transport and storage. This is done by eliminating some effect in the reference model and comparing the resulting fluxes to those calculated with the effect present. The effects considered are listed below:

1. Heat of wetting
2. Temperature coefficient of matric potential
3. Temperature coefficient of hydraulic conductivity
4. Water vapor
5. Hysteresis

For each effect, a simulation is performed with each of the soil/forcing combinations. The duration of these test simulations is four days. This is approximately the period of the deterministic forcing sequences. Although this may lie entirely within the initial period of transience associated with the specification of a constant initial moisture potential, it was found to be sufficiently long to exhibit any differences that occurred in longer tests. Conclusions will later be checked using longer random forcing sequences.

The philosophy underlying this section is that negligibility of physical effects cannot necessarily be

inferred directly by inspection of the dynamic and diagnostic equations of the system, but that it may be demonstrable through simulation. The former approach is difficult to apply rigorously. For instance, by inspection of the equations, one may conclude that vapor transport effects are negligible when the soil is not too dry. Since a dry boundary layer will often develop at the bare soil surface, even in a humid climate, the qualification that the soil must not be too dry is quite a restriction on generality. The question of interest for many purposes is really the following: "Even given the possibility that a certain mechanism (mathematically, perhaps a term in the equations) may be significant locally at some times, what is its overall impact on the system behavior as evidenced by the sensitivity, say, of system outputs to it?" Through comparative simulations of typical combinations of soil and weather, we may determine the importance of soil vapor to evaporation, for instance.

3.3.2 Heat of Wetting

It can be shown using (2.35) and the data in Table 2.2 that the magnitude of the heat of wetting should almost always be negligible. The possible exception occurs for soils of large specific surface or high clay content when the magnitude of ψ is very large, on the order of its air-dry value.

Table 3.11 gives data on the main components of the surface heat balance for silt loam/Winslow. The latent heat term is essentially proportional to evaporation, so the most important (for our application) and most sensitive term in the water balance is also represented. Mean values from the complete reference model are tabulated, along with values of the mean error and root-mean-square error of the reduction, relative to the reference model. It is apparent that the heat of wetting is negligible, as the results are almost identical. The silt loam at Winslow, which has a large specific surface and a very negative initial matric potential, is the combination that would most likely have been affected by the heat of wetting. This is confirmed by the data for the other combinations, which show mean and RMS errors of less than 0.05 ly/day.

3.3.3 Temperature Coefficient of Matric Potential

Due to the dependence of the $\psi(\theta)$ relation on temperature, matric potential gradients will be affected by the temperature distribution for a given distribution of moisture in the soil. This leads to what may be viewed as thermally-induced liquid flow. By using typical values of the variables, one can show that the magnitude of this flow term may be significant with respect to the isothermal liquid flow component. The question of whether or not the

	Rn	G	H	LE
Reference Mean	285.7	20.8	202.0	62.8
Reduction ME	-0.1	0.0	0.2	0.0
Reduction RMSE	0.3	0.4	0.8	0.5

Table 3.11

EFFECTS ON SIMULATED FLUXES OF THE REDUCTION ELIMINATING THE HEAT OF WETTING. DATA ARE FOR SILT LOAM/WINSLOW. ME = MEAN ERROR, RMSE = ROOT-MEAN-SQUARE ERROR. UNITS ARE ly/day.

net fluxes are significantly altered by this effect remains unanswered by such an analysis, however, as there is the possibility that a compensating reverse flow due to moisture content gradients will be established. Here again we are arguing that local, instantaneous system behavior is not necessarily representative of the global, dynamic system response. We therefore examine the latter to study the importance of the temperature coefficient of matric potential.

The specific reduction made in this section is to set the constant a', defined by (2.16), to zero. Hysteretic moisture retention is then a temperature-independent process. This reduction eliminates the liquid water storage coefficients of temperature in the conservation equations (2.1) and (2.2). In addition, moisture retention calculations are more straightforward without the temperature factor in (2.15).

The results of this reduction are tabulated in Table 3.12. Tabulated means of fluxes and errors are based on the 96 hourly values. In general, the errors of largest absolute magnitude are those associated with evaporation. These values are quite small, however, equalling less than 2% of actual evaporation. The small values of the root-mean-square error (RMSE) indicate that the small mean errors are not merely a result of averaging over the 96 periods. Rather, good agreement between reference model and reduction

		Rn	G	H	LE
	Reference Mean	285.7	20.8	202.0	62.8
Silt loam/Winslow	Reduction ME	0.4	0.1	0.5	-0.2
	Reduction RMSE	0.6	2.0	1.1	2.4
	Reference Mean	231.1	31.4	104.1	95.6
Sand/Winslow	Reduction ME	0.4	0.0	-0.8	1.3
	Reduction RMSE	0.8	1.4	1.9	3.4
	Reference Mean	225.1	18.9	14.6	191.6
Silt/loam/Dulles	Reduction ME	1.0	-0.3	-1.3	2.7
	Reduction RMSE	2.3	2.6	3.0	7.2
	Reference Mean	150.7	21.6	7.9	121.2
Sand/Dulles	Reduction ME	0.4	-0.3	-0.9	1.6
	Reduction RMSE	0.8	1.7	2.0	4.0

Table 3.12

EFFECTS ON SIMULATED FLUXES OF THE REDUCTION ELIMINATING THE TEMPERATURE COEFFICIENT OF MATRIC POTENTIAL. ME = MEAN ERROR, RMSE = ROOT-MEAN-SQUARE ERROR. UNITS ARE ly/day.

is observed throughout.

These results demonstrate the negligibility of the temperature effect on matric potential, at least in the simulations examined. Should these results be confirmed in further simulations with more general random forcing, they would provide justification for neglecting this effect in soil moisture simulations. This would be a useful result, eliminating one of the theoretical couplings between moisture and heat fluxes in soils. It would also allow one to avoid the necessity of quantifying the temperature dependence of matric potential, a subject on which there seems to be little agreement, either experimentally (Milly and Eagleson, 1980) or theoretically (Milly, 1982).

3.3.4 Temperature Coefficient of Hydraulic Conductivity

Another effect that couples the moisture and heat fields in soil is the temperature dependence of the hydraulic conductivity. This dependence enters through the viscosity of water, as seen in (2.23). Hydraulic conductivity increases by a factor of two between 10°C and 40°C. In assessing the significance of this sensitivity, it is important to realize that a bare soil surface is often subjected to large diurnal variations in temperature, as the surface is the major site of conversion of radiant to thermal energy and vice versa.

In a first reduction eliminating the temperature dependence of hydraulic conductivity, we evaluate the temperature factor only once, at the start of the simulation, using the initial soil temperature (14°C at Dulles, 24°C at Winslow). A comparison of this reduction with the reference simulations is presented in Table 3.13. As we saw in Section 3.3.3, the largest errors are in the evaporation term. In each case, evaporation is underpredicted. The largest mean error is a little over 5% of the total evaporation for the sand/Winslow case. The fairly low RMSE values suggest that this average bias is not much smaller than the typical hourly error. This is confirmed by Figure 3.5, which shows how the reduction underpredicts evaporation during the daytime of the first two days. This, of course, is when the reduction underpredicts the hydraulic conductivity.

The results of this section, which show a minor importance for the temperature factor, can be improved by evaluating this factor at a temperature closer to an average surface soil temperature. The average should be weighted more heavily during the daytime, when most evaporation occurs. Keeping in mind that soil surface temperatures usually exceed air temperatures in the heat of the day, we repeated the above analysis using the maximum air temperature to evaluate the conductivity. Temperature is referenced to the air since the soil temperature is not known

		Rn	G	H	LE
	Reference Mean	285.7	20.8	202.0	62.8
Silt loam/Winslow	Reduction ME	-0.1 (-0.1)	0.0 (0.0)	0.0 (0.1)	-0.1 (-0.2)
	Reduction RMSE	0.6 (0.9)	1.3 (1.7)	1.0 (1.4)	2.7 (3.5)
	Reference Mean	231.1	31.4	104.1	95.6
Sand/Winslow	Reduction ME	-1.4 (0.1)	0.3 (-0.1)	3.5 (-0.1)	-5.4 (0.3)
	Reduction RMSE	2.8 (1.8)	5.8 (5.7)	6.7 (3.4)	12.1 (9.6)
	Reference Mean	255.1	18.9	14.6	191.6
Silt loam/Dulles	Reduction ME	-2.6 (-0.8)	1.0 (0.3)	4.0 (1.6)	-7.6 (-2.7)
	Reduction RMSE	5.8 (3.0)	8.4 (5.2)	9.4 (6.1)	21.6 (13.1)
	Reference Mean	150.7	21.6	7.9	121.2
Sand/Dulles	Reduction ME	-0.6 (-0.7)	0.4 (0.3)	1.3 (1.4)	-2.4 (-2.4)
	Reduction RMSE	1.0 (1.2)	2.5 (2.5)	2.9 (3.4)	5.8 (6.2)

Table 3.13

EFFECTS ON SIMULATED FLUXES OF THE REDUCTION THAT EVALUATES THE HYDRAULIC CONDUCTIVITY AT A CONSTANT TEMPERATURE. VALUES OUTSIDE PARENTHESES USE INITIAL SOIL TEMPERATURE, WHILE VALUES INSIDE USE MAXIMUM AIR TEMPERATURE. ME = MEAN ERROR, RMSE = ROOT-MEAN-SQUARE ERROR. UNITS ARE ly/day.

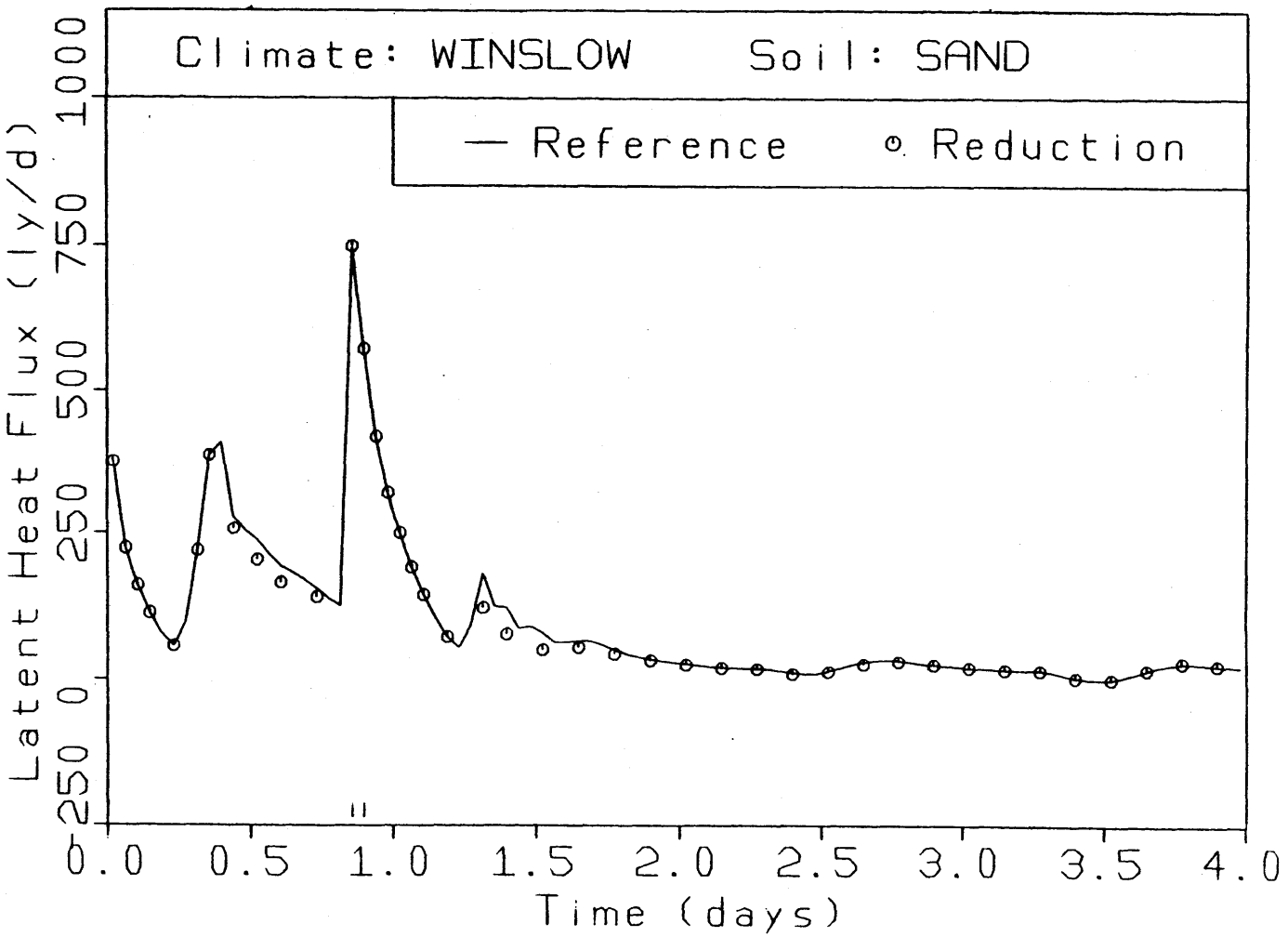

Figure 3.5

EVAPORATION CALCULATED FOR SAND/WINSLOW WITH HYDRAULIC CONDUCTIVITY EVALUATED AT THE INITIAL CONDITION ("REDUCTION").

a priori. The effects of this change on the flux predictions are shown in parentheses in Table 3.13. With the new approximation, the evaporation bias is reduced to less than two percent for all simulations. The time variation of the temperature factor is therefore negligible, provided an average soil surface temperature, or an appropriate surrogate, is used.

3.3.5 Water Vapor

Water vapor accounts for several of the transport and storage terms in the conservation and flux equations, (2.1)-(2.4). If the vapor phase could be ignored, this would lead to considerable simplifications. For instance, aside from the slight thermal influences on liquid moisture retention and hydraulic conductivity, the vapor provides the only mechanism by which the temperature distribution can directly enter the moisture conservation equation.

As our first reduction of the governing equations with respect to vapor, we set the humidity equal to zero everywhere in the soil. To calculate evaporation, we employ (2.45), with ρ_{vg} evaluated using (2.14) with the initial value of temperature and the time-varying value of ψ at the surface.

The results of the comparison are summarized in Table 3.14. As usual, the largest error is in the evaporation. It is consistently underpredicted, by as much as

		Rn	G	H	LE
	Reference Mean	285.7	20.8	202.0	62.8
Silt loam/Winslow	Reduction ME	-5.3 (0.0)	1.1 (-0.4)	16.3 (0.5)	-22.6 (-0.2)
	Reduction RMSE	13.1 (5.3)	33.9 (7.6)	35.5 (13.1)	49.6 (19.2)
	Reference Mean	231.1	31.4	104.1	95.6
Sand/Winslow	Reduction ME	-5.4 (-1.0)	-2.6 (-6.1)	16.7 (5.2)	-19.5 (-0.1)
	Reduction RMSE	12.4 (6.1)	22.9 (28.7)	32.8 (15.6)	41.9 (14.1)
	Reference Mean	225.1	18.9	14.6	191.6
Silt loam/Dulles	Reduction ME	-6.6 (-0.2)	3.8 (-0.1)	17.9 (1.0)	-28.3 (-1.1)
	Reduction RMSE	15.3 (1.5)	38.7 (4.1)	39.9 (4.6)	87.5 (8.9)
	Reference Mean	150.7	21.6	7.9	121.2
Silt loam/Winslow	Reduction ME	-1.4 (-0.2)	-1.5 (-2.6)	5.3 (2.0)	-5.2 (0.4)
	Reduction RMSE	4.4 (2.8)	13.2 (13.5)	13.8 (8.5)	19.2 (7.4)

Table 3.14

EFFECTS ON SIMULATED FLUXES OF THE REDUCTION ELIMINATING VAPOR. VALUES OUTSIDE PARENTHESES FOR STRAIGHT REDUCTION. VALUES INSIDE COMPUTED WITH VAPOR ENTERING ONLY THROUGH $D_{\psi v}$. ME = MEAN ERROR, RMSE = ROOT-MEAN-SQUARE ERROR. UNITS ARE ly/day.

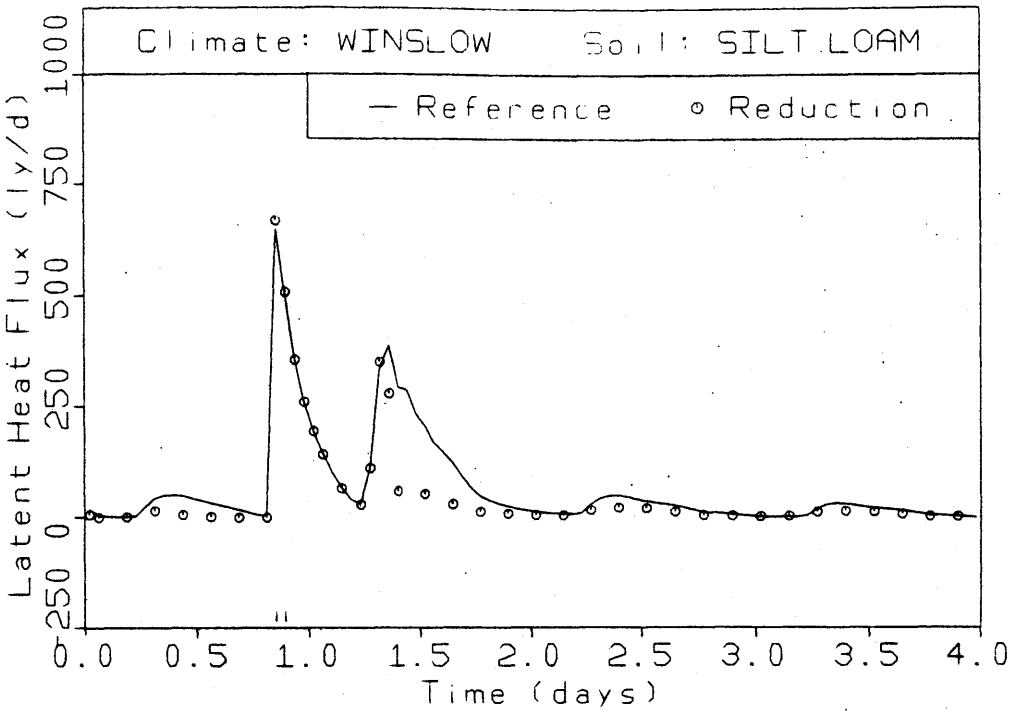

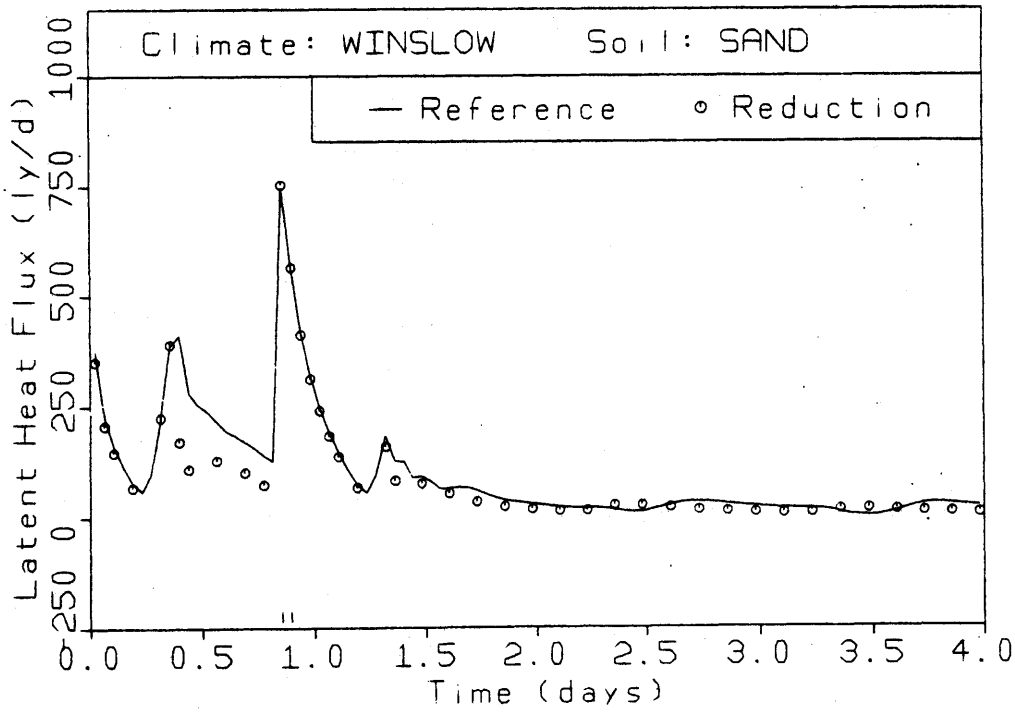

Figure 3.6

EVAPORATION ERRORS INDUCED BY NEGLECTING WATER VAPOR.

(Continued on next page.)

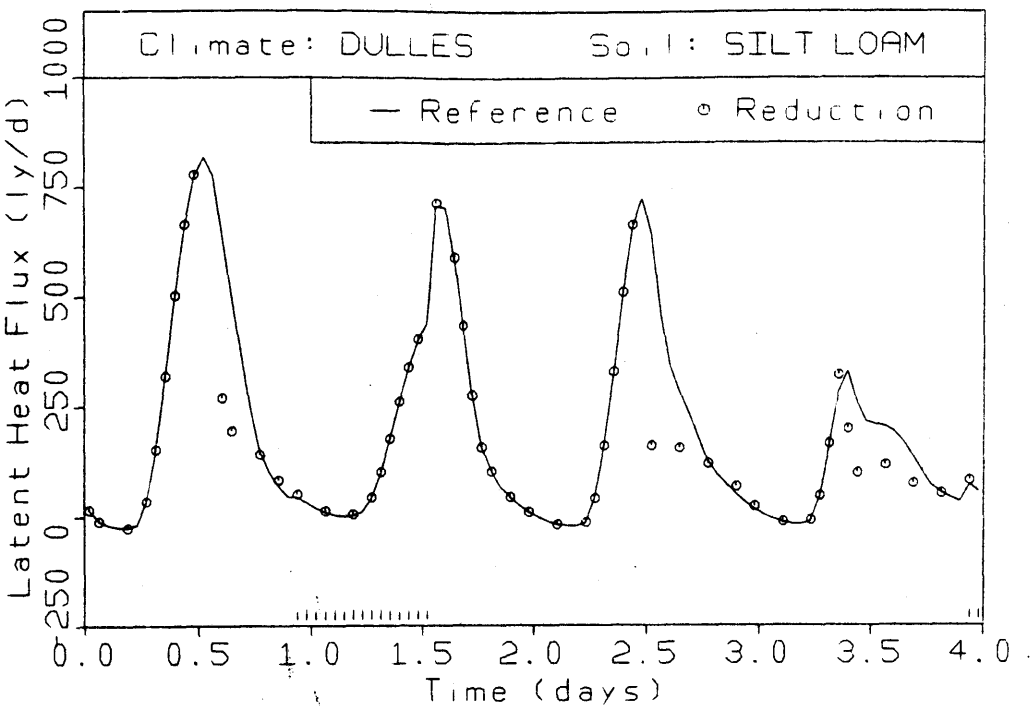

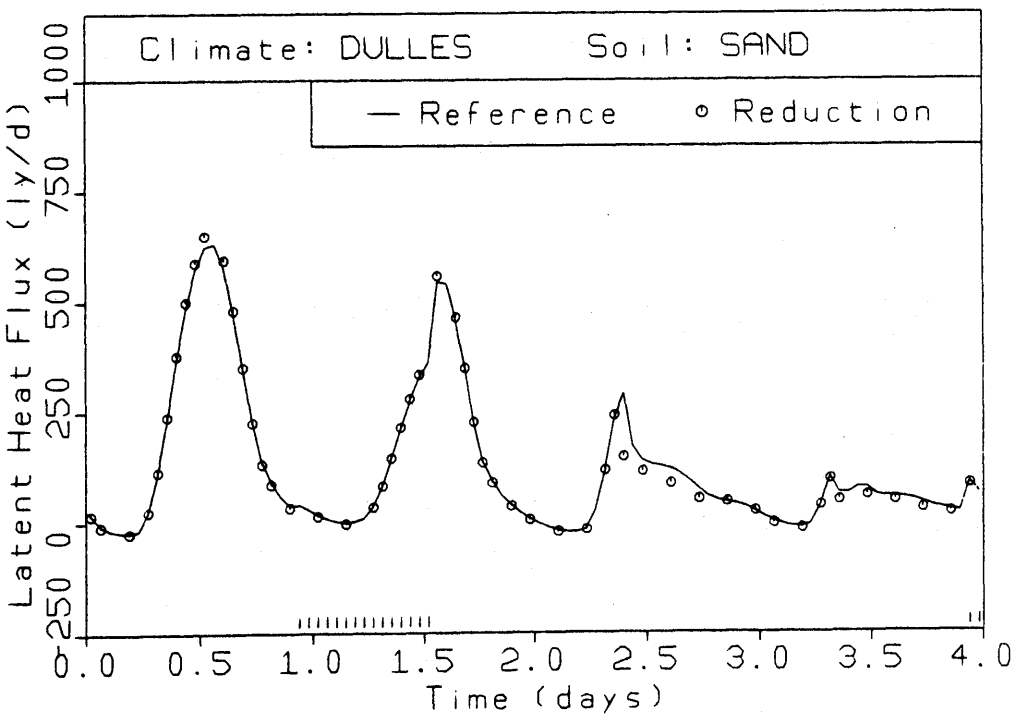

Figure 3.6

(Continued.)

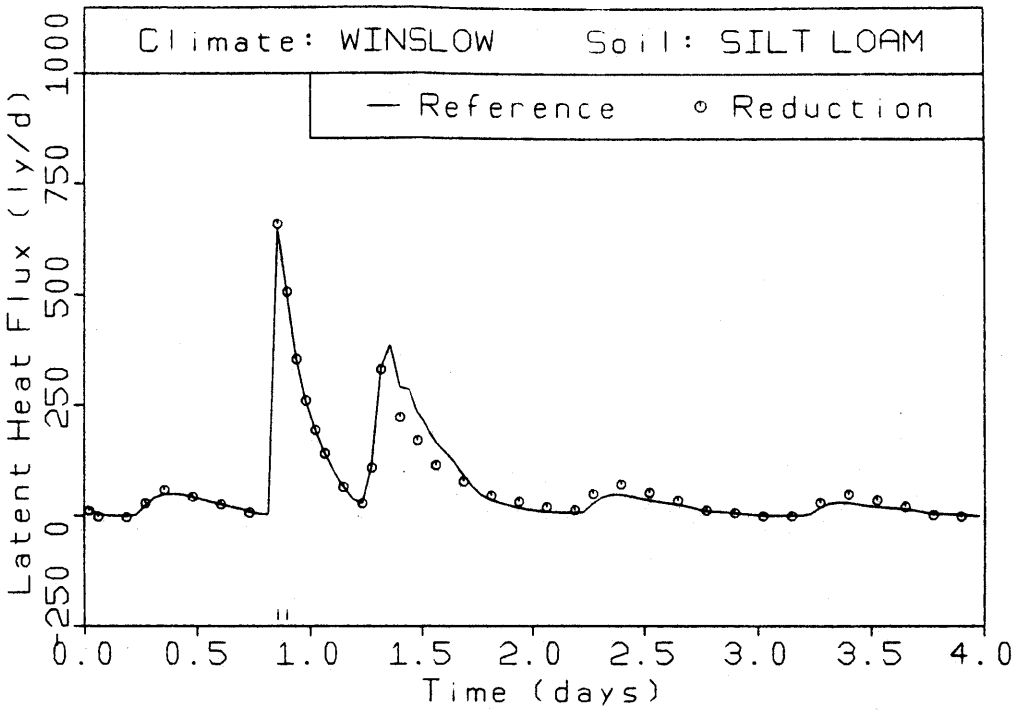

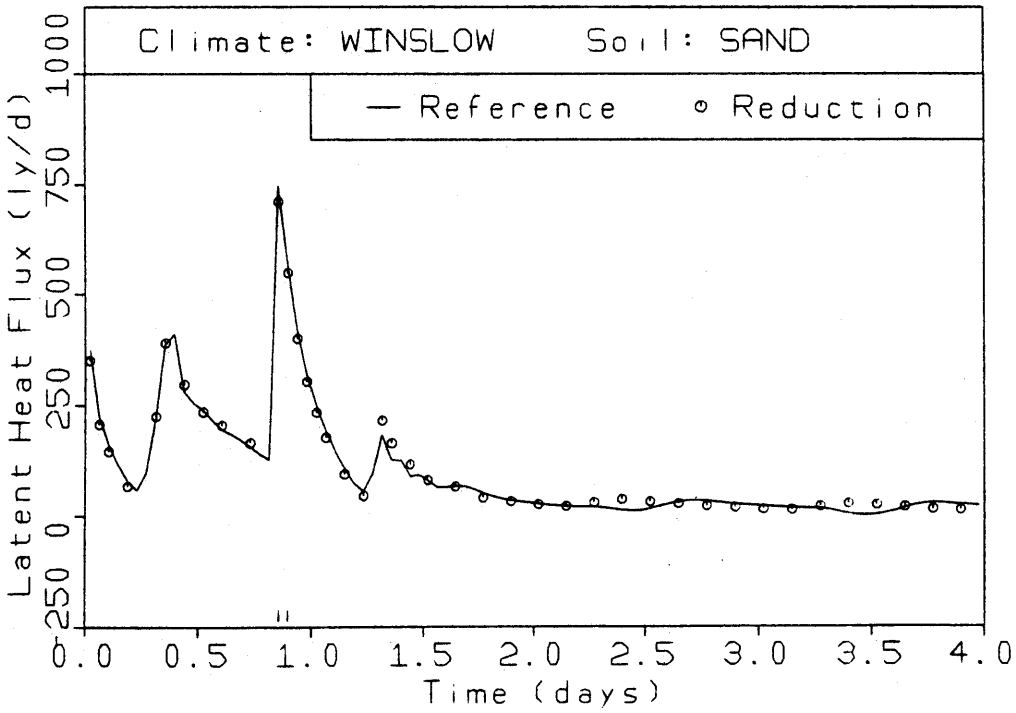

Figure 3.7

EVAPORATION CALCULATED BY NEGLECTING WATER VAPOR, EXCEPT IN $D_{\psi v}$.

(Continued on next page.)

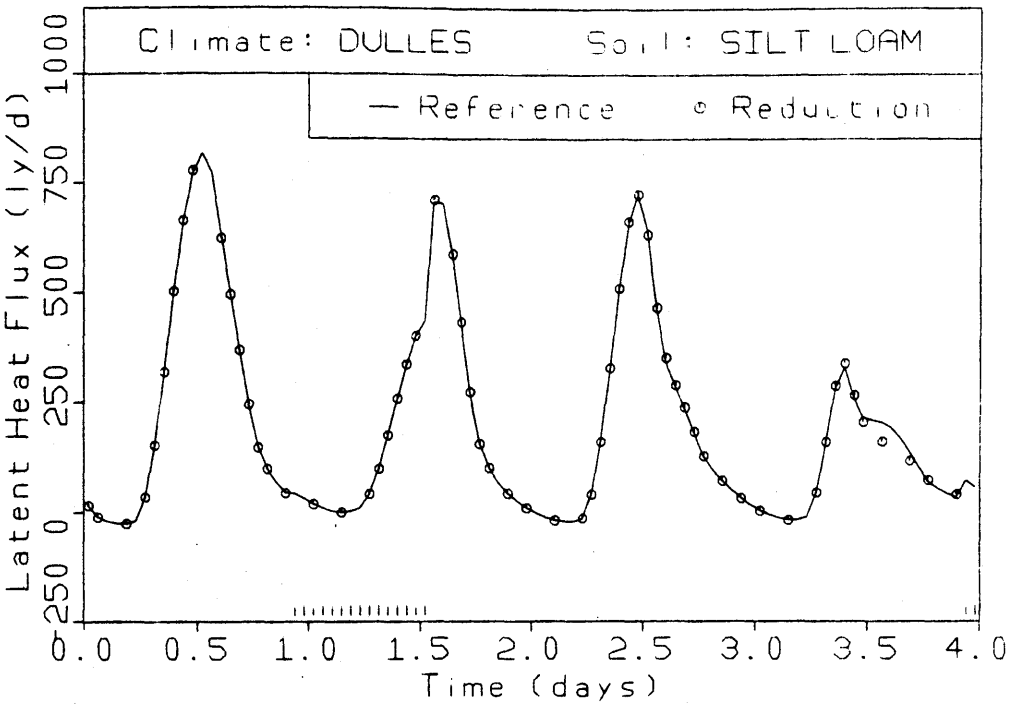

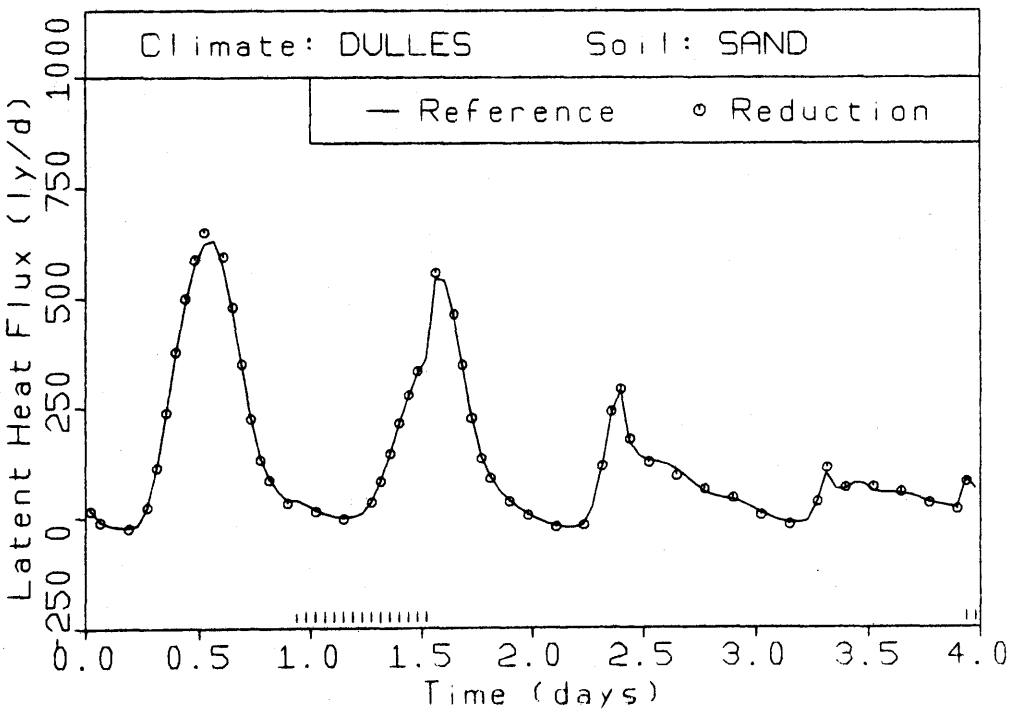

Figure 3.7
(Continued.)

36 percent at Winslow with the silt loam. Clearly, the ability of water to evaporate beneath the soil surface is important, especially in the dry scenarios. Figure 3.6 illustrates the time variation of the error in calculated evaporation induced by neglecting vapor.

Given the various ways in which vapor enters the governing equations, it is logical to ask if any particular effect can be isolated as the most important, and, if such a dominant effect exists, how it can be parameterized. We hypothesize that the vapor analog of hydraulic conductivity, $D_{\psi v}$ in (2.3) and (2.26), is the most important. Figure 2.5 shows that $D_{\psi v}$ greatly exceeds K when either soil is dry.

In order to test the aforementioned hypothesis, we keep ρ_v equal to zero everywhere in the governing equations except in (2.26). Furthermore, we shall evaluate $D_{\psi v}$ with (2.26) using a typical temperature, the initial temperature, instead of the actual time- and space-varying temperature. This latter decoupling of moisture and heat is analogous to the reduction applied to hydraulic conductivity in Section 3.3.4.

The improved results obtained with this $D_{\psi v}$ parameterization appear in the parentheses in Table 3.14. As far as the means are concerned, the results are greatly improved. A comparison of the time variation of evaporation is presented in Figure 3.7 for all four scenarios. Improvement over Figure 3.6 is evident. The most significant

errors are in the two Winslow sequences. In the silt loam, evaporation is slightly underpredicted during day 2 and slightly overpredicted during the next two days. In the sand, the low evaporation during the dry days is out of phase with the reference model. In the reference model, downward temperature gradients during the day suppress evaporation through the thermal vapor effect. In the reduction, no such opposing force exists and evaporation reaches a maximum near noon. As far as total evaporation is concerned, the thermal effect does not appear to be crucial. It appears that the isothermal vapor conductivity, $D_{\psi v}$, is indeed the dominant mechanism by which vapor in the soil affects surface fluxes and that its temperature dependence is not crucial.

3.3.6 Hysteresis

Given the magnitude of the hysteresis loop usually observed in soils (Figures 2.3 and 2.4), the application of a single $\theta(\psi)$ curve to a process involving both wetting and drying may lead to significant errors. However, when such errors can be shown to be negligible, the resultant simplifications in the relation between θ and ψ facilitate calculations in mathematical analyses, either analytic or numerical.

In an attempt to assess the importance of hysteresis in a soil undergoing repeated wetting and drying,

we perform another reduction experiment. In the reduction, an average moisture retention curve is defined by

$$\bar{\theta}(\cdot) = \frac{1}{2}[\theta_w(\cdot) + \theta_d(\cdot)] \qquad (3.4)$$

where $\theta_w(\cdot)$ and $\theta_d(\cdot)$ are the main wetting and drying curves, given by (2.19) and (2.21). Since the initial condition for the reference simulations has been specified to lie on the main drying curve, and not on $\bar{\theta}(\cdot)$, it is impossible to assign identical initial ψ and θ to the reference model and to the reduction. Since the hydraulic conductivity, which is the main controller of moisture flow in the soil, depends uniquely on θ, rather than on ψ, we shall apply to the reduction that value of ψ that produces the same initial θ as in the reference model. Then

$$\bar{\theta}(\psi_{red}) = \theta_d(\psi_{ref}) \qquad (3.5)$$

where ψ_{red} is the initial matric potential applied to the reduction and ψ_{ref} is the initial value assigned in the reference model, given already in Table 3.10. In Table 3.15, the values of ψ_{red} are presented for each scenario, together with the ψ_{ref} values. In each case, ψ_{red} is smaller in magnitude than ψ_{ref}, as should be expected on the basis of Figures 2.3 and 2.4.

Because the initial conditions are not precisely equivalent (i.e., θ, but not ψ, is matched), there is an initial discrepancy in the simulations that is due more to

	Reduction	Reference
Silt loam/Winslow	-5.4×10^5 cm	-10^6 cm
Sand/Winslow	-121	-330
Silt loam/Dulles	-128	-500
Sand/Dulles	-51	-70

Table 3.15

INITIAL MATRIC POTENTIAL APPLIED IN THE HYSTERESIS REDUCTION. CORRESPONDING REFERENCE VALUES ARE ALSO LISTED.

the initial condition than to the dynamics of hysteresis. This period is one to two days in duration. In order to get beyond this initial transient, we run these simulations for ten days instead of the four days used up until now for the reduction tests.

Comparisons of the calculated evaporative heat fluxes are presented in Figure 3.8 for each scenario. For both soils at Winslow, the calculated fluxes differ somewhat during daytime evaporation from a wet surface, but are otherwise quite similar. Differences are much more pronounced in the humid Dulles climate, especially for the sand. Peak evaporation from a drying surface is significantly overpredicted in each case.

Table 3.16 is a summary of the average errors in surface fluxes. The first 48 hours are excluded from the calculations, because of the discrepancy discussed earlier. Evaporation is usually overpredicted, and the largest bias is 31.5 ly/day, over 35 percent of the average evaporation calculated by the reference model, for the sand at Dulles.

It is apparent from the foregoing analysis that moisture retention hysteresis is a physically significant process, directly affecting the average water and heat balances on time scales up to at least several days, particularly in the sand.

		Rn	G	H	LE
	Reference Mean	280.9	10.3	211.3	59.2
Silt loam/Winslow	Reduction ME	-0.9	0.1	0.7	-1.8
	Reduction RMSE	8.1	12.1	11.1	26.4
	Reference Mean	214.9	19.3	138.5	57.1
Sand/Winslow	Reduction ME	2.4	-2.4	-5.5	10.3
	Reduction RMSE	5.6	14.5	13.6	14.5
	Reference Mean	214.4	13.2	30.8	170.4
Silt loam/Dulles	Reduction ME	1.4	-1.0	-2.7	5.1
	Reduction RMSE	10.4	16.4	17.6	38.9
	Reduction Mean	139.1	17.6	32.7	88.9
Sand/Dulles	Reduction ME	-4.5	-4.5	-19.4	31.8
	Reduction RMSE	26.1	26.1	31.5	63.5

Table 3.16

EFFECTS ON SIMULATED FLUXES OF THE REDUCTION ELIMINATING HYSTERESIS. DAYS 3 THROUGH 10. ME = MEAN ERROR, RMSE = ROOT-MEAN-SQUARE ERROR. UNITS ARE ly/day.

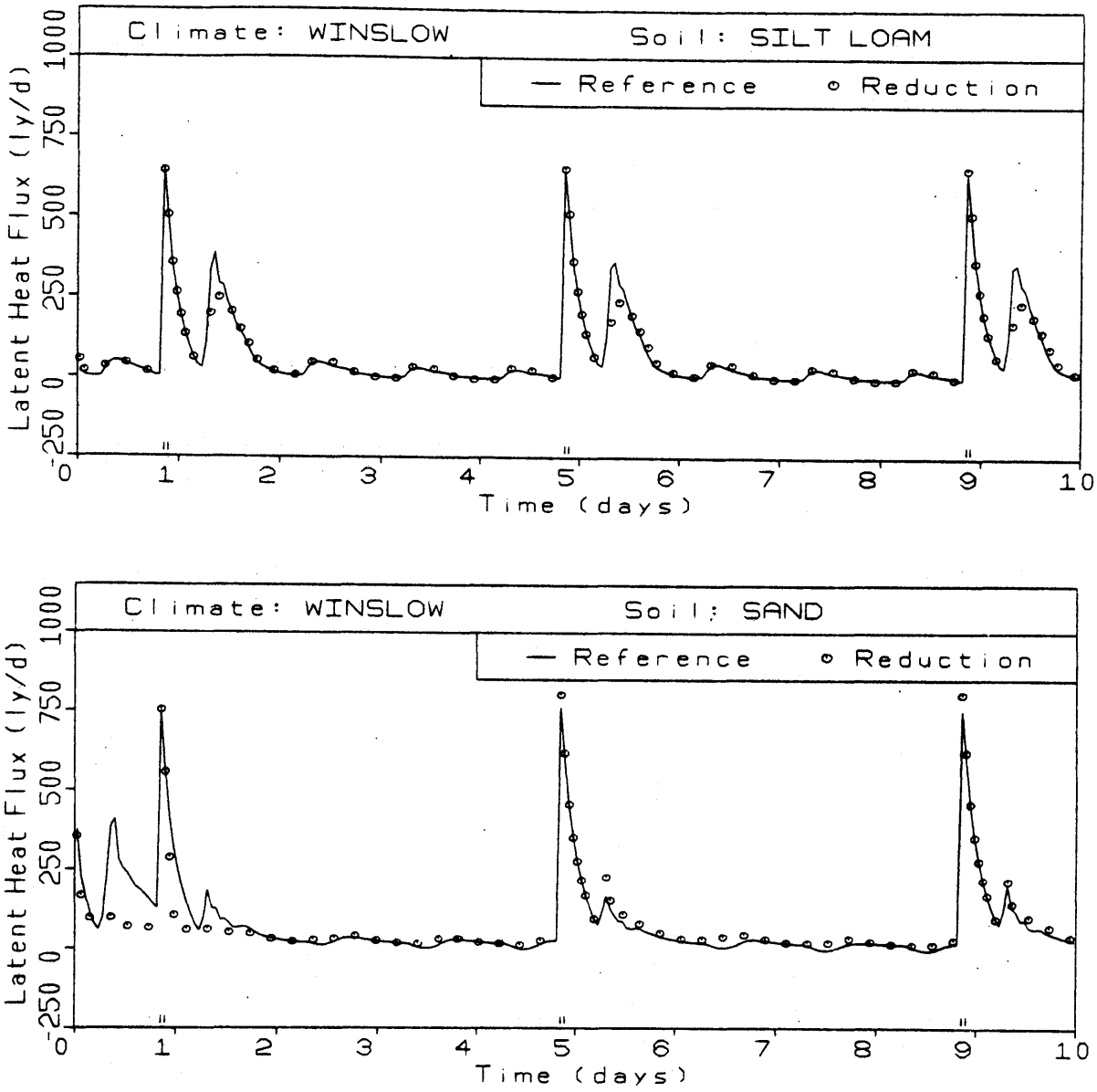

Figure 3.8

EVAPORATION CALCULATED BY NEGLECTING HYSTERESIS.

(Continued on next page.)

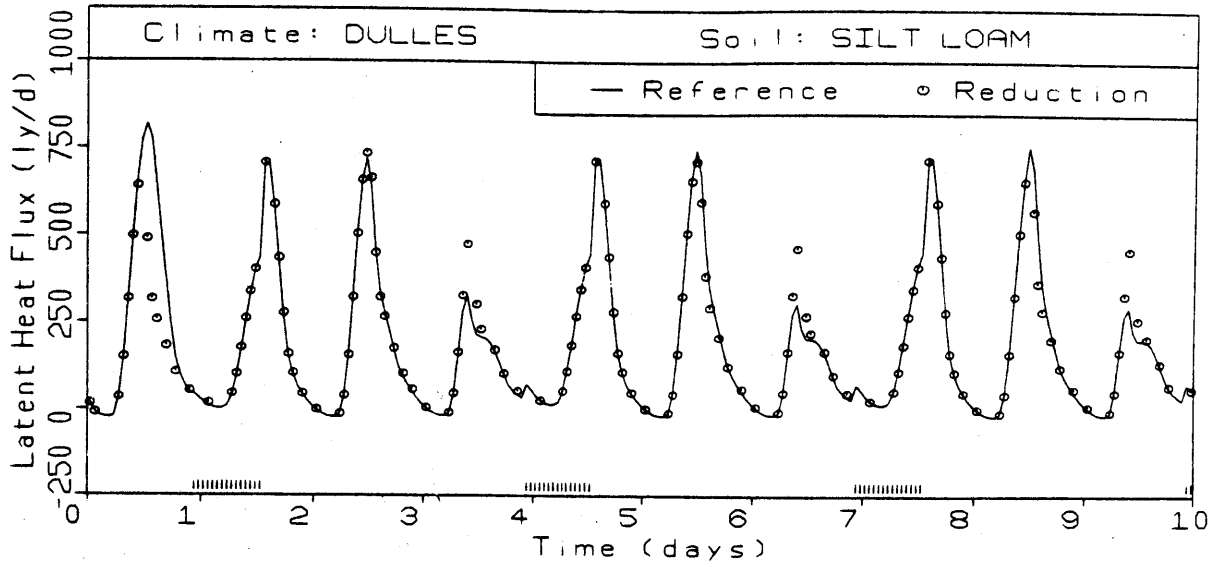

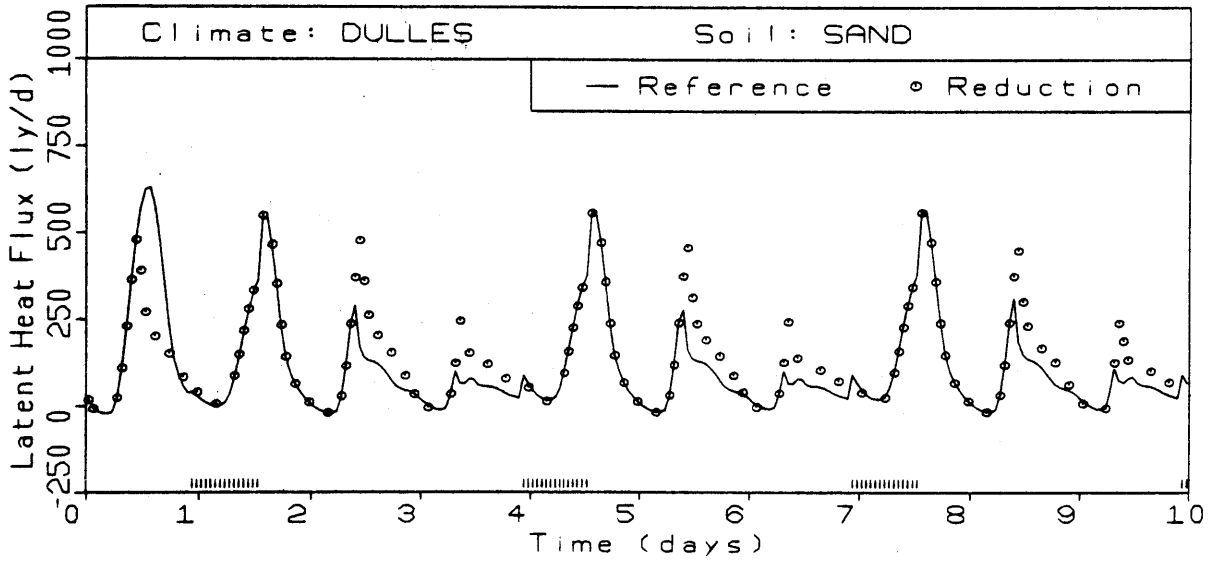

Figure 3.8

(Continued.)

3.3.7 Verification of Reductions using Random Forcing

In the preceding sections, we studied various simplifications of the equations governing moisture and heat in a soil. The validation of these reductions was performed using short, periodic sequences of forcing, and only one simplification at a time was tested. In order to verify our findings under longer, random forcing, a final set of experiments is presented.

As before, four scenarios are considered. The difference here is that the forcing sequences for Winslow and Dulles are based directly on the three-hourly observations reported in "Local Climatological Data" for those stations during July 1968 and May 1972. For Winslow, hourly precipitation reports are used together with interpolated hourly values of 3-hourly reports of other meteorological variables. For Dulles, 6-hourly rainfall amounts were reported. The intensity is assumed constant during these 6-hour periods in order to specify hourly values of rainfall. For the other variables, interpolation of 3-hourly values is again used to obtain hourly forcing. Both sequences are 744 hours (31 days) long.

All simplifications considered in earlier sections, except the hysteresis one, are applied jointly. The heat of wetting and the temperature dependence of moisture retention are ignored. The temperature factor in the hydraulic

		Rn	G	H	LE
	Reference Mean	273.3	5.3	226.6	41.4
Silt loam/Winslow	Reduction ME	-0.1	0.0	-0.2	0.1
	Reduction RMSE	4.9	11.9	12.4	15.9
	Reference Mean	209.0	9.0	152.4	47.5
Sand/Winslow	Reduction ME	0.2	-1.8	1.6	0.4
	Reduction RMSE	5.1	18.4	12.1	16.1
	Reference Mean	182.0	9.4	0.2	172.4
Silt loam/Dulles	Reduction ME	-0.3	-0.1	0.8	-1.0
	Reduction RMSE	4.0	7.7	7.5	17.1
	Reference Mean	109.1	13.7	19.3	76.1
Sand/Dulles	Reduction ME	-0.4	-1.3	2.2	-1.3
	Reduction RMSE	3.4	11.4	9.5	9.6

Table 3.17

EFFECTS ON SIMULATED FLUXES OF THE JOINT REDUCTION DESCRIBED IN SECTION 3.3.7 FOR 31-DAY SIMULATIONS. ME = MEAN ERROR, RMSE = ROOT-MEAN-SQUARE ERROR. UNITS ARE ly/day.

conductivity is evaluated using the average daily maximum air temperature, an approach that was shown to yield good results in Section 3.3.4. Water vapor is ignored in the soil, except for its effect on isothermal vapor flow through $D_{\psi v}$, as in Section 3.3.5. The reference simulation involves none of these simplifications.

Results of the comparisons of the joint reductions with the reference model using one month of random forcing are presented in Table 3.17. The reduced model performs very well. Maximum average heat flux errors are on the order of one ly/day. The RMS values of hourly errors are in the range of 3 to 20 ly/day, indicating very good agreement of hourly values.

3.4 Summary and Discussion

In this chapter, we have performed various experiments using a detailed numerical simulation model of soil moisture and heat dynamics under atmospheric excitation. The first section was devoted to the practical problem of determining the degree of discretization in time and space necessary for an accurate solution. For the scenarios considered here, it is sufficient to use 20 elements to represent the soil moisture zone, with most of those elements concentrated within the top 50 cm of the soil. A sufficiently small time step size is one that prevents the

moisture content (and temperature) at any node from changing by more than 0.002 (1°C) during any step.

Due to the very long time constants ($\sim$ months) governing moisture storage within the top meters of the soil, we find it necessary to specify initial conditions that are consistent (i.e., in dynamic equilibrium) with the forcing. Otherwise, system behavior will be dominated by long-term storage effects. Equilibrium rates of deep percolation to groundwater were presented in Table 3.10 for the four scenarios. These values may be underestimated, especially in silt loam, because the numerical model does not take into account the existence of cracks and other macropores that allow rapid, deep infiltration of water during storms. A complementary overestimate of evaporation would accompany this effect.

The final part of this chapter demonstrates how the moisture flow equations (2.1) and (2.3) may be simplified greatly without causing significant changes in predicted evaporation, sensible heat flux, etc. Our results provide rigorous justification for the use of an isothermal flow equation to model evaporation from a bare soil. On the other hand, it appears that soil moisture retention hysteresis is generally not negligible. Neglecting it leads to serious overestimation of average evaporation from sands in our examples.

Chapter 4

PARAMETERIZATIONS OF SOIL MOISTURE AND HEAT

4.1 Introduction

Chapter 3 provides the basis for simplification of the equations governing soil moisture dynamics originally presented in Chapter 2. In particular, it supports the application of isothermal moisture flow theory in the prediction of the surface moisture and heat fluxes. The validated simplified theory for moisture dynamics forms the basis for further analysis in this chapter.

Whereas the goal of Section 3.3 was to simplify the reference model with respect to physical processes, the aim here can be viewed as an attempt to simplify the mathematical (more specifically, the computational) representation of a given set of physical laws. The finite element method applied so far generally requires a large number of states and small computational time increments, leading to heavy demands for computer time. Improved economy, with reasonable accuracy, can come only with a reduction of the state set and/or an increase in the allowable time step size.

In this chapter, we are primarily concerned with simplified models of the moisture dynamics. The corresponding problem of soil temperature prediction has been dealt with by

Deardorff (1978), whose parameterization using the force-restore method, described in Section 4.4, will be coupled here with three proposed moisture parameterizations. Deardorff showed that a simple two-state temperature model can provide efficient and accurate prediction of the ground surface temperature when the forcing is dominated by a deterministic, periodic component (e.g., the diurnal cycle). It is our goal to develop an efficient scheme of similar complexity to represent the soil moisture dynamics, which, unlike the heat dynamics, are governed by extreme nonlinearities.

The parameterizations outlined in this chapter will be evaluated in Chapter 5. As a result of that analysis, a modified version of the most promising moisture model will be proposed and tested.

4.2 A Two-Node Model of Soil Moisture Dynamics

Our parameterizations of the soil moisture dynamics are to be based on the physical theory introduced in Chapter 2 and simplified in Chapter 3. Given the reductions that were validated in Section 3.3, we may reduce (2.1) and (2.3) to

$$\frac{d\theta}{d\psi}\frac{\partial\psi}{\partial t} = \frac{\partial}{\partial z}\left\{[K(\theta) + D_{\psi v}(\psi,\theta)]\frac{\partial\psi}{\partial z} + K(\theta)\right\} \qquad (4.1)$$

where

$$\theta = \theta_H(\psi) \qquad (4.2)$$

in which the H subscript indicates that θ is a hysteretic function of ψ, as prescribed in Section 2.3.4.1. Examples of the functional forms of $K(\theta)$ and $D_{\psi v}(\theta)$ have also been presented in Chapter 2 and are used here. Their temperature dependences are eliminated as described in Section 3.3.

The value of $D_{\psi v}$ can be significant relative to K only when $\frac{\partial \psi}{\partial z}$ is much greater than unity. This justifies rewriting (4.1) as

$$\frac{d\theta}{d\psi} \frac{\partial \psi}{\partial t} = \frac{\partial}{\partial z} \left\{ [K(\theta) + D_{\psi v}(\psi, \theta)] \left(\frac{\partial \psi}{\partial z} + 1 \right) \right\} \qquad (4.3)$$

since the added term is always negligible.

As a starting point for our parameterizations, we shall apply Galerkin's finite element method to (4.3). In contrast to the previous application that yielded the reference model, however, we shall employ only two elements (and eventually only one). We shall thereby preserve the fundamental physics of the process. The numerical accuracy of the scheme will not be immediately guaranteed, though, due to the extreme coarseness of the grid. By judicious selection of the element lengths, we shall attempt to reproduce the predictions of the reference model.

Details of the application of finite elements to (4.1) are not presented here. Milly and Eagleson (1980) describe the approach used here and derive a finite element

description of (2.1) through (2.4), which are a generalization of (4.1). We can therefore apply our reductions directly to their finite element equations. For two elements, this yields

$$\begin{bmatrix} \frac{\Delta_1}{2}\left(\frac{d\theta}{d\psi}\right)_1 & 0 & 0 \\ & \frac{\Delta_1+\Delta_2}{2}\left(\frac{d\theta}{d\psi}\right)_2 & \\ & & \frac{\Delta_2}{2}\left(\frac{d\theta}{d\psi}\right)_3 \end{bmatrix} \begin{Bmatrix} \frac{d\psi_1}{dt} \\ \frac{d\psi_2}{dt} \\ \frac{d\psi_3}{dt} \end{Bmatrix}$$

$$\begin{bmatrix} \frac{K_{e1}}{\Delta_1} & -\frac{K_{e1}}{\Delta_1} & 0 \\ -\frac{K_{e1}}{\Delta_1} & \frac{K_{e1}}{\Delta_1}+\frac{K_{e2}}{\Delta_2} & -\frac{K_{e2}}{\Delta_2} \\ 0 & -\frac{K_{e2}}{\Delta_2} & \frac{K_{e2}}{\Delta_2} \end{bmatrix} \begin{Bmatrix} \psi_1 \\ \psi_2 \\ \psi_3 \end{Bmatrix} + \begin{Bmatrix} K_{e1} \\ K_{e2}-K_{e1} \\ -K_{e2} \end{Bmatrix} = \begin{Bmatrix} f \\ 0 \\ -R_g \end{Bmatrix} \tag{4.4}$$

In this system of equations, ψ_1, ψ_2, and ψ_3 are the values of matric potential at the surface, at some shallow depth, and at a greater depth, in that order. (We have reversed the ordering used by Milly and Eagleson.) The subscript of $\frac{d\theta}{d\psi}$ is the same depth index. The length of the top element is Δ_1 and that of the second is Δ_2. Nodes 2 and 3 are thus at depths Δ_1 and $\Delta_1+\Delta_2$, respectively. The variables f and $-R_g$ are fluxes of water into the system across its top and bottom. Physically, f is infiltration (or minus exfiltration), and R_g is the deep percolation rate. Although we shall not specify the functional forms of these fluxes at this point, it

should be noted that they are dependent upon the state at the surface node.

The K_{ei} in (4.4) refers to an effective value of the sum of K and $D_{\psi v}$ over element i. While strict application of the finite element method would require

$$K_{ei} = \frac{1}{\Delta_i} \int_{\text{element } i} [K(\theta(z)) + D_{\psi v}(\theta(z), \psi(z))]dz \quad (4.5)$$

which can be approximated as

$$K_{ei} = \frac{1}{2\Delta_i} \sum_{n=1}^{2} (K + D_{\psi v})_n \quad (4.6)$$

where n denotes the element endpoints, experiments with the reference model have demonstrated improved rates of convergence using

$$K_{ei} = [(K + D_{\psi v})_1 \ (K + D_{\psi v})_2]^{1/2} \quad (4.7)$$

which is a geometric mean. Haverkamp et al. (1977) have also found this to be an optimal weighting procedure.

During initial testing of the model described in this section, we discovered that (4.7) was unworkable as a formula for the effective hydraulic conductivity between the two nodes. It yields an excessive K_{el}, and therefore excessive evaporation, when the difference in moisture content between the two nodes is great. (Of course, (4.6) would be

even worse, as the arithmetic mean is larger than the geometric mean.) Apparently, the coarse lumping of this system requires that the effective hydraulic conductivity be parameterized more carefully.

Consider a steady, unsaturated, vertical flow between two points. The flux is given by

$$q = -K\left(\frac{d\psi}{dz} + 1\right) \tag{4.8}$$

Rearrangement, using the fact that q is constant, and integration between levels 2 and 1, separated by distance Δ_1, yields

$$\Delta_1 = \int_{\psi_1}^{\psi_2} \frac{d\psi}{1+q/K} \tag{4.9}$$

In order to obtain a simple formula for an effective hydraulic conductivity, we now drop the gravity term (unity) in the denominator, and assume that K and ψ are related through (Eagleson, 1978)

$$K = K_o(\psi_o/\psi)^{mc} \tag{4.10}$$

Although this is inconsistent with our representation of soil properties and does not allow for hysteresis, it should eventually yield a better estimate of K_e than (4.6) or (4.7).

With these assumptions, (4.9) becomes

$$\frac{q\Delta_1}{K_o} = \frac{\psi_o}{mc-1}\left[\left(\frac{\psi_1}{\psi_o}\right)^{-mc+1} - \left(\frac{\psi_2}{\psi_o}\right)^{-mc+1}\right] \qquad (4.11)$$

or

$$q\Delta_1 = \frac{1}{mc-1}\,(\psi_1 K_1 - \psi_2 K_2) \qquad (4.12)$$

where K_1 and K_2 are values of K at nodes 1 and 2. Defining the effective hydraulic conductivity as the "apparent" constant value for the interval Δ_1, we can write

$$K_e = \frac{q}{(\psi_2-\psi_1)/\Delta_1} \qquad (4.13)$$

Cancellation of the flux between (4.12) and (4.13) yields

$$K_e = [(mc-1)(\psi_2 - \psi_1)]^{-1}\,(\psi_1 K_1 - \psi_2 K_2) \qquad (4.14)$$

The factor mc varies with soil texture. For our soils, mc $\sim$ 3, a value which is used here. The simulation results are insensitive to this quantity. In the results reported for this model, (4.14) is used together with a restriction that K_e be bounded by K_1 and K_2.

In our parameterizations, we shall deal with the same physical situation considered in defining the lower moisture boundary condition of the reference model in Section 2.3.2. That is, the water table is deep and water flux at the bottom of the model is equal to the hydraulic conductivity, the matric potential gradient being zero. We therefore set

$\psi_2 = \psi_3$ and disregard the third line in (4.4). The first two lines of (4.4) then become

$$\begin{bmatrix} \frac{\Delta_1}{2}\left(\frac{d\theta}{d\psi}\right)_1 & 0 \\ 0 & \frac{\Delta_1+\Delta_2}{2}\left(\frac{d\theta}{d\psi}\right)_2 \end{bmatrix} \begin{Bmatrix} \frac{d\psi_1}{dt} \\ \frac{d\psi_2}{dt} \end{Bmatrix} + \frac{K_{el}}{\Delta_1}\begin{bmatrix} 1 & -1 \\ -1 & 1 \end{bmatrix} \begin{Bmatrix} \psi_1 \\ \psi_2 \end{Bmatrix}$$

$$+ K_{el} \begin{Bmatrix} 1 \\ -1 \end{Bmatrix} = \begin{Bmatrix} f \\ -K_{e2} \end{Bmatrix} \qquad (4.15)$$

The rate of moisture supply, f, to the soil at the surface is equal to the precipitation rate minus the evaporation rate, except when the infiltration capacity (f_i^*) is exceeded, at which times it equals the latter, i.e.,

$$f = \min\left\{P - \frac{C_w u_a}{\rho_\ell}\left[\rho_o(T_1)\exp(\psi_1 g/RT_1) - \rho_{va}\right],\ f_i^*\right\} \qquad (4.16)$$

where T_1 is the land surface temperature.

Let us now summarize the proposed two-node model of soil moisture dynamics. The expansion of the time derivative with respect to ψ is unnecessary. We re-write (4.15) as

$$\frac{d\theta_1}{dt} = -\frac{K_{el}}{2\ell_1^2}(\psi_1 - \psi_2 + 2\ell_1)$$

$$+ \frac{1}{\ell_1}\min\left\{P - \frac{C_w u_a}{\rho_\ell}\left[\rho_o(T_1)\exp(\psi g/RT_1) - \rho_{va}\right],\ f_i^*\right\} \qquad (4.17)$$

and

$$\frac{d\theta_2}{dt} = \frac{K_{el}}{2\ell_1\ell_2}(\psi_1 - \psi_2 + 2\ell_1) - \frac{1}{\ell_2}K_{e2} \tag{4.18}$$

where

$$\ell_1 \equiv \frac{\Delta_1}{2} \tag{4.19}$$

$$\ell_2 \equiv \frac{\Delta_1 + \Delta_2}{2} \tag{4.20}$$

Equations of state are, from (4.2),

$$\theta_i = \theta_H(\psi_i) \tag{4.21}$$

(4.14) for K_{el}, and

$$K_{e2} = K(\theta_2) + D_{\psi v}(\theta_2, \psi_2) \tag{4.22}$$

Finally, f_i^* is the quantity that satisfies (4.16) with P large, θ_1 constant in time, and ψ_1 equal to zero,

$$f_i^* = \frac{K_{el}}{2\ell_1}(-\psi_2 + 2\ell_1) \tag{4.23}$$

Knowing the initial conditions, the atmospheric forcing (u_a and ρ_{va}), the forms of $\theta_H(\cdot)$, $K(\cdot)$, and $D_{\psi v}(\cdot,\cdot)$, the parameters ℓ_1 and ℓ_2, and the surface temperature, T_1, we can integrate the system (4.17)/(4.18) in time.

The surface temperature, of course, cannot be predicted independently, since the evaporation rate enters into the surface heat balance. For this reason, the system

of equations presented above must be solved simultaneously with a heat balance equation. In this work, the force-restore method of soil temperature prediction (Section 4.4) will be used.

Equations (4.17) and (4.18) have direct physical interpretations. The first equates the depth-averaged storage change in a reservoir of depth ℓ_1 to the loss of water by drainage to a lower layer (which is proportional to total head difference between layers) plus a gain or loss due to rain or evaporation. The second equation states that drainage from the upper layer will tend to increase the depth-averaged moisture content in the lower layer of depth ℓ_2, while gravity drainage out the bottom will tend to lower it.

The performance of this moisture parameterization, and of the others, is discussed in Chapter 5. In that chapter, we shall discuss the sensitivity of this model to the as-yet-undefined parameters ℓ_1 and ℓ_2.

4.3 One-Node Models of Soil Moisture Dynamics

4.3.1 General Framework

We can introduce a family of one-node, or one-cell, moisture accounting models by following the entire line of logic that led to (4.17) and (4.18), and then taking it one step further. We multiply (4.17) by ℓ_1, (4.18) by ℓ_2, and add the two, obtaining

$$(\ell_1 + \ell_2)\ \frac{d\bar{\theta}}{dt} = \min\left\{P - \frac{C_w u_a}{\rho_\ell}\left[\rho_o(T_1)\exp(\psi_1 g/RT_1) - \rho_{va}\right],\ f_i^*\right\} - K_{e2} \tag{4.24}$$

where

$$\bar{\theta} \equiv \ell_1\theta_1 + \ell_2\theta_2 \tag{4.25}$$

is a depth-averaged moisture content. With no explicit relation between ψ_1 (a surface value) and $\bar{\theta}$, we must replace (4.24) by

$$Z\ \frac{d\bar{\theta}}{dt} = \min[P - E,\ f_i^*] - K_e(\bar{\theta}) \tag{4.26}$$

where we have estimated the drainage rate using $\bar{\theta}$, and in which

$$Z \equiv \ell_1 + \ell_2 \tag{4.27}$$

In analogy to the treatment of infiltration as the lesser of the precipitation rate and a soil-controlled infiltration capacity, we may express the actual evaporation rate between storms as

$$E = \min[E_p,\ f_e^*] \tag{4.28}$$

where E_p is the potential evaporation rate,

$$E_p \equiv \frac{C_w u_a}{\rho_\ell}[\rho_o(T_1) - \rho_{va}] \tag{4.29}$$

and f_e^* is the exfiltration capacity of the soil, a function of the soil state.

Using (4.28), and assuming that $E = E_p$ during rain events, we can re-write (4.26) as

$$Z \frac{d\bar{\theta}}{dt} = - \min(E_p, f_e^*) - K_e(\bar{\theta}) \qquad P = 0 \qquad (4.30a)$$

and

$$Z \frac{d\bar{\theta}}{dt} = \min(P - E_p, f_i^*) - K_e(\bar{\theta}) \qquad P > 0 \qquad (4.30b)$$

We must add to (4.30a) the explicit restriction that E goes to zero when $\bar{\theta}$ goes to zero. This condition is otherwise not satisfied by the f_e^* parameterization given in (4.3.2), because it is based on a semi-infinite medium.

Given E_p, which is determined through simultaneous solution of a heat balance equation, we can solve (4.30) if the dynamic values of f_i^* and f_e^* are known. There is no simple way to calculate these variables exactly, as that would require continuous integration of (4.1). The problem of soil moisture accounting within the framework of any one-cell model hinges upon the specification of f_i^* and f_e^* in terms of $\bar{\theta}$ and the model forcing. The following subsections present two distinctly different approaches to this problem.

4.3.2 Surface Fluxes Based on Nonlinear Diffusion and the Time Compression Assumption

Here we shall specify parameterizations for f_i^* and f_e^* by applying existing idealized nonlinear diffusion solutions

to our problem. Our first assumption is that the flux capacity at a given time is a unique function of the cumulative surface flux since the start of the current event (infiltration or exfiltration). Then

$$f_i^* = f_i^*(F_i) \tag{4.31}$$

$$f_e^* = f_e^*(F_e) \tag{4.32}$$

where

$$F_i(t) = \int_{t_1}^{t} f_i(\tau)d\tau \tag{4.33}$$

$$F_e(t) = \int_{t_2}^{t} f_e(\tau)d\tau \tag{4.34}$$

in which $F_i(t)$ is the cumulative infiltration, at time t, since the start of the most recent rain at time t_1, $F_e(t)$ is the cumulative exfiltration since the end of the most recent rain at time t_2, and f_i and f_e are the actual rates of infiltration and exfiltration. These correspond to the "minimum" operators in (4.30). The statements of (4.31) and (4.32) that unique relations exist between soil-limited flux rates and cumulative fluxes are variations of the time compression assumption (Reeves and Miller, 1975).

Eagleson (1978) has applied (4.31) and (4.32) implicitly for the cases of constant precipitation and

constant potential evaporation. He uses for (4.31) and (4.32) a particular pair of solutions of the appropriate nonlinear diffusion equation (4.1) with constant initial conditions, and with step changes (to saturation for infiltration, to dryness for exfiltration) in surface moisture content. These solutions can be expressed, in the form of (4.31) and (4.32), as

$$f_i^* = A_o\left\{1 + \left[-1 + \left(1 + \frac{4A_oF_i}{S_i^2}\right)^{1/2}\right]^{-1}\right\} \qquad (4.35)$$

and

$$f_e^* = S_e^2/2F_e \qquad (4.36)$$

in which A_o is a hydraulic conductivity term and S_i and S_e are the infiltration sorptivity and the exfiltration desorptivity. These parameters are dependent upon the initial (constant in space) moisture content, the moisture content applied as a boundary condition, and the soil properties.

Eagleson (1978) uses

$$A_o(\theta_o,\theta_b) = \frac{1}{2}\,[K(\theta_o) + K(\theta_b)] \qquad (4.37)$$

and

$$S_i(\theta_o,\theta_b) = 2(\theta_b - \theta_o)(D_i/\pi)^{1/2} \qquad (4.38)$$

for infiltration with θ_o being the initial condition, θ_b the boundary condition, and D_i an effective diffusion coefficient

for the infiltration process. In terms of the nonlinear soil moisture diffusion coefficient, defined in the absence of hysteresis and vapor flow as

$$D(\theta) = K(\theta) \frac{d\psi(\theta)}{d\theta} \tag{4.39}$$

the effective diffusion coefficient is approximated using the weighted-average (Crank, 1956, p. 256)

$$D_i(\theta_o, \theta_b) = \frac{5}{3} (\theta_b - \theta_o)^{-5/3} \int_{\theta_o}^{\theta_b} (\theta - \theta_o)^{2/3} D(\theta) d\theta \tag{4.40}$$

We have seen in Sections 3.3.5 and 3.3.6 that it is sometimes important to account also for the effects of vapor flow and hysteresis. Accordingly, we propose that (4.40) be modified for these effects. Substituting (4.39) into (4.40), and adding an isothermal vapor flow conductivity to the hydraulic conductivity, we arrive at

$$D_i(\theta_o, \theta_b) = \frac{5}{3} (\theta_b - \theta_o)^{-5/3} \int_{\psi_o}^{\psi_b} [\theta_H(\psi) - \theta_o]^{2/3} \left\{ K[\theta_H(\psi)] + D_{\psi v}[\theta_H(\psi), \psi] \right\} d\psi \tag{4.41}$$

In (4.41), we assume that not only θ, but also the wetting history (and hence $\psi = \psi_o$) is constant initially. Then the wetting process proceeds along the same scanning curve at all depths. On this particular scanning curve, θ is a unique function of ψ, so (4.41) can be evaluated. The limits of

the integral in (4.41) are given by

$$\theta_H(\psi_o) = \theta_o \tag{4.42}$$

$$\theta_H(\psi_b) = \theta_b \tag{4.43}$$

We must still specify how the particular scanning curve for integration of (4.41) is to be chosen. One approach would be to keep track of the history of $\bar{\theta}$, the depth-averaged moisture content, and to use the appropriate scanning curve, with $\theta_o = \bar{\theta}$, to evaluate (4.41) at the start of an evaporation period. Noting the insensitivity of D_i to θ_o near dryness and the likelihood of an initially dry near-surface soil zone, we shall evaluate (4.41) using $\theta_o = 0$ (and $\theta_b = \theta_u$), integrating along the main wetting curve. This integration path is illustrated schematically in Figure 4.1 as Γ_1. This procedure will yield a unique value of D_i, applicable to all storms, and therefore represents a considerable computational simplification. To be consistent, we use these same values of θ_o and θ_b in (4.37) and in (4.38), obtaining unique infiltration parameters for a given soil.

We note here that, although the vapor term has been included in (4.41), its contribution is actually negligible during wetting, when the conductivity at high θ dominates the integral in (4.41). For exfiltration, however, it will be important. With the various assumptions set forth above, we

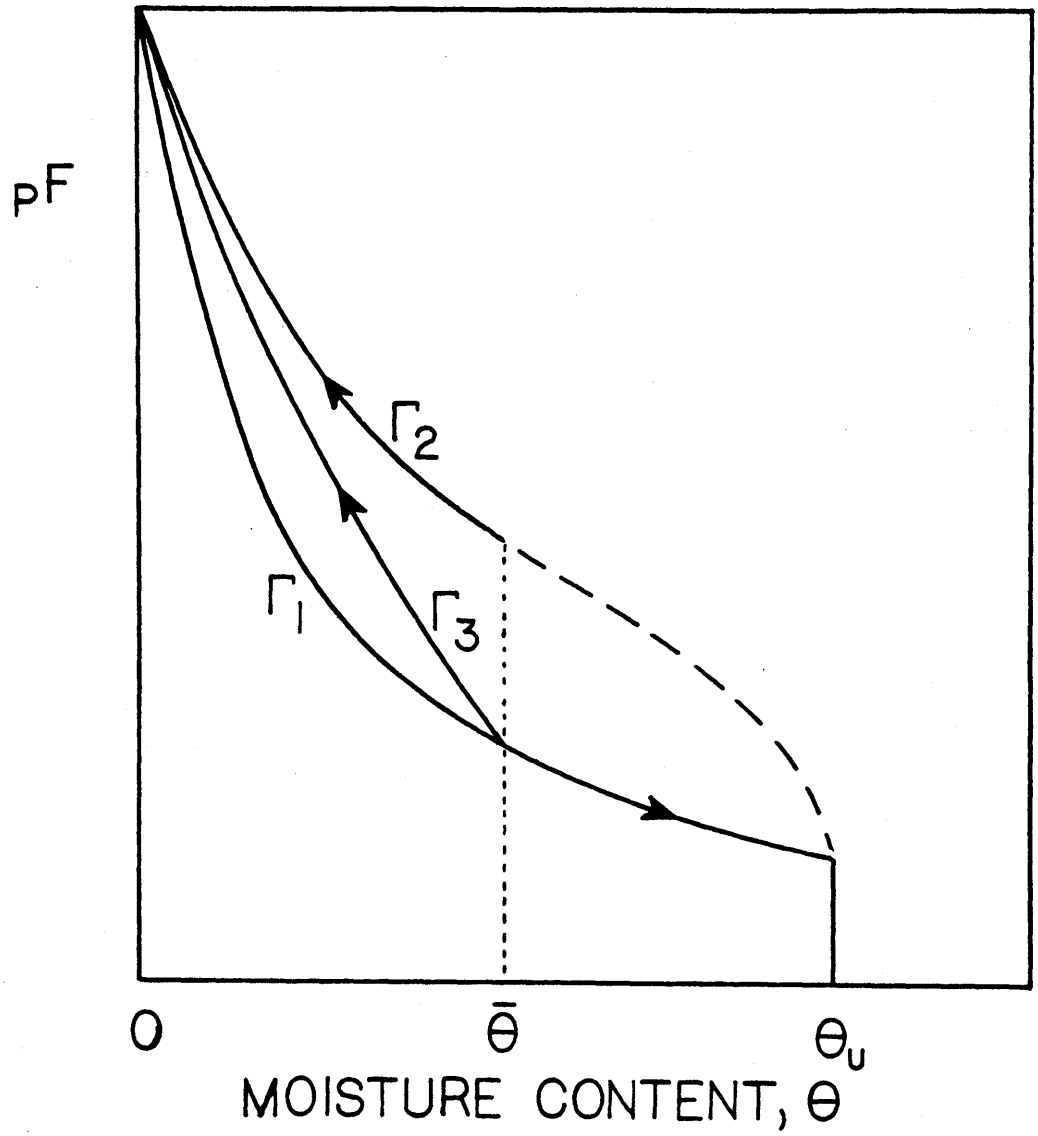

Figure 4.1

BRANCHES OF THE MOISTURE RETENTION FUNCTION USED TO EVALUATE SORPTIVITY (CURVE Γ_1), AND DESORPTIVITY (CURVE Γ_3). CURVE Γ_2 OVERESTIMATES THE DESORPTIVITY.

obtain, from (4.37), (4.38), and (4.41),

$$A_o(0,\theta_u) = \frac{1}{2} K(\theta_u) \tag{4.44}$$

$$S_i(0,\theta_u) = \left\{ \frac{20\theta_u^{1/3}}{3\pi} \int_{-\infty}^{0} [\theta_w(\psi)]^{2/3} K[\theta_w(\psi)] d\psi \right\}^{1/2} \tag{4.45}$$

For exfiltration ($\theta_b < \theta_o$), Eagleson (1978) uses

$$S_e(\theta_o, \theta_b) = 2(\theta_o - \theta_b)(D_e/\pi)^{1/2} \tag{4.46}$$

where D_e is the effective desorption diffusivity, given by (Crank, 1956, p. 256)

$$D_e(\theta_o, \theta_b) = 1.85(\theta_o - \theta_b)^{-1.85} \int_{\theta_1}^{\theta_o} (\theta_o - \theta)^{0.85} D(\theta) d\theta \tag{4.47}$$

Again, we change the integration variable and introduce hysteresis and vapor. Setting θ_b equal to zero and θ_o equal to $\bar{\theta}$, we arrive at

$$D_e(\bar{\theta}) = 1.85\ \bar{\theta}^{-1.85} \int_{-\infty}^{\bar{\psi}} [\bar{\theta} - \theta_H(\psi)]^{0.85} \left\{ K[\theta_H(\psi)] + D_{\psi v}[\theta_H(\psi), \psi] \right\} d\psi \tag{4.48}$$

where

$$\theta_H(\bar{\psi}) = \bar{\theta} \tag{4.49}$$

We must identify the branch of θ_H to be used for evaluation of (4.48). Initial experiments using the main drying curve, with θ_o equal to $\bar{\theta}$ at the start of the interstorm period (Γ_2 in Figure 4.1), resulted in excessive evaporation due to overestimation of D_e. A method that is physically more realistic is to integrate (4.48) using a primary drying scanning curve (Γ_3 in Figure 4.1). This approach is used to obtain the results presented in the next chapter. Along the primary drying scanning curve, we have (Milly and Eaglenon, 1980)

$$\theta_H(\psi) = \theta_w(\psi)\{1 + [\theta_{rev} - \theta_w(\psi)]\theta_u^{-1}\} \qquad (4.50)$$

where θ_{rev} is the value of θ at which the wetting reversal occurs, equal to $\bar{\theta}$ at the end of the rain.

If $\bar{\theta}$ were to change during an interstorm period only as a result of evaporation, then the proper approach would be to evaluate (4.48) and (4.46) at the end of a storm and to use the resulting desorptivity throughout the period. However, immediately after the storm, the process of redistribution -- gravity drainage and capillary diffusion of water to lower levels -- begins. In the absence of evaporation, it would result in a fairly uniform decrease in moisture content near the surface. As a result, we expect that the desorptivity also will decrease following a storm. In this first parameterization, we shall incorporate this

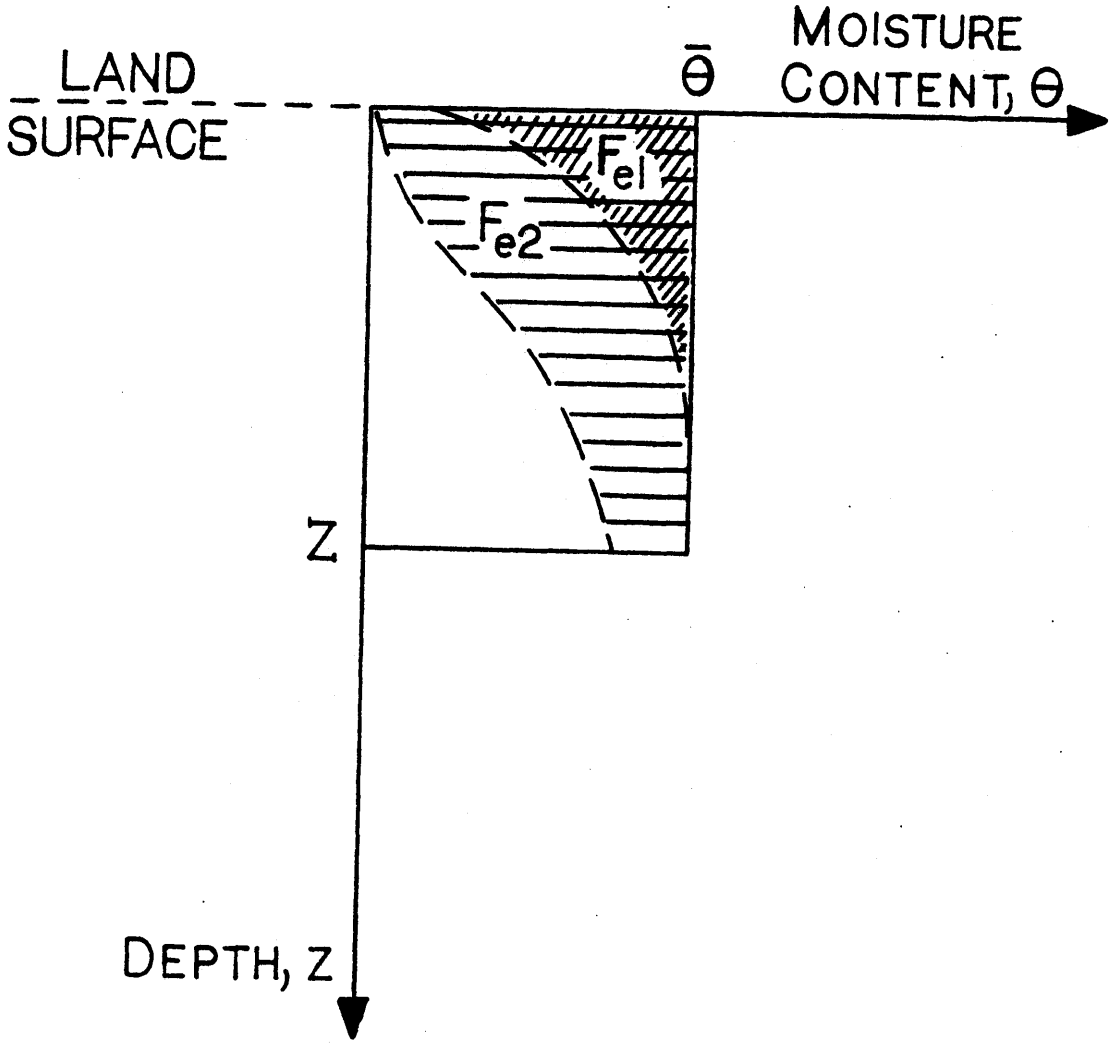

Figure 4.2

SQUARE-WAVE REPRESENTATION OF WETTED SOIL MASS FOLLOWING RAINFALL, AND SUBSEQUENT LOSSES OF MOISTURE (F_{e1} AND F_{e2}) TO EVAPORATION AT TWO LATER TIMES.

redistribution implicitly by the choice of Z, the storage cell depth. We assume that the optimal value of Z determined in the next chapter automatically smears the moisture content after a storm to a value that might occur following the initial rapid phase of redistribution. We use $\bar{\theta}$ at the start of the interstorm period to evaluate S_e once for the entire period. In the second version of this parameterization, presented later, we shall explicitly track S_e. Figure 4.2 depicts our conceptualization of the moisture distribution following rainfall.

Our statement of this one-cell parameterization of the water balance is now complete. The average moisture content, $\bar{\theta}$, within the surface soil layer of depth Z, varies in time according to (4.30). The infiltration and exfiltration capacities have been defined in (4.35) and (4.36), whose parameters are evaluated, accounting for hysteresis, by (4.44), (4.45), and the combination of (4.46), (4.48) and (4.50). All basic parameters, except for Z, have been defined in physical terms, unambiguously, in Chapter 2.

It may be expected that Z, if it can be uniquely defined, is a measure of the depth over which dynamic storage of soil moisture is important. It will therefore be soil- and climate-dependent. We shall examine this dependence further in the next chapter.

4.3.3 Surface Fluxes Based on a Simple Conceptual Model -- GFDL Hydrology

The ground hydrology parameterization used in the GCM of the Geophysical Fluid Dynamics Laboratory (Manabe, 1969) has the form of (4.30). Here we define the functions f_i^* and f_e^* implicit in that model.

Runoff (combined surface and ground water) occurs when the "field capacity" of the soil, θ_{fc}, is reached. Therefore,

$$f_i^* = \begin{cases} \infty & \bar{\theta} < \theta_{fc} \\ 0 & \bar{\theta} = \theta_{fc} \end{cases} \tag{4.51}$$

Since groundwater runoff is viewed as rejected infiltration in this parameterization, the final drainage term in (4.30) is set to zero.

The exfiltration capacity of the soil is expressed using a Budyko-type supply function of the form

$$f_e^* = E_p \min\left(\frac{4\bar{\theta}}{3\theta_{fc}}, 1\right) \tag{4.52}$$

One structural shortcoming of (4.52) is that it is scaled by E_p, even though we would expect f_e^* to be totally under soil control when the soil nears dryness.

We shall express the conceptual parameter θ_{fc} first in terms of the physical soil characteristics using

$$\theta_{fc} = \frac{1}{2} [\theta_d(\psi_{fc}) + \theta_w(\psi_{fc})] \qquad (4.53a)$$

in which ψ_{fc} has a value of -350 cm (Buckman and Brady, 1969, p. 166). It should be kept in mind, however, that the concept of field capacity is a very approximate one. In fact the field capacity is a dynamic result of the interaction of soil and climate. We shall thus try also a second estimate for it, given by

$$\theta_{fc} = \theta_i \qquad (4.53b)$$

where the initial condition, θ_i, is the same one that has been shown to be in dynamic equilibrium with the forcing for each scenario in Section 3.2.

The GFDL hydrology model specifies a fixed value of $Z\theta_{fc}$ of 15 cm. We shall not specify Z a priori.

4.4 The Force-Restore Method of Soil Temperature Prediction

4.4.1 General Formulation

Deardorff (1978) has shown that the force-restore method is an efficient means of parameterization of the ground surface temperature. Because of its firm physical basis, its accuracy, and its simplicity, we shall employ it in conjunction with each of the moisture parameterizations.

Consider a homogeneous semi-infinite medium subjected to a simple sinusoidal input of heat,

$$G = B \sin(2\pi t/\tau + \pi/4) \tag{4.54}$$

If we impose the condition that

$$T \to T_2 , \qquad x \to \infty \tag{4.55}$$

where x is the distance into the medium, then the well-known analytic solution to the heat diffusion equation yields the surface temperature, T_1, after any initial transient has died away,

$$T_1 = T_2 + B\left(\frac{\tau}{2\pi\lambda C}\right)^{1/2} \sin(2\pi t/\tau) \tag{4.56}$$

The essence of the force-restore method is the replacement of the linear partial differential equation of diffusion by an equivalent linear ordinary differential equation of the form

$$\frac{dT_1}{dt} = c_1 G - c_2(T_1 - T_2) \tag{4.57}$$

This is the simplest dynamic equation for surface temperature that includes both heat input from the atmosphere (G, which <u>forces</u> T_1) and a diffusion-like conduction of heat into the underlying soil (which tends to <u>restore</u> T_1 to the deep temperature, T_2). Furthermore, the constants c_1 and c_2 can be chosen so that (4.57) yields the exact solution, (4.56), to the heat diffusion equation, given the forcing (4.54). This

means (4.57) can be tuned to the forcing period τ. The values of c_1 and c_2 are (Deardorff, 1978)

$$c_1 = 2\left(\frac{\pi}{\lambda C \tau}\right)^{1/2} \tag{4.58}$$

$$c_2 = 2\pi/\tau \tag{4.59}$$

where λ and C are the thermal conductivity and the volumetric heat capacity of the homogeneous medium.

When G is not sinusoidal, or λ or C are not constant in time and space, (4.57)-(4.59) will no longer yield the exact solution for surface temperature, but they will still be a good approximation if the forcing is dominated by a particular frequency and if λ and C vary little. This is in fact the case for a soil subjected to natural diurnal forcing by solar radiation and other variables. The period, τ, is one day. We therefore use (4.57) to predict the surface temperature, T_1, which is required by each of our moisture parameterizations in order to calculate E or E_p.

The heat flux G can be expressed, using the surface heat balance equation, (2.10), as

$$G = (1-A)I_s + \varepsilon I_{\ell d} - I_{\ell u} - \rho_\ell (L + c_\ell T_1) E$$

$$-H + \rho_\ell c_\ell T_a P - \rho_\ell c_\ell T_1 R_s - \rho_\ell c_\ell \frac{d}{dt}(hT_1) \tag{4.60}$$

Recall that A is the surface albedo, I_s the incoming shortwave radiation, ε the emissivity, $I_{\ell d}$ the downward longwave

radiation, $I_{\ell u}$ the upward longwave radiation, E the evaporation rate, ρ_ℓ and c_ℓ the density and specific heat of water, H the sensible heat loss to the atmosphere by turbulent diffusion, T_a the air temperature, P the precipitation, R_s the surface runoff, and h the depth of detention storage on the surface. Using several of the relations given in Chapter 2, we can write (4.60) as

$$G = f_1(T_1, \theta_1, E) \tag{4.61}$$

where only the unknown system states and the evaporation rate are explicitly indicated. The surface temperature enters through $I_{\ell u}$ and H; the surface moisture content affects A and ε; and the evaporation rate appears explicitly.

In general, T_2 will vary slowly due to the annual cycle of forcing. We model this with a simple linear forcing equation (Deardorff, 1978)

$$\frac{dT_2}{dt} = (\lambda C\, N_d\, \tau)^{-1/2}\, G \tag{4.62}$$

Deardorff suggests N_d should equal 365, the number of days (recall τ = 1 day) in the annual cycle. However, our simulations are relatively short (10 or 31 days) and begin from a constant initial condition. At early time, the analytic solution for a constant initial temperature and a step change, ΔT, at the boundary yields a heat flux

$$G = \left(\frac{\lambda C}{\pi t}\right)^{1/2} \Delta T \tag{4.63}$$

Then the total heat flux between the initial time, t = 0, and any later time t_o is

$$\int_o^{t_o} G dt = 2\left(\frac{\lambda C t_o}{\pi}\right)^{1/2} \Delta T \tag{4.64}$$

An integration of (4.62) yields

$$\Delta T_2 = (\lambda C N_d \tau)^{-1/2} \int_o^{t_o} G dt \tag{4.65}$$

If we equate ΔT to ΔT_2, we obtain

$$N_d = \frac{4 t_o}{\pi \tau} \tag{4.66}$$

This value of N_d can be used for simulations (such as ours) starting from a constant initial condition and having a total duration t_o significantly less than a year. For all of our simulations, we have t_o equal to either 10 or 31 days. Since results are not overly sensitive to N_d, we fix it at 20.

4.4.2 Coupling to the Soil Moisture Parameterizations

The coupling between the moisture parameterizations and the force-restore equations has been shown explicitly in the theoretical development. Certain aspects of their interaction require special mention here, however. These involve the moisture content, which enters into the albedo, the emissivity, the thermal conductivity, and the heat capacity. Not all of the moisture parameterizations explicitly predict

θ_1, and none predict the subsurface distribution of θ. Furthermore, it is not clear what value of θ should be used to evaluate the product of the thermal parameters appearing in (4.58) and (4.62). In this section, we briefly describe how these problems are handled.

The first moisture parameterization, the two-node model, explicitly predicts θ_1, the surface moisture content, so A and ε can be evaluated directly. The product λC is evaluated, using the expressions for λ and C appearing in Chapter 2 (but neglecting vapor effects), at the initial moisture content for use in (4.62),

$$(\lambda C)_2 = \lambda(\theta_i)\ C(\theta_i) \tag{4.67}$$

where θ_i is the initial moisture content and the subscript "2" refers to the prediction equation for T_2. We know that the value of θ at which $(\lambda C)_2$ should be evaluated is an average value over the depth of the annual temperature wave. For our relatively short experiments, this will not depart far from the initial condition. In order to evaluate λC for use in (4.58), it is more important to account for the time-varying surface moisture content. We use

$$(\lambda C)_1^{1/2} = 0.3[\lambda(\theta_1)\ C(\theta_1)]^{1/2} + 0.7(\lambda C)_2^{1/2} \tag{4.68}$$

which is a slight simplification of a procedure proposed by Deardorff (1978).

In order to evaluate A, ε, and (by means of (4.68)) $(\lambda C)_1$ using the one-node moisture models, we need to estimate θ_1, since it is not explicitly predicted. In the nonlinear diffusion model, we know that θ_1 becomes zero when f_e^* drops below E_p. At other times, we shall approximate θ_1 by the depth-averaged moisture content. Thus, for the nonlinear diffusion model, we have

$$\theta_1 = \begin{cases} 0 & f_e^* \leq E_p \\ \bar{\theta} & f_e^* > E_p \end{cases} \tag{4.69}$$

The same approximation is used in the GFDL hydrology model.

4.5 Numerical Solution of Proposed Models

Each of the moisture parameterizations is coupled to the force-restore temperature model, with which it is solved simultaneously. The time derivatives of T_1, θ_1, and $\bar{\theta}$ are finite-differenced using a fully implicit procedure, while T_2 and θ_2 are treated explicitly, since they vary much more slowly. The time step of integration is one hour in all cases. The details of the algorithm used for the one-node models, coupled to the force-restore procedure, are presented by Milly and Eagleson (1982).

Chapter 5

EVALUATION OF PROPOSED PARAMETERIZATIONS

5.1 Introduction

In this chapter, we shall describe the results of simulations of soil moisture and heat obtained using the parameterizations set forth in Chapter 4. In particular, we shall focus on the ability of each parameterization to predict evaporation, as this is the variable that is most sensitive to the parameterization and that is usually the most poorly predicted.

Each of the parameterizations has been defined in terms of a storage cell depth, whose value has been left undefined. We would expect this conceptual parameter to be dependent upon the soil type and the climate, if its definition is even valid at all. A good parameterization would be one, first, that predicts evaporation well for some value of the cell depth. Second, the cell depth must be identifiable for a given soil/climate combination, preferably through physical reasoning. Failing that, the cell depth can be fitted to a particular sequence of data, but it must then yield satisfactory predictions for other inputs. In this chapter, we concentrate on the latter approach. In the following chapter, we propose, essentially, to calculate a dynamic cell depth, using physical theory in the framework

of the one-cell nonlinear diffusion model.

For each of the three parameterizations, we follow the same general course in the presentation of the results. First we look at the sensitivity of the mean error and the RMSE of LE to the cell depth. This is done using the periodic weather sequences. An optimal cell size is chosen for each scenario by forcing the error in total evaporation to zero. Representative plots of the resulting evaporation series are presented and errors are summarized. Finally, the predetermined optimal cell depths are used to simulate evaporation during the 31-day sequences of actual hourly meteorologic data, and the results are compared to those of the reference model. Identical soil data and initial conditions are used in all models.

5.2 The Two-Node Model

There is a basic difference between the two-node model and the others in that the former is defined in terms of two cell depths, rather than one. To simplify our analysis here, we present results only for a fixed value of one meter for the lower cell depth. Numerous sensitivity runs indicated that the top cell size was much more important in determining the response of the model to atmospheric excitation. For example, the results presented in this section are changed little if a value of ten centimeters is used instead of one meter for the lower cell depth.

Figure 5.1 illustrates the sensitivity of the mean error and the RMSE of hourly LE to the top cell depth. (These and other error data presented in this chapter are all based on comparisons beginning at the end of day 2. In most of the plots of evaporation against time, an initial transient error, due to non-equivalence of initial conditions, is visible. It usually decays within two days.) The mean error at Winslow is rather insensitive to the cell depth. Decreasing cell depth then leads to increased surface moisture content during storms and hence to increased percolation to the lower cell. As the top cell becomes very small, there is a decrease in its resistance to flow from below during evaporation periods, and evaporation begins to increase again. The latter effect can be seen for the silt loam at Winslow. The RMSE has a minimum at a cell depth significantly lower than the one that gives zero average error.

For Dulles, the total evaporation and the RMSE are very sensitive to the cell depth. As for Winslow, the minimum-RMSE cell depth gives average evaporation rates biased downwards.

Table 5.1 (first three columns) gives the cell depth and RMSE associated with zero mean error for each scenario, along with actual average evaporative heat fluxes for reference. The cell depths are in the range of 0.8 to 10 cm. The RMSE values give a rough idea as to how well the

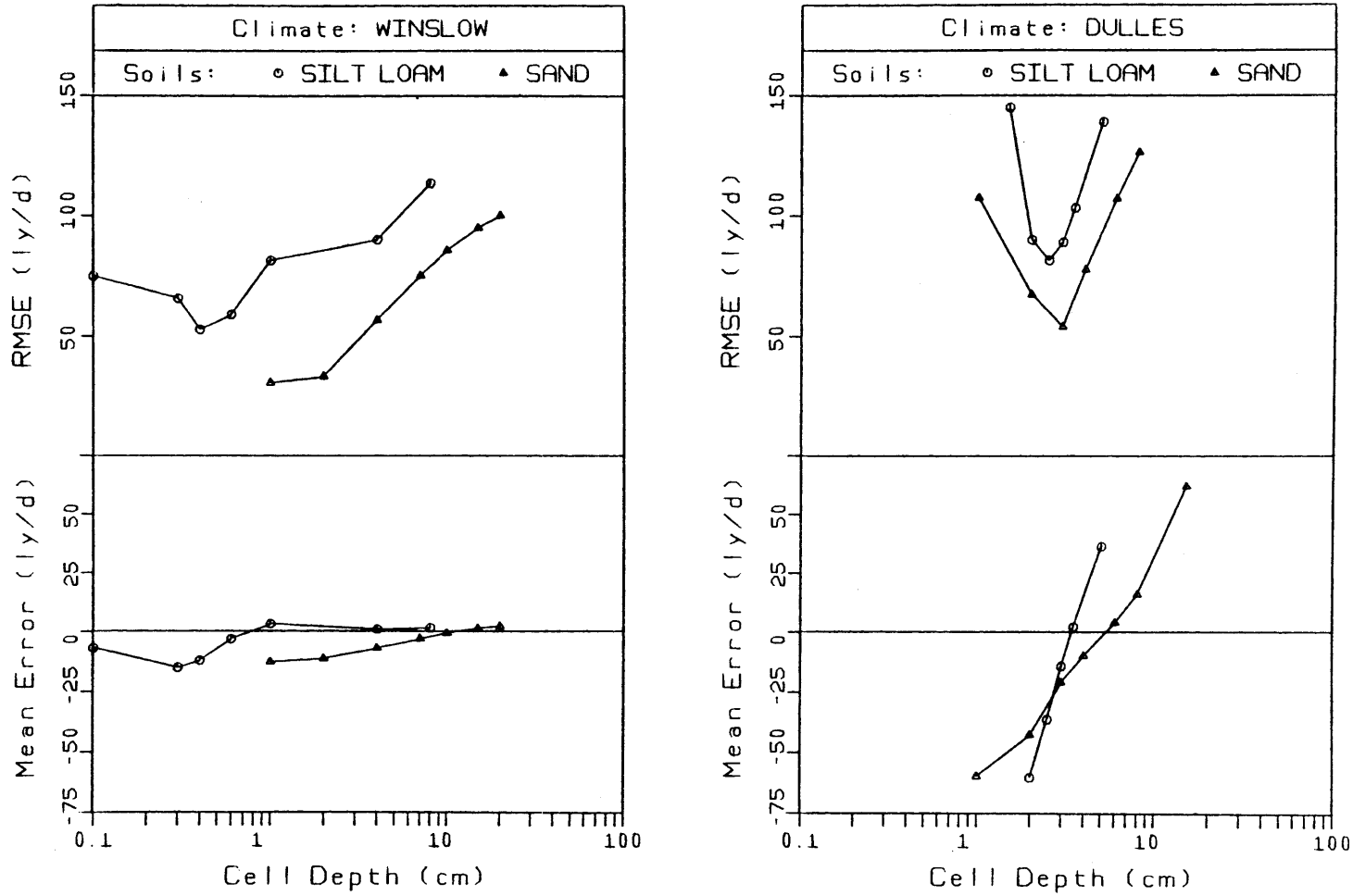

Figure 5.1

COMPUTED ERRORS IN LE AS FUNCTIONS OF THE TOP CELL DEPTH, ℓ_1, USING THE TWO-NODE PARAMETERIZATION (ℓ_2 = 100 cm, PERIODIC FORCING).

	Periodic Forcing			Actual Forcing		
	Actual Average LE (ly/d)	Fitted Cell Depth (cm)	RMSE (ly/d)	Actual Average LE (ly/d)	Mean Error (ly/d)	RMSE (ly/d)
Silt loam/Winslow	59	0.8	70	43	-10	66
Sand/Winslow	57	10	86	42	0	79
Silt loam/Dulles	170	3.5	103	171	-35	76
Sand/Dulles	189	5	100	70	26	126

Table 5.1

SUMMARY OF ERRORS IN LE ASSOCIATED WITH THE TWO-NODE PARAMETERIZATION

(ℓ_2 = 100 cm)

time distribution of evaporation matches that of the reference model.

The calculated major components of the surface heat balance are shown as functions of time in Figures 5.2 and 5.3 for the sand at Winslow. Vertical bars at the bottom of each picture indicate the occurrence of rain. Relatively speaking, the calculations of net radiation, heat flux into the ground, and sensible heat flux into the atmosphere, all dependent mainly on surface temperature, are simulated well, in contrast to the evaporation, which is controlled by the soil moisture supply. (In fact, evaporation is also predicted well while under atmospheric control, i.e., on the falling curves shortly after the rains on days 1, 5, and 9.) This implies that the force-restore procedure is doing a good job predicting surface temperature, while the moisture parameterization is less accurate. This result was observed consistently with all of the models. Henceforth, we shall present plots only of the critical evaporative heat fluxes.

Before leaving the sand/Winslow example, we note (Fig. 5.3) the behavior of the error in predicted evaporation as a function of time. With the parameterization, the surface dries later than in the reference model, as evidenced by the higher peak evaporation during days 2, 6, and 10 after the rain. Once it dries, however, evaporation rates calculated by the parameterization fall much more rapidly,

yielding lower evaporation on the dry days. This transition from high to low evaporation corresponds to a change from free evaporation from the top cell to soil-controlled exfiltration by diffusion from the lower cell. The out-of-phase behavior of LE during the dry periods has already been noted in Chapter 3, where it was shown to result from our neglect of the flow of water due to thermal gradients.

The time variation of evaporation for another scenario, the silt loam at Dulles, is shown in Figure 5.4. During the second day after the rain, evaporation becomes soil-limited in the reference model, and the peak rate is halved on the third day. In the parameterization, the transition from atmosphere- to soil-control is more abrupt, as seen in the falling curves on days 4, 7, and 10. This rapid decline is similar to that observed in the sand/Winslow case. On the hourly time scale, this appears to be a consistent feature of this parameterization.

Using the cell depths determined to fit the periodic forcing sequences with zero mean error, we have simulated the moisture and heat balances of the two soils given the month of actual hourly weather data at both sites. The resulting errors are tabulated in columns 4 through 6 of Table 5.1, together with the actual average LE. Significant errors in the mean are apparent. This suggests that a single cell depth cannot be consistently defined,

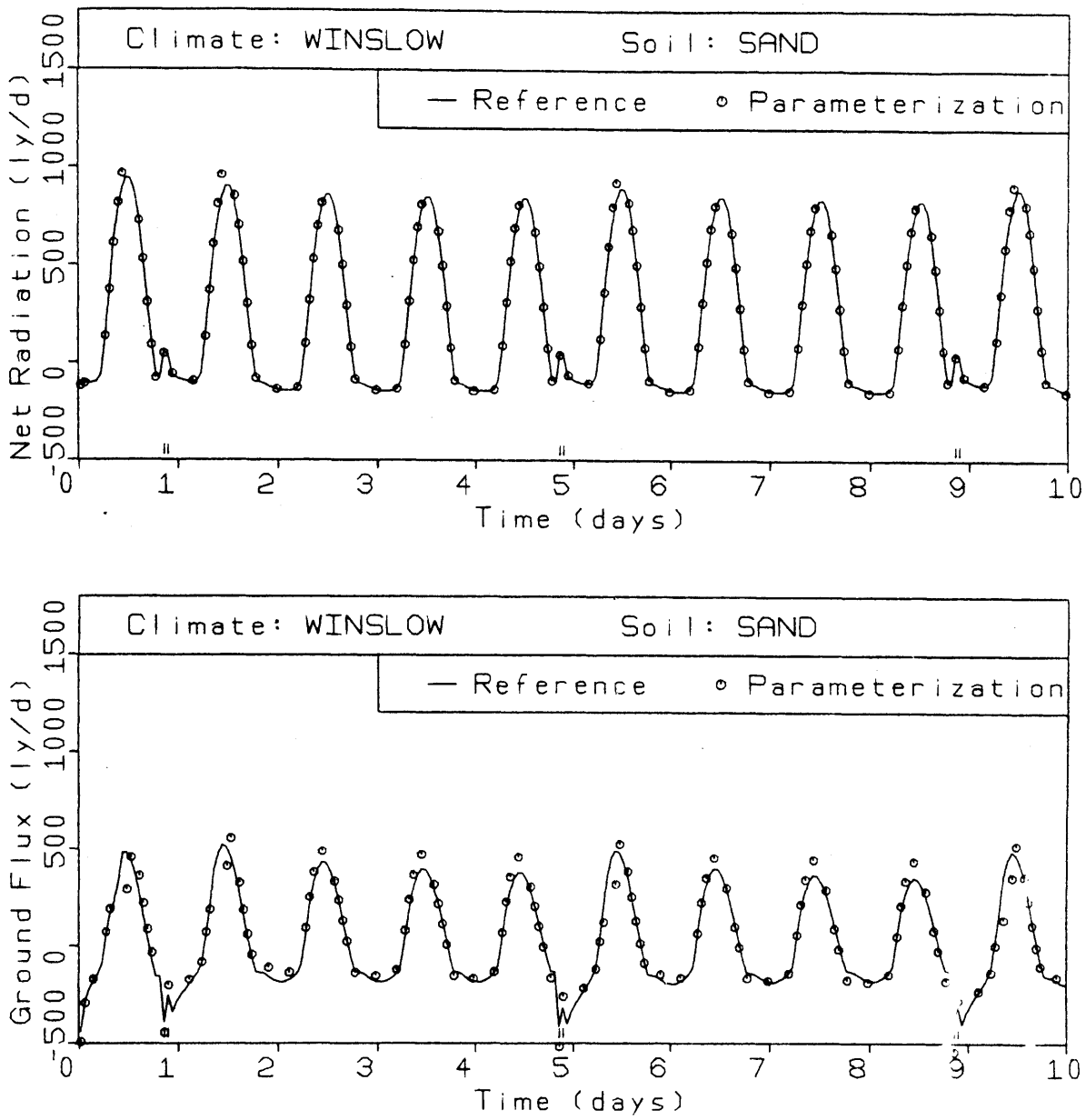

Figure 5.2

COMPARISONS OF NET RADIATION AND GROUND HEAT FLUX COMPUTED BY THE REFERENCE MODEL AND BY THE TWO-NODE PARAMETERIZATION. SAND, PERIODIC WINSLOW SCENARIO, ℓ_1 = 10 cm, ℓ_2 = 100 cm

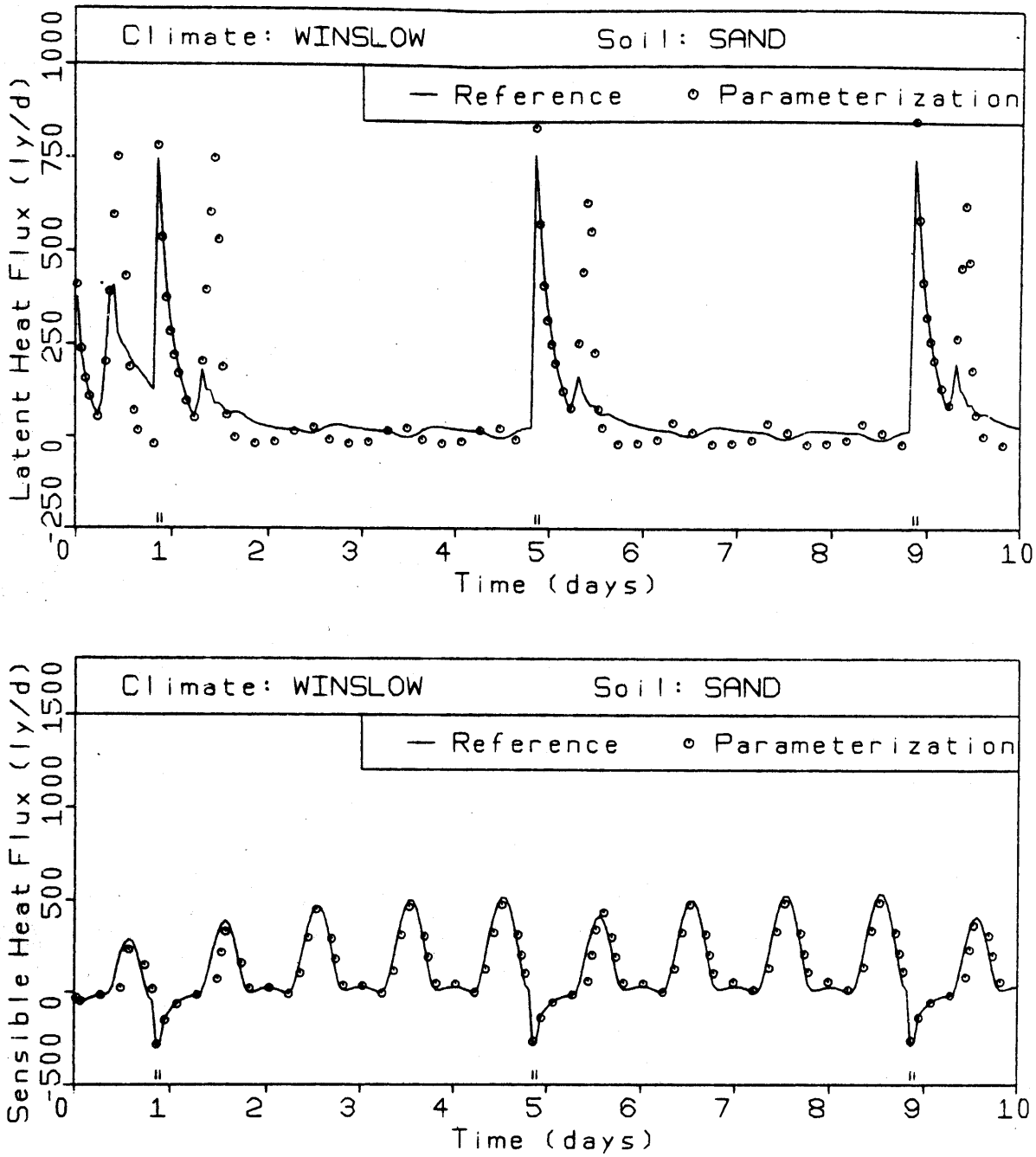

Figure 5.3

COMPARISONS OF LATENT AND SENSIBLE HEAT FLUXES COMPUTED BY THE REFERENCE MODEL AND BY THE TWO-NODE PARAMETERIZATION. SAND, PERIODIC WINSLOW SCENARIO, ℓ_1 = 10 cm, ℓ_2 = 100 cm.

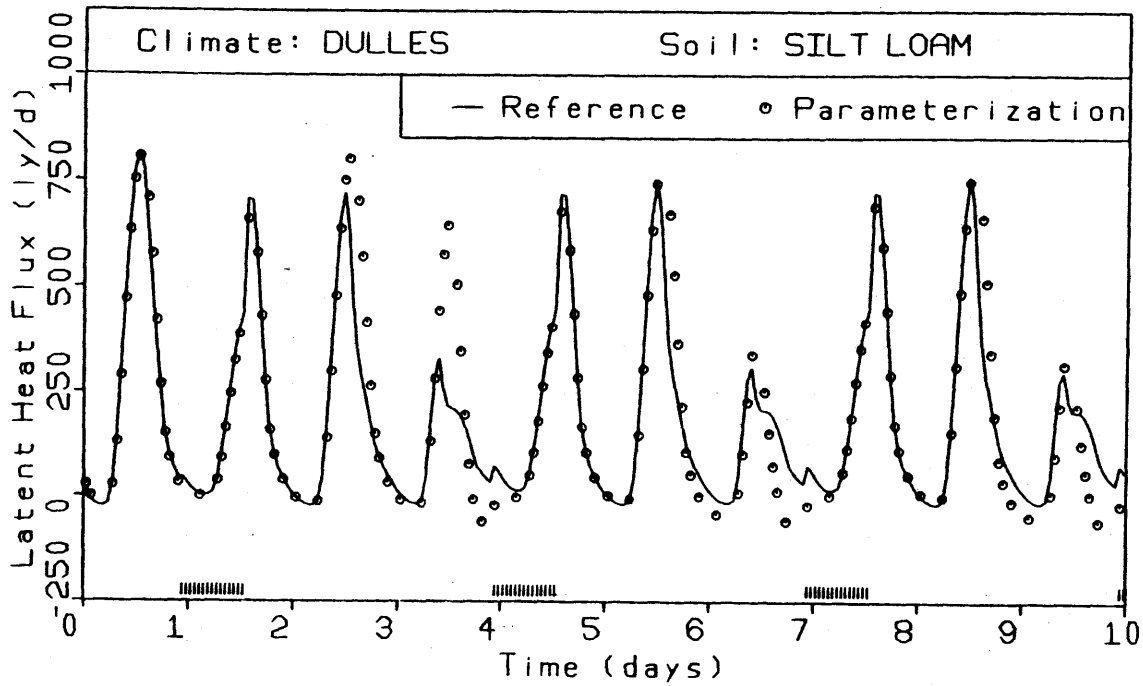

Figure 5.4

COMPARISON OF LATENT HEAT FLUXES COMPUTED BY THE REFERENCE MODEL AND BY THE TWO-NODE PARAMETERIZATION. SILT LOAM, PERIODIC DULLES SCENARIO, ℓ_1 = 3.5 cm, ℓ_2 = 100 cm.

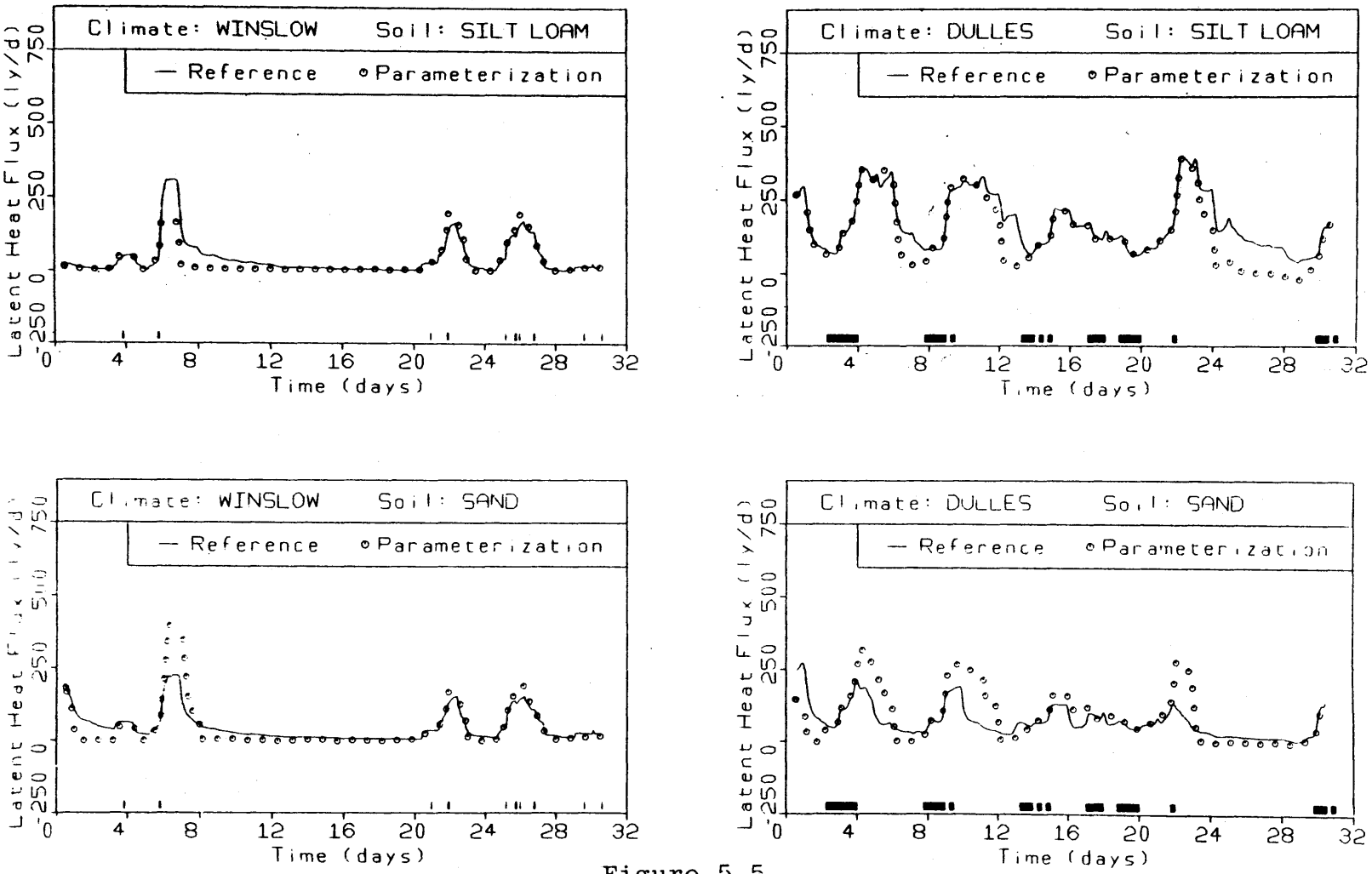

Figure 5.5

COMPARISONS OF LATENT HEAT FLUXES COMPUTED BY THE REFERENCE MODEL AND BY THE TWO-NODE PARAMETERIZATION. ACTUAL WEATHER DATA AS INPUT. CELL DEPTHS AS OPTIMIZED FOR PERIODIC FORCING.

even for a given soil/climate pair.

The time variation of evaporation for the 31-day sequences are shown in Figure 5.5. The data have been snoothed by applying a 25-point ($\sim$ 1 day) moving average to the hourly values. As a consequence, the short-term discrepancies noted in Figures 5.3 and 5.4 are not apparent, though they are still there. At Winslow the evaporation after the second (and deepest) storm is underpredicted for the silt loam and overpredicted for the sand. For the silt loam at Dulles, evaporation, which is mostly at the potential rate, is well estimated until it comes under soil-control during the dry period at the end of the month, at which time the parameterization underpredicts evaporation. For the sand at Dulles, the availability of moisture for evaporation is grossly overestimated.

In its present form, this moisture parameterization, essentially a super-coarse-grid finite difference model, has little predictive value. Furthermore, even when a given data sequence is fitted to the model, the fit is imperfect, as illustrated in Figures 5.3 and 5.4.

5.3 The One-Cell Model with Nonlinear Diffusion

Figure 5.6 illustrates the sensitivity of the mean evaporation and the RMSE of hourly LE to the cell depth. In all cases, the total evaporation first increases with increasing cell size, indicating increased capacity of the

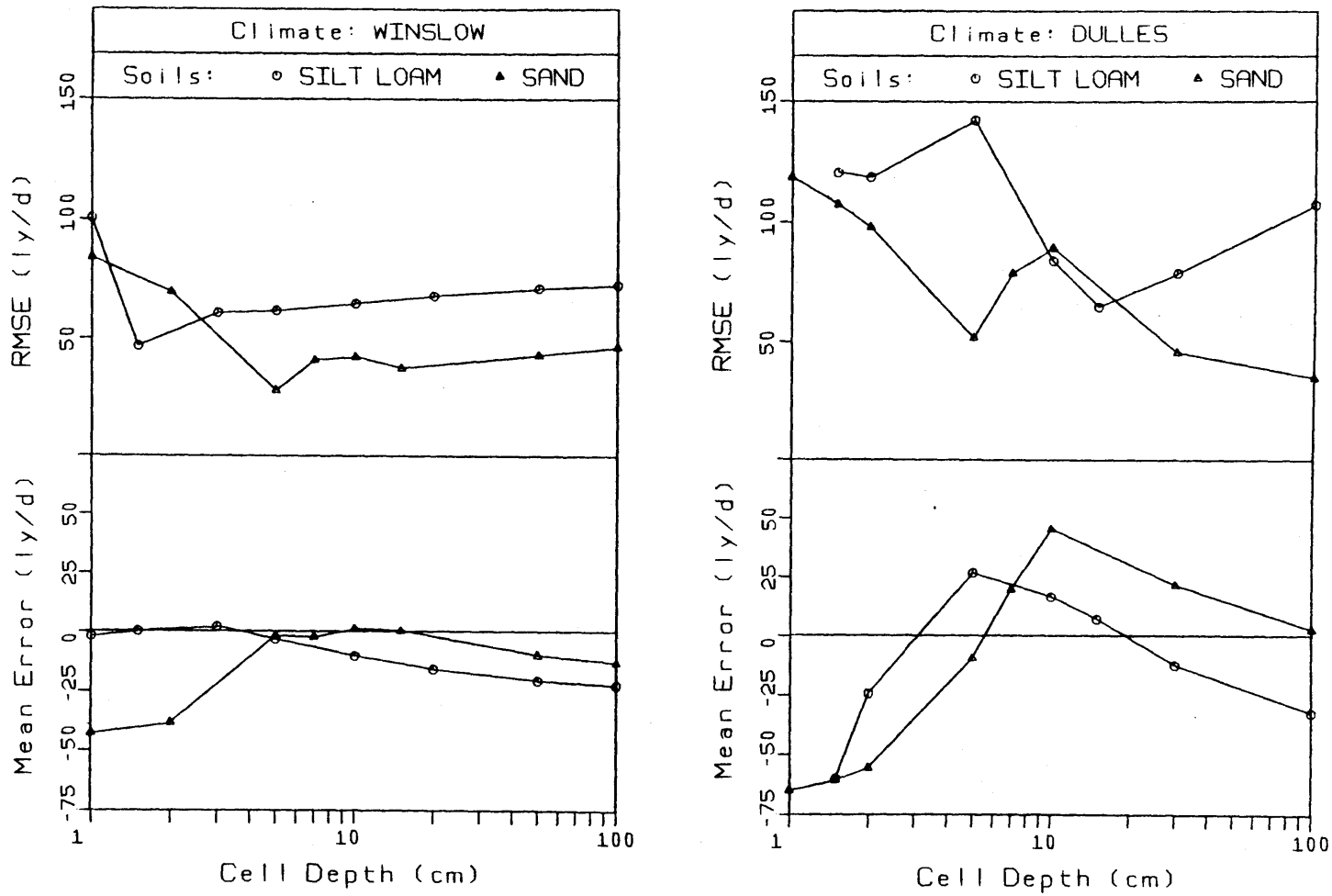

Figure 5.6

COMPUTED ERRORS IN LE AS FUNCTIONS OF THE CELL DEPTH, Z, USING THE ONE-CELL DIFFUSION MODEL. PERIODIC FORCING.

cell to hold rainwater for later evaporation. As the cell size is increases further, the capacity becomes more than sufficient to hold the water. Rain then results in smaller increased of moisture content, so desorptivities and total evaporation decrease.

In general, then, there are two cell sizes at which the mean LE is correctly predicted. The smaller corresponds to a situation where the evaporation is limited by the physical depth of the cell, while the larger corresponds to a limit due to desorptivity. The larger is therefore the one corresponding to physical reality.

Table 5.2 lists the larger cell depths for which the mean error in LE is zero. Physically, these should approximate the depth to which water redistributes itself within, say, one day after a storm. The values appear to be in agreement with this. The greater storm depth at Dulles causes deeper distribution for both soils, as does the higher permeability of the sand for both climates.

The fit of this parameterization to the reference model is remarkably better than the fit of the two-node parameterization, as can be seen by comparing RMSE's in the third columns of Tables 5.1 and 5.2.

Figure 5.7 shows the evaporation for the sand/Winslow scenario. Overall, the parameterization performs well. The structure of the error is significant, however.

	Periodic Forcing			Actual Forcing		
	Actual Average LE (ly/d)	Fitted Cell Depth (cm)	RMSE (ly/d)	Actual Average LE (ly/d)	Mean Error (ly/d)	RMSE (ly/d)
Silt loam/Winslow	59	3.5	60	43	1	64
Sand/Winslow	57	15	37	42	0	55
Silt loam/Dulles	170	20	68	171	-1	64
Sand/Dulles	89	100	35	70	23	50

Table 5.2

SUMMARY OF ERRORS IN LE ASSOCIATED WITH THE ONE-CELL NONLINEAR DIFFUSION PARAMETERIZATION

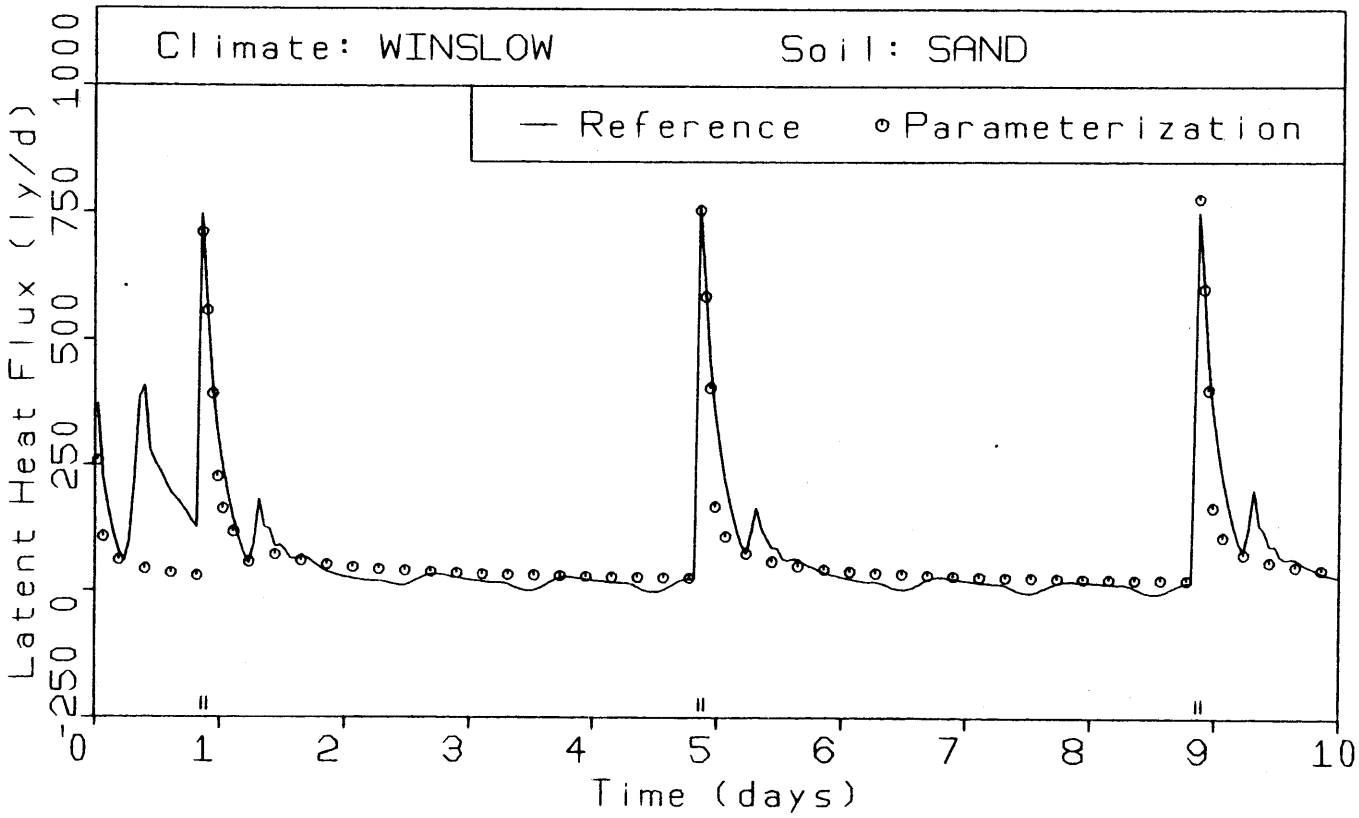

Figure 5.7

COMPARISON OF LATENT HEAT FLUXES COMPUTED BY THE REFERENCE MODEL AND BY THE ONE-CELL DIFFUSION PARAMETERIZATION. SAND, PERIODIC WINSLOW SCENARIO, Z = 15 cm.

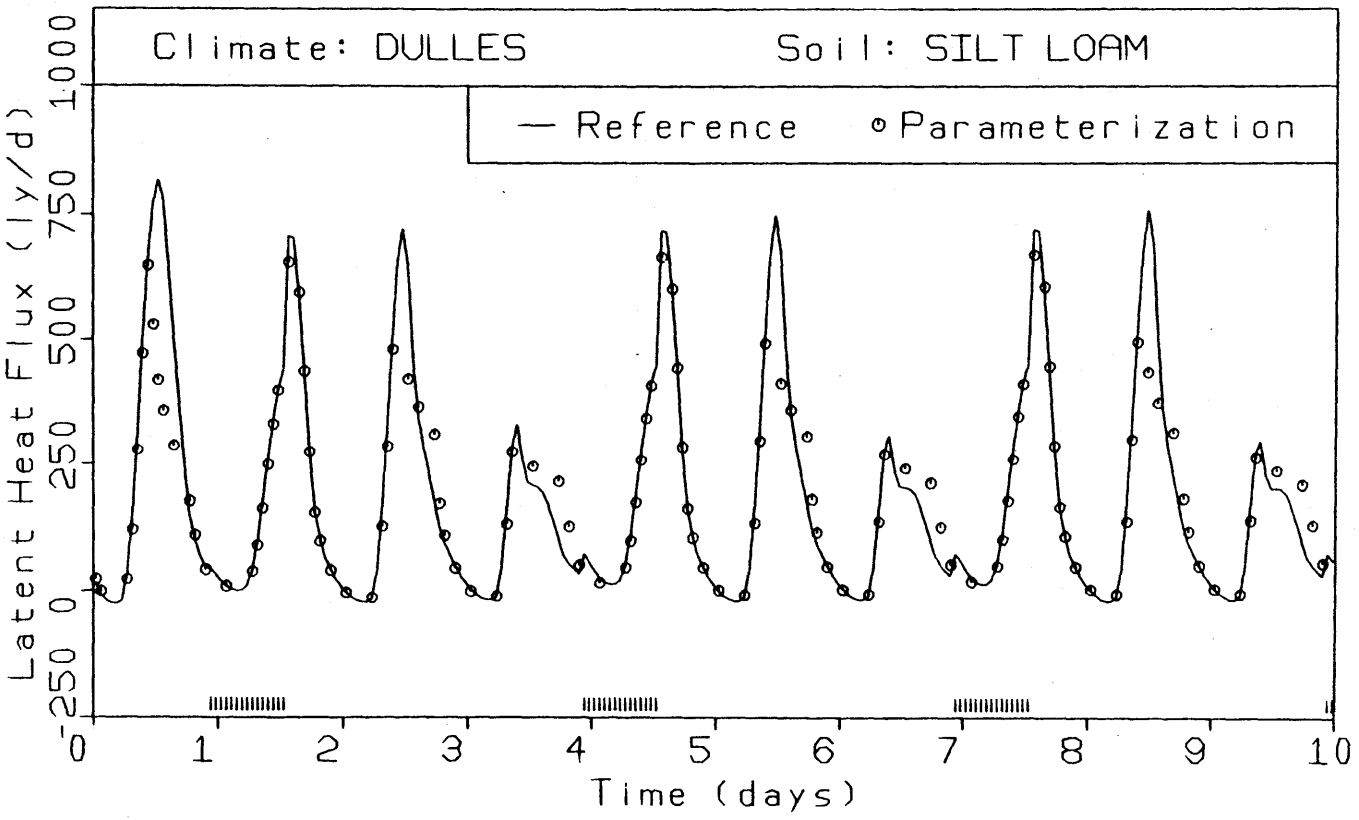

Figure 5.8

COMPARISON OF LATENT HEAT FLUXES COMPUTED BY THE REFERENCE MODEL AND BY THE ONE-CELL DIFFUSION PARAMETERIZATION. SILT LOAM, PERIODIC DULLES SCENARIO, Z = 20 cm.

After a storm, the exfiltration capacity decreases more rapidly than the actual at first, and then more slowly. This may be due to our assumption that desorptivity is a constant throughout an evaporation period. In fact, the near-surface moisture content decreases over time due to redistribution, even in the absence of evaporation. This causes a decrease in the exfiltration capacity that is faster than the F_e^{-1} behavior of the present model.

Evaporation as a function of time for the silt loam/ Dulles scenario is depicted in Figure 5.8. Behavior similar to that just described for Figure 5.7 is seen. Evaporation falls below the potential (and the reference) too early, but then does not fall as fast, say, during the afternoons before the second and third storms. The consistent, though minor, error in the results of this parameterization add support to the argument for a decreasing sorptivity.

Despite the discrepancy in the decay of the exfiltration capacity, this model appears to perform quite well on the whole. In the next chapter, one of our goals will be to parameterize the desorptivity variation in order to improve on this model.

Using the optimized cell depths from the periodic forcing sequences, we calculate evaporation using the month-long weather sequences. The results are tabulated in Table 5.2 and plotted in Figure 5.9. Mean and root-mean-square

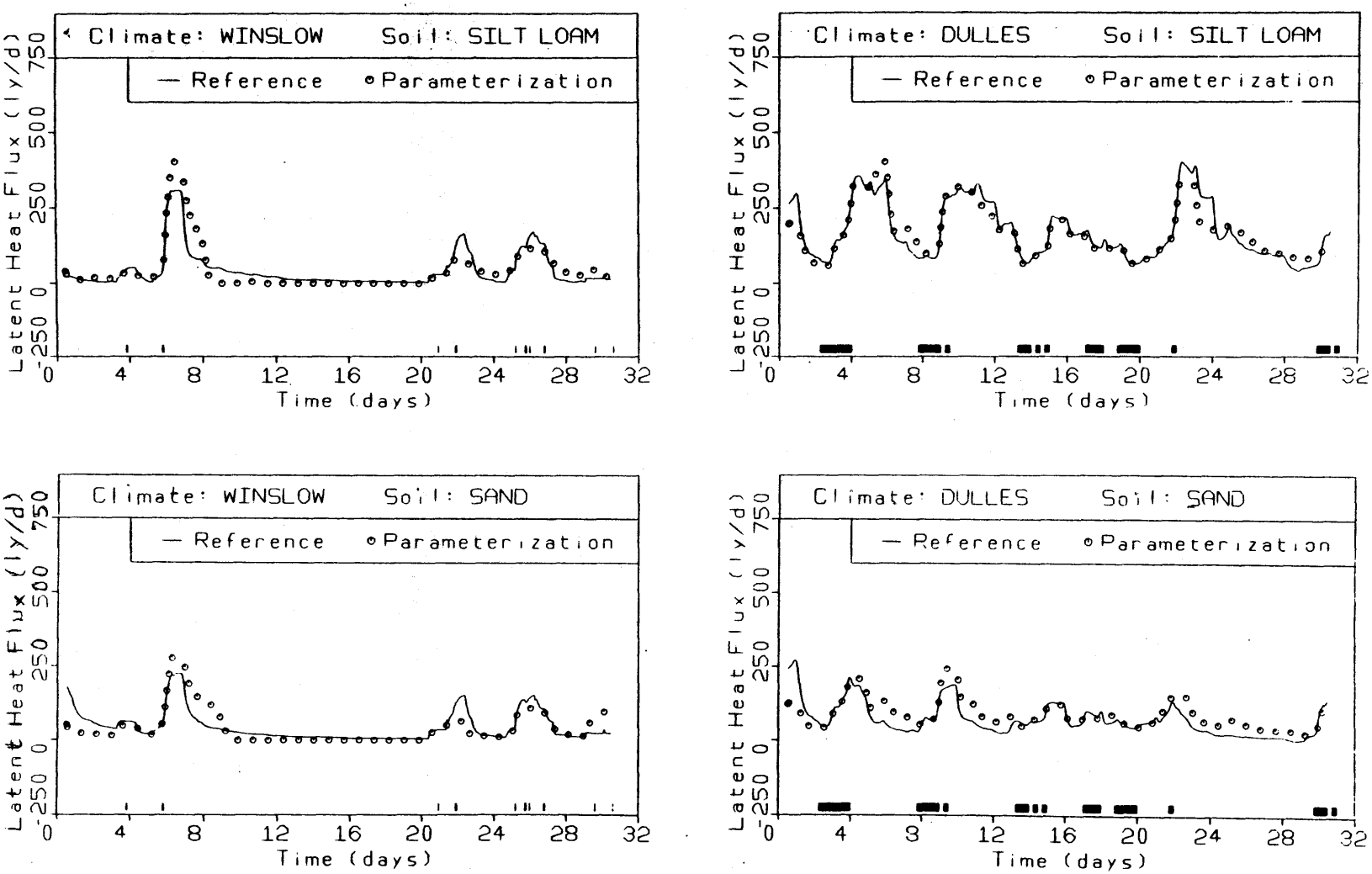

Figure 5.9

COMPARISONS OF LATENT HEAT FLUXES COMPUTED BY THE REFERENCE MODEL AND BY THE ONE-CELL DIFFUSION PARAMETERIZATION. ACTUAL WEATHER DATA AS INPUT. CELL DEPTHS AS OPTIMIZED FOR PERIODIC FORCING.

errors show marked improvement over the two-node model. The mean evaporation from the sand at Dulles, however, is underpredicted by one-third. This is due to the fact that the cell depth which tunes the model to one storm is not the best depth to use for any sequence of forcing. In fact, the optimal depth will vary from storm to storm in a given sequence due to several factors in the forcing, chiefly the rainfall depth and the subsequent time between storms. To account for this variability automatically will be another goal of the next chapter.

5.4 The One-Cell Model with GFDL Hydrology

In Chapter 4, we proposed two methods by which to evaluate the field capacity for use in the GFDL parameterization. Our computations revealed that the better predictions were obtained if the field capacity was considered to be the initial condition determined in Chapter 3. This moisture content is approximately a time-space mean resulting from the interaction of soil and climate. We use that value for the field capacity in this section.

The sensitivity of the LE errors to the cell depth is shown in Figure 5.10 for all periodic scenarios. For Winslow, there is little difference in the initial conditions for the two soils and hence little difference in evaporation. (Recall that no soil properties other than field capacity

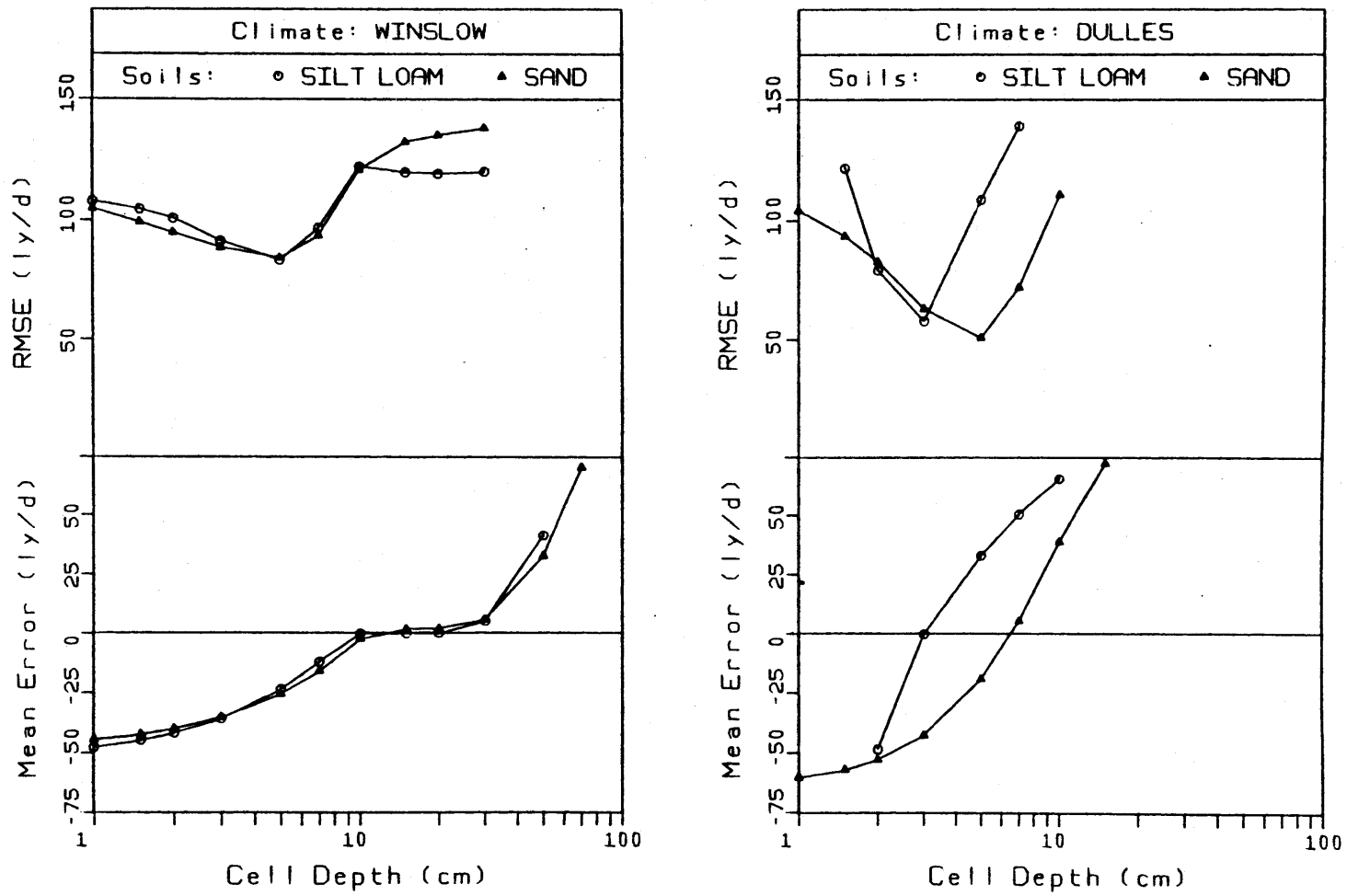

Figure 5.10

COMPUTED ERRORS IN LE AS FUNCTIONS OF CELL DEPTH USING THE GFDL HYDROLOGY MODEL. PERIODIC FORCING.

enter the GFDL parameterization explicitly.) The ledges in the mean error curves at zero error occur where total evaporation approximately equals total precipitation. For smaller cell sizes, runoff occurs when the cell fills, and evaporation then decreases. The increase in evaporation at higher cell sizes is due to an increase in the initial amount of water stored. For the dry Winslow situations, this does not become important until the size becomes large, hence the ledge. For Dulles, the curves are continuous, as the two effects overlap.

The fit of the tuned model to the reference model is uneven. For the Dulles sequences it is good, while it is bad for Winslow. This is reflected by the RMSE values for periodic forcing in Table 5.3, and can be seen also in Figures 5.11 and 5.12. In contrast to the two previous parameterizations, there appears to be no systematic structure to the errors here.

The tuned parameterization is employed to predict evaporation during the months of actual data. The results appear in Table 5.3 and in Figure 5.13. In each case, the evaporation is underpredicted (from 9 to 43 percent). This appears to be a result of tuning the model using an average storm depth. Larger storms then cause excess runoff due to the limited space in the cell, and evaporation is reduced.

	Periodic Forcing			Actual Forcing		
	Actual Average LE (ly/d)	Fitted Cell Depth (cm)	RMSE (ly/d)	Actual Average LE (ly/d)	Mean Error (ly/d)	RMSE (ly/d)
Silt loam/Winslow	59	20	120	43	-5	75
Sand/Winslow	57	13	132	42	-11	80
Silt loam/Dulles	170	3	58	171	-73	148
Sand/Dulles	89	6.5	65	70	-6	54

Table 5.3

SUMMARY OF ERRORS IN LE ASSOCIATED WITH THE ONE-CELL GFDL HYDROLOGY PARAMETERIZATION

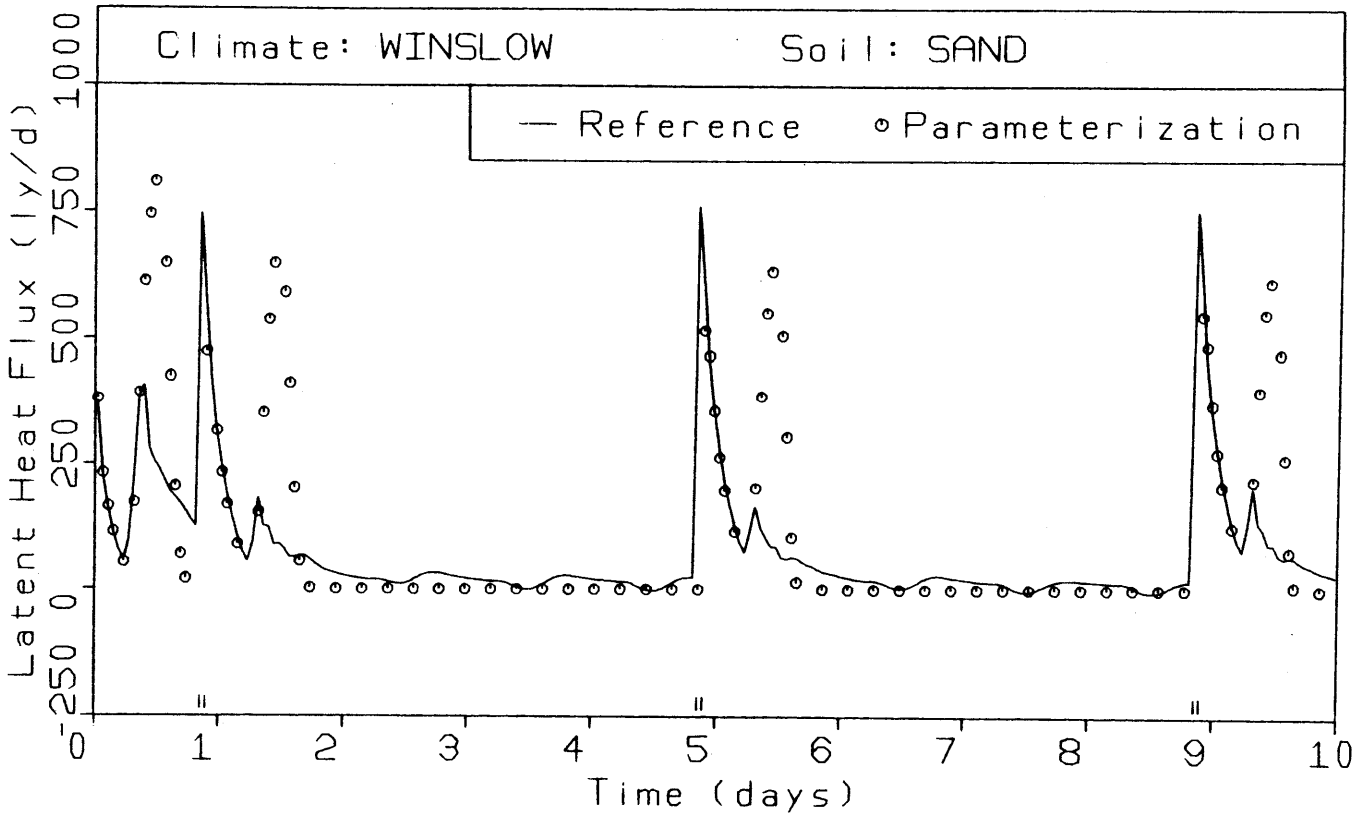

Figure 5.11

COMPARISON OF LATENT HEAT FLUXES COMPUTED BY THE REFERENCE MODEL AND BY THE GFDL PARAMETERIZATION. SAND, PERIODIC WINSLOW SCENARIO, Z = 13 cm.

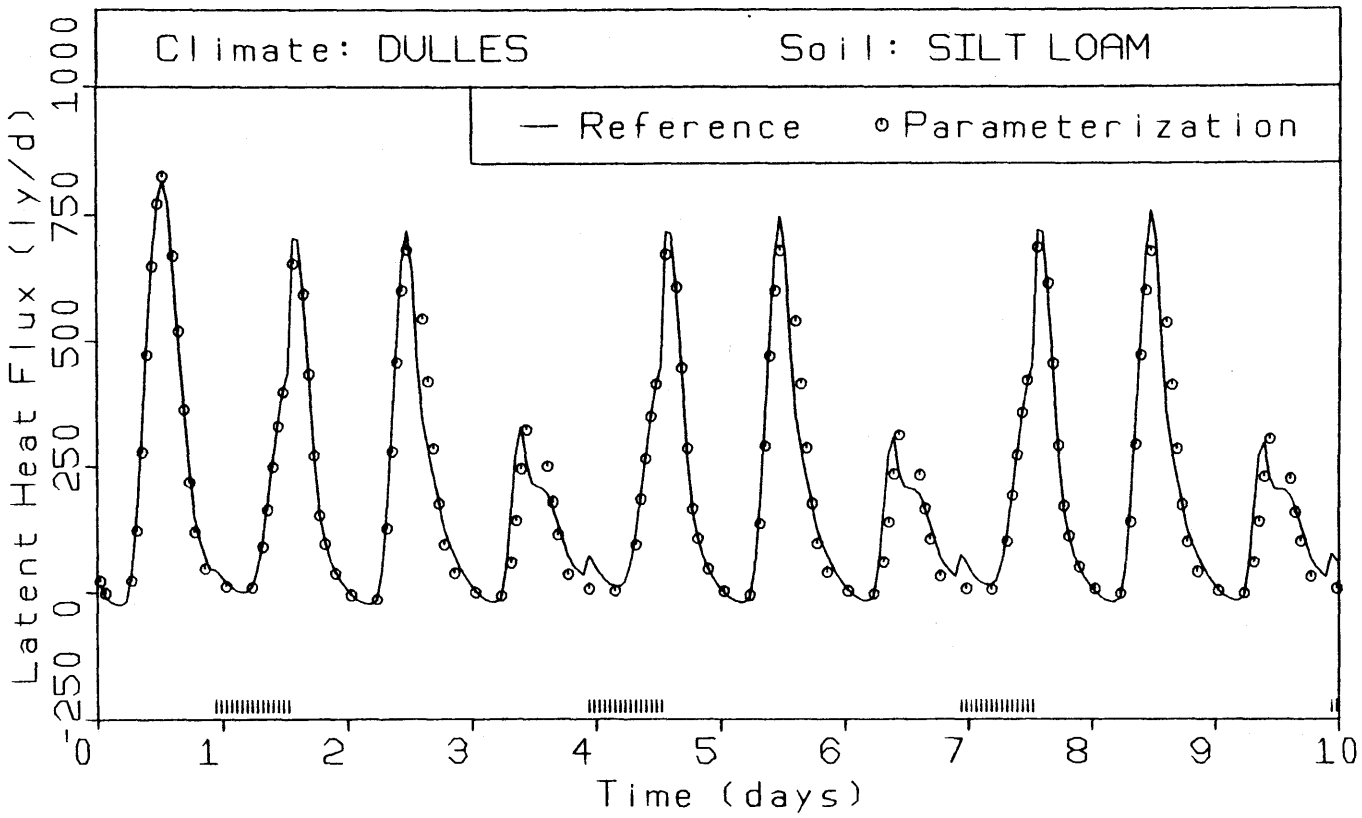

Figure 5.12

COMPARISON OF LATENT HEAT FLUX COMPUTED BY THE REFERENCE MODEL AND BY THE GFDL PARAMETERIZATION. SILT LOAM, PERIODIC DULLES SCENARIO, Z = 3 cm.

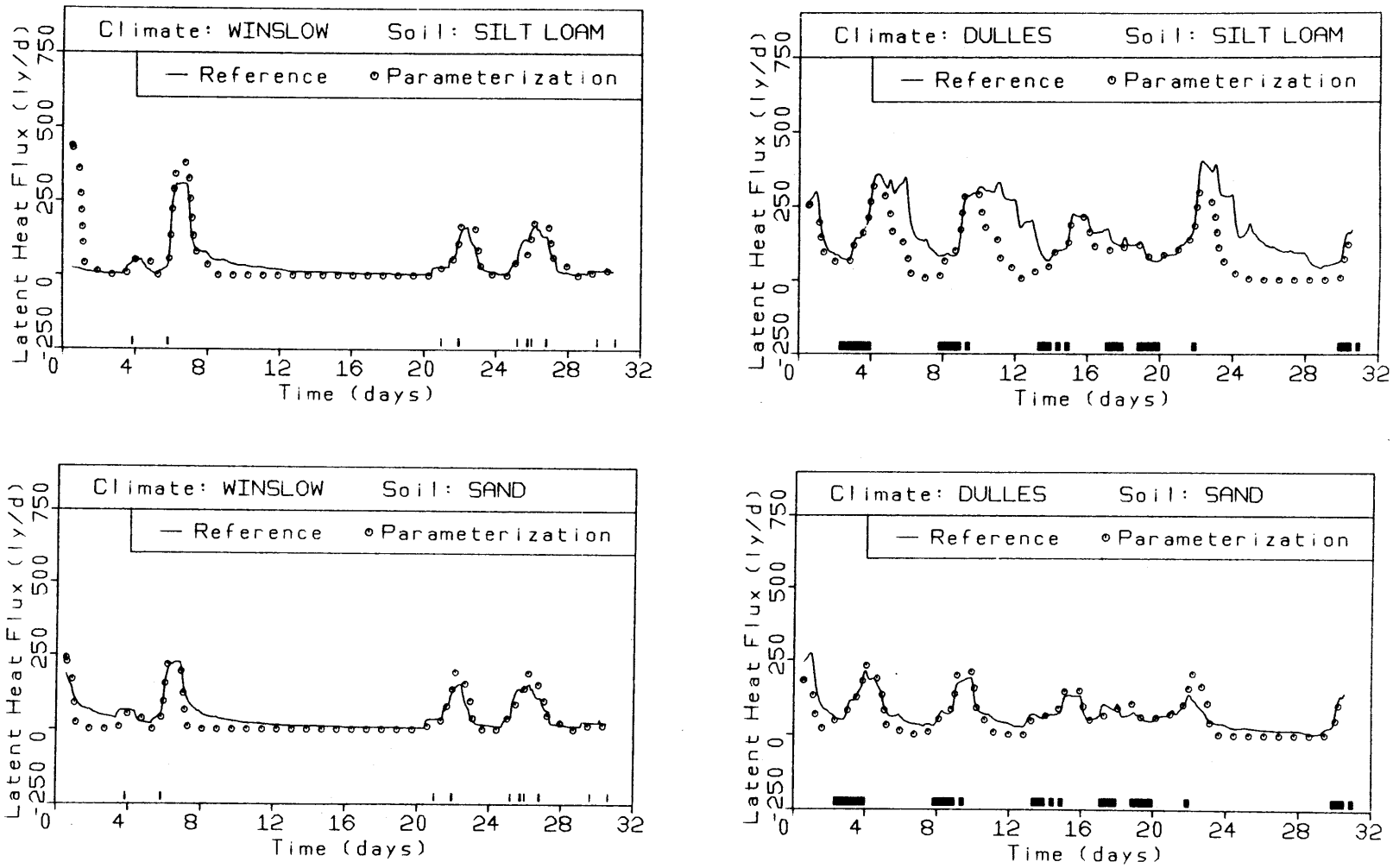

Figure 5.13

COMPARISONS OF LATENT HEAT FLUXES COMPUTED BY THE REFERENCE MODEL AND BY THE GFDL PARAMETERIZATION. ACTUAL WEATHER DATA AS INPUT. CELL DEPTHS AS OPTIMIZED FOR PERIODIC FORCING.

5.5 Summary and Conclusions

Three models of soil moisture have been tested, in conjunction with the force-restore temperature scheme, against the reference model. In the first stage of evaluation, the parameterizations are tuned by variation of a storage cell depth in order to match total evaporation. With the two-node model, the resulting time variation of evaporation differs consistently in structure from the actual series. The virtual neglect of the depth variability of soil moisture content leads to an initial period of drying of the surface cell at the potential rate, followed by a period of minimal flow from below to the surface. The model does not allow for a gradual transition between the two.

The tuned evaporation sequences from the one-cell nonlinear diffusion model give improved fits to the reference data. This is because the basic diffusion solution underlying the parameterization is realistically based on the physics. A second-order error appears in the tuned sequences, however, apparently resulting from the neglect of soil moisture redistribution between storms. An interesting feature of this parameterization is that the mean evaporation can be fitted by two distinct cell sizes, of which only the larger is arguably realistic physically.

Evaporation predictions for the tuned sequences of the GFDL parameterization are uneven in quality. There seems

to be no simple structure to the errors. The optimal cell depth for the tuned sequences ranges from 3 to 20 cm, significantly less than the value of one meter currently applied in that parameterization for climate predictions.

A common problem affects all three parameterizations when we attempt to use the cell depth obtained from one set of data to predict evaporation for another set. Apparently, the cell depth is sufficiently sensitive to the forcing, and the forcing is sufficiently variable, to make such a parameterization, using a fixed cell depth, inaccurate. The results of the nonlinear diffusion model showed this the least. Due to the structure of the GFDL model, evaporation under random forcing is underpredicted using a cell depth corresponding to the average forcing. In the next chapter, a modification of the nonlinear diffusion model is proposed in an attempt to get around the problem of defining the cell depth. The nonlinear diffusion model will be chosen, not only because its predictions so far are the best, but also because its physical formulation provides a sound framework for the estimation of a dynamic cell depth.

The force-restore parameterization of ground surface temperature performed well in conjunction with all of the moisture parameterizations. Clearly, its level of accuracy equals or exceeds that of any of the moisture models. This justifies a focus of attention on the hydrology, whose

mathematical complexity requires a more sophisticated model in order to achieve the same level of accuracy as for heat.

Chapter 6

INCORPORATION OF REDISTRIBUTION IN THE ONE-CELL NONLINEAR DIFFUSION MODEL

6.1 Introduction

In the previous chapter, we found that even the best of the three proposed moisture parameterizations, the nonlinear diffusion model, has the drawback that it must be tuned through optimization of the cell depth. Furthermore, the optimal cell depth undoubtedly varies from storm to storm, even for a given soil in a given climate. Another minor, yet consistent, idiosyncracy of that parameterization is the slow decay of the exfiltration capacity computed by it, relative to the reference model. This has been seen in Figures 5.8 and 5.9. In this chapter, we incorporate a sub-parameterization of the soil moisture redistribution process into this model, explicitly addressing both of the above-mentioned issues.

6.2 Theoretical Formulation

We employ here the basic theoretical framework of the nonlinear diffusion parameterization outlined in Section 4.3.2. The exception is that we employ a new procedure for the calculation of $\bar{\theta}$, the near-surface soil moisture content, instead of using (4.30). Let us suppose that a storm has just ended. We have calculated the total infiltration, F_i,

during that storm using (4.31), (4.33), and (4.35). We hypothesize that $\bar{\theta}$, immediately following the storm, has the value that would have caused the total infiltration to equal F_i if the surface moisture content were held at $\bar{\theta}$ throughout the storm. The solution of the gravity-affected nonlinear diffusion equation for infiltration into a dry medium, with surface moisture content $\bar{\theta}$, is approximated by (Eagleson, 1978)

$$\frac{dF_i}{dt} = A_o(0,\bar{\theta}) + \frac{1}{2} S_i(0,\bar{\theta})\ t^{-1/2} \qquad (6.1)$$

or

$$F_i(t_r) = A_o(0,\bar{\theta})\ t_r + S_i(0,\bar{\theta})\ t_r^{1/2} \qquad (6.2)$$

where A_o and S_i have already been defined in (4.37) and (4.38), and t_r is the storm duration. Given F_i and t_r, we can solve (6.2) to obtain $\bar{\theta}$, the near-surface soil moisture content.

If wished only to avoid the specification of a cell depth, we might stop at this point, since we have obtained a value for $\bar{\theta}$ without using a prediction equation involving Z. However, if we wish to parameterize the redistribution process, it is useful to re-introduce Z. We view Z as the depth of soil wetted to moisture content $\bar{\theta}$ as a result of infiltration during the preceding storm. If we view the wetting front as a square wave advancing into a dry medium, then

$$Z = F_i / \bar{\theta} \qquad (6.3)$$

In fact, the wetting front will not always be so sharp, but this assumption is probably adequate. Also, there may be moisture already in storage at the surface, in which case Z will be greater than predicted by (6.3). Tests of the parameterization, using reasonable alternatives to (6.3), revealed that Z the parameterization is not sensitive to the assumption regarding initial moisture content.

We have re-introduced Z so that it may be used to scale a new prediction equation for $\bar{\theta}$, this one based on the concept of soil moisture redistribution. Given the initial values of $\bar{\theta}$ and Z immediately following a storm, we model their subsequent evolution over time by

$$Z \frac{d\bar{\theta}}{dt} = - g(\bar{\theta}) \qquad (6.4)$$

where $g(\bar{\theta})$ is some function to be defined, in conjunction with (6.3). This formulation accounts for the persistence of the square-wave shape, the attenuation of its magnitude, and the consequent deepening of its penetration depth.

The function $g(\bar{\theta})$ should parameterize the effects of gravity and of capillary diffusion in transporting water downward following a rain. A truly physically-based formulation of $g(\bar{\theta})$ in terms of nonlinear diffusion is difficult because both sorption and desorption are occurring simultaneously and because the boundary separating these two

processes is moving. We shall therefore adopt an alternative conceptual sub-parameterization. Noting the predominant role of the hydraulic conductivity in both diffusion and gravity drainage of soil moisture, we scale the redistribution function $g(\bar{\theta})$ by the hydraulic conductivity,

$$g(\bar{\theta}) = RK(\bar{\theta}) \tag{6.5}$$

where R is assumed to be a constant. We shall call it the redistribution parameter. The value of (6.5) will depend on the degree of constancy of R for various forcing and soil types. In essence, we have substituted one conceptual parameter -R- for another - the Z used in Section 4.3 - with the expectation that the former will prove to be more stable than the latter. Ideally, a single, "universal" value for R would exist, and it would thereby cease to be a true "parameter."

Substitution of (6.3) and (6.5) into (6.4) yields

$$\frac{d\bar{\theta}}{dt} = - \frac{R\bar{\theta}K(\bar{\theta})}{F_i} \tag{6.6}$$

In order to estimate $\bar{\theta}$, then, throughout an interstorm period, we calculate an initial value using (6.2) and then update it periodically (we use a one-hour time step) by integrating (6.6). Figure 6.1 depicts the interstorm dynamics of $\bar{\theta}$ and Z.

Our interest in a dynamic $\bar{\theta}$ stemmed from the need for a desorptivity that decreases over time. Each time step,

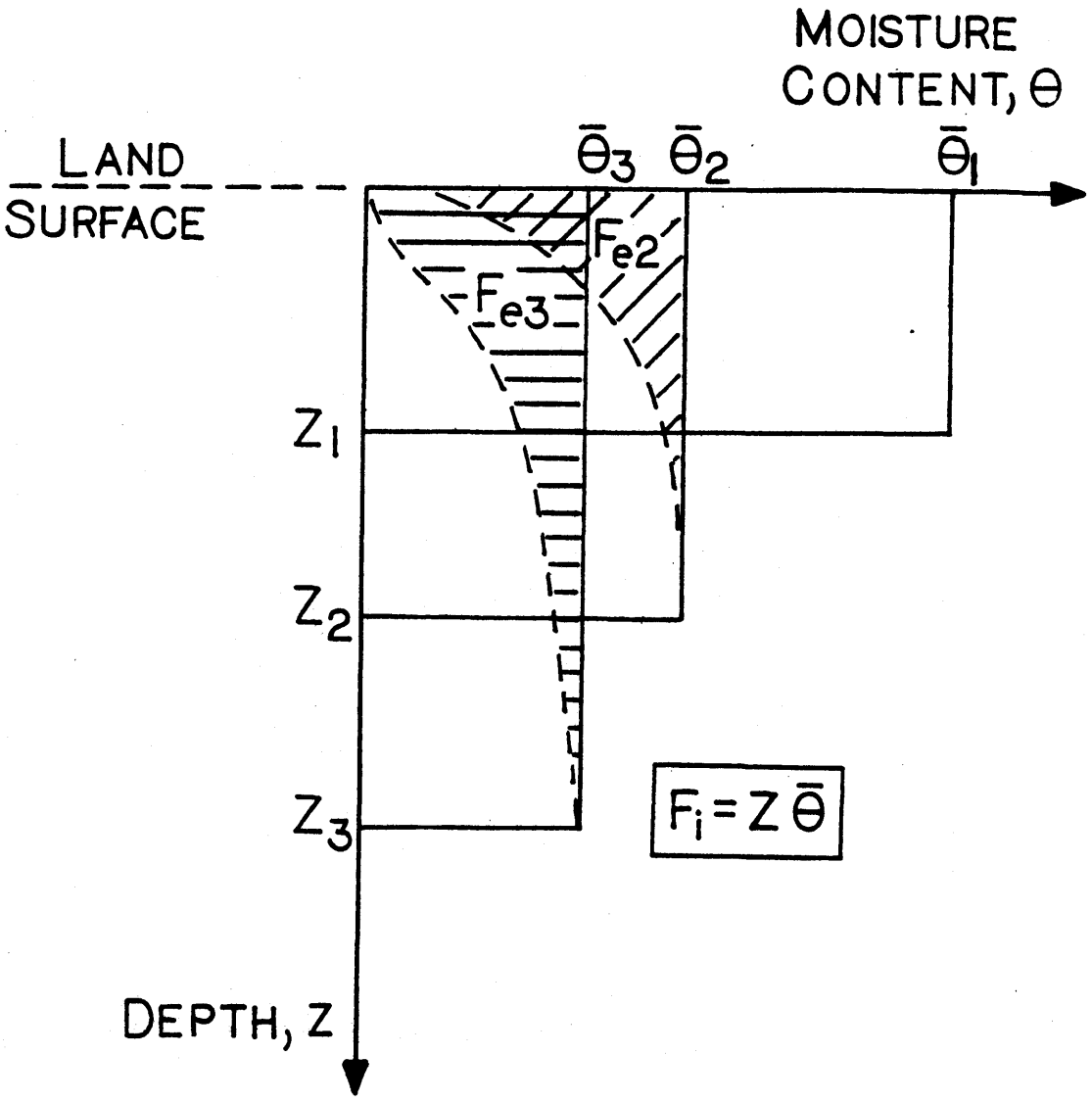

Figure 6.1

DYNAMIC SQUARE-WAVE REPRESENTATION OF WETTED SOIL MASS FOLLOWING RAINFALL, AND LOSSES OF MOISTURE (F_{e2} AND F_{e3}) TO EVAPORATION.

we update S_e using the new (smaller) value of $\bar{\theta}$. In order that our time compression procedure yield a continuously decreasing value for f_e^*, we must modify (4.36) to allow the new discontinuity in S_e. We introduce a new variable, F_e', the apparent cumulative exfiltration, and write

$$f_e^* = S_e^2/2F_e' \tag{6.7}$$

Whenever the value of S_e is updated, F_e' is changed, according to

$$(F_e')_{new} = [(S_e)_{new}/(S_e)_{old}]^2(F_e')_{old} \tag{6.8}$$

thereby maintaining continuity of f_e^*. During a time step, F_e' is increased (in analogy to the actual exfiltration depth, F_e) according to

$$\frac{dF_e'}{dt} = E \tag{6.9}$$

In previous parameterizations, we employed a restriction that exfiltration could not exceed the amount of water stored in the cell at the start of an interstorm period. Here we introduce an analogous limitation that evaporation not exceed F_i from the previous storm. Both of these restrictions are necessary in order to apply the diffusion solution for a semi-infinite medium to a problem where the virtual depth of moisture storage is finite. Clearly, however, the restriction

that the cumulative evaporation following a storm be bounded by the infiltration depth of that storm is physically unrealistic. Such an assumption prevents evaporation from occurring when a long, soaking storm is followed by a brief shower. Several improvements to this procedure could be adopted. These include the following:

1. The forcing data could be pre-processed in order to lump the small showers with the more significant storms.
2. The values of $\bar{\theta}$ and Z at the end of an interstorm period could be stored in memory. On the occasion when cumulative evaporation reached previous cumulative values, $\bar{\theta}$ and Z could be re-set to their earlier values and calculations resumed.
3. Equations (6.2) and/or (6.3) could be modified to include information on conditions before the storm, especially if the most recent storm was a small one.

In preliminary testing of this parameterization with the actual weather data for Dulles and Winslow, we found that none of the modifications suggested above was needed, because there was sufficient time between storms and sufficient evaporative potential relative to the maximum storm depth. For Dulles, using the six-hourly records of precipitation,

Sequence Number	Time between Storms (hrs)	Storm Duration (hrs)	Storm Depth (inches)	Ratio of Storm Depth to Previous Storm Depth
1	54	42	1.20	-
2	90	30	1.21	1.0
3	6	6	0.04	0.03
4	90	30	0.25	6.3
5	6	6	0.30	1.2
6	48	24	0.18	0.6
7	18	30	0.93	5.2
8	42	6	0.08	0.09
9	186	18	0.21	2.6
10	6	6	0.12	0.6

Table 6.1

RAINFALL DATA FOR DULLES, VA; MAY 1972

the anticipated problem did arise. The rainfall data for Dulles appears in Table 6.1. The two smallest storms, numbers 3 and 8, resulted in subsequent underprediction of evaporation. Note that both of these follow two of the deepest storms of the month, numbers 2 and 7. Number 3 follows number 2 by only six hours. Both pairs of storms (2/3 and 7/8) stand out when the ratios of consecutive storm depths are calculated, as shown in Table 6.1.

For the calculations to be reported in the next section, we have lumped together the abovementioned pairs of storms. This is the first approach suggested earlier. We also tried the second approach which yielded similar results.

6.3 Evaluation of the Parameterization

We began the evaluation of the earlier parameterizations by showing their sensitivity to the cell depth and by determining an optimal cell depth. Here we perform the analogous exercise for the redistribution parameter, R. The results are plotted in Figure 6.2 and tabulated in Table 6.2. The mean evaporation is predicted well for all scenarios with a value of R near 2. For Winslow, the mean evaporation is insensitive to R (except for the sand with large R) because all precipitation evaporates sooner or later, no matter how deeply the water redistributes itself. For Dulles, increasing redistribution reduces the availability of water at the surface

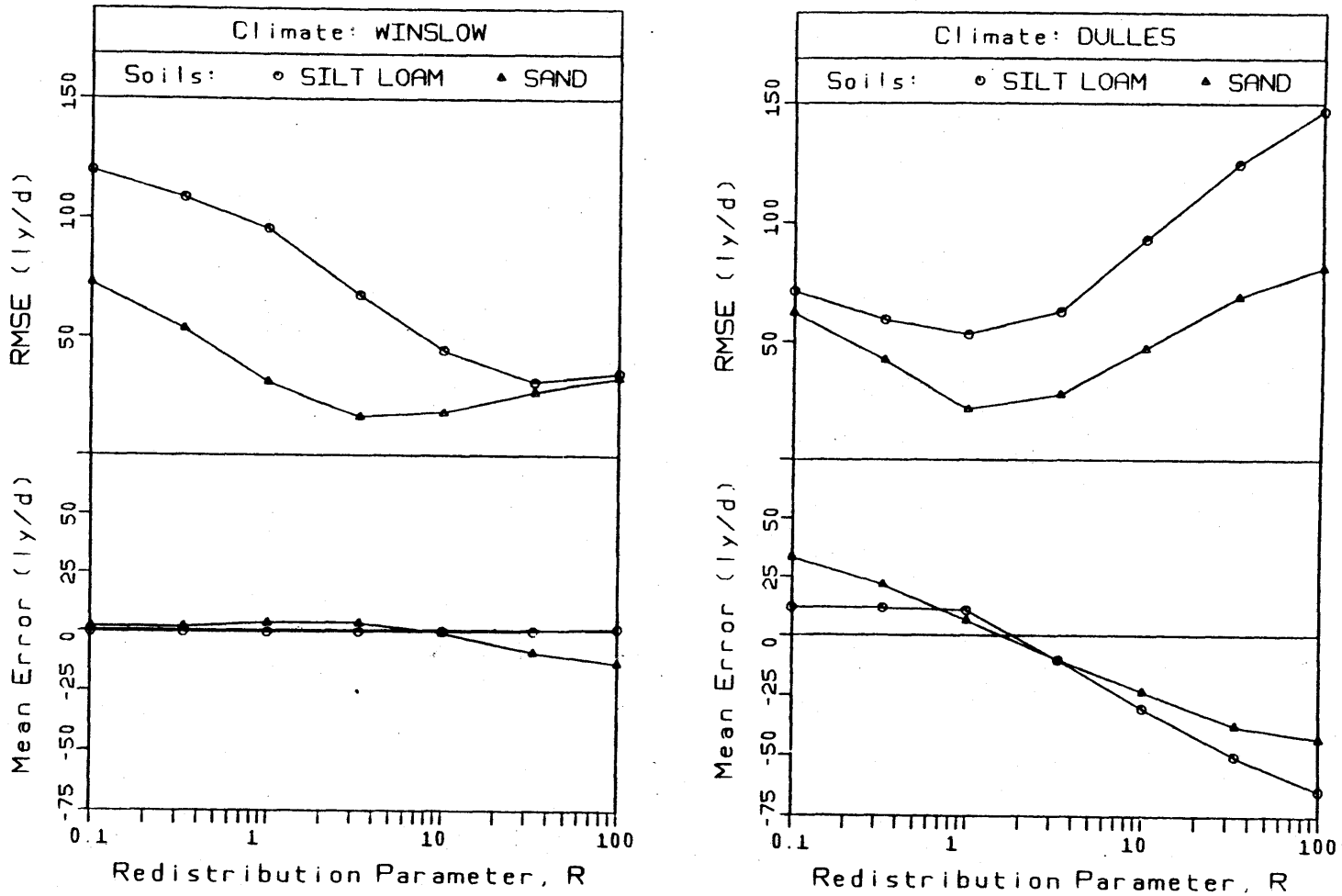

Figure 6.2

COMPUTED ERRORS IN LE AS FUNCTIONS OF THE REDISTRIBUTION PARAMETER, R, USING THE DIFFUSION MODEL WITH THE CELL-DEPTH SUBPARAMETERIZATION.

	Periodic Forcing					Actual Forcing (R = 2)		
	Actual Average LE (ly/d)	Fitted R	RMSE with Fitted R (ly/d)	Mean Error with R = 2 (ly/d)	RMSE with R = 2 (ly/d)	Actual Average LE (ly/d)	Mean Error (ly/d)	RMSE (ly/d)
Silt loam/ Winslow	59	45	32	-1	80	43	0	69
Sand/ Winslow	57	8	18	3	22	42	0	38
Silt loam/ Dulles	170	2	55	0	58	171	-24	100
Sand/ Dulles	89	1.6	20	-2	25	70	6	26

Table 6.2

SUMMARY OF ERRORS IN LE ASSOCIATED WITH THE PARAMETERIZATION PROPOSED IN THIS CHAPTER

and thereby decreases evaporation.

The values of R that yield zero mean error for each scenario are given in Table 6.2. They range from 1.6 and 2 at humid Dulles to 8 and 45 at Winslow. The larger values in each pair correspond to the silt loam, in which we might expect that diffusive redistribution is more important than in the sand. The difference between soils is larger at Winslow, where the drier average initial moisture content before rain should significantly enhance sorption at lower levels.

The RMSE values associated with the optimal R values are all smaller than any of the corresponding RMSE values from the earlier parameterizations (Tables 5.1, 5.2, and 5.3). Previously, the best values were obtained for the nonlinear diffusion model with fixed cell size. The new parameterization, with a dynamic cell size, almost halves the RMSE values for three of the four cases, indicating a very significant improvement in model structure.

The fitted sequences of evaporation are depicted in Figures 6.3 through 6.6. The parameterization clearly performs well in all cases. The results for the sand appear to be slightly better than for the silt loam. At Winslow, evaporation from the silt loam (Figure 6.4) falls off somewhat too slowly during days 2, 6, and 10, then goes to zero rather abruptly. This occurs when the calculated sorptivity is still large enough to allow evaporation, but all of the water from

the last rain has evaporated, so there is no available water left. (Recall our restriction that evaporation not exceed the previous infiltration depth.) In the silt loam at Dulles (Figure 6.5), the evaporation rate becomes soil-limited a little too early, as seen in the lower peaks of the parameterization on days 6 and 9, and does not fall quite so rapidly as the reference data on days 7 and 10. These differences are small, however. The predictions for sand (Figures 6.3 and 6.6) are very good.

We saw in Figure 6.2 and Table 6.2 that there is a wide range in the optimal value of R, the redistribution parameter. Although these differences can be explained, at least qualitatively, in terms of the soil type and climate, a quantitative description of them must account for simultaneous sorption and desorption, and will not be attempted here.

In the interest of maintaining the simplicity of the model structure, it is informative to examine the predictions of the model when a constant, "universal" value of R is used. We choose a value of R that approximately minimizes the mean errors of the four scenarios in a least-squares sense. This value is 2, dictated mainly by the Dulles scenarios, whose mean errors are much more sensitive to R than are the Winslow errors. In Table 6.2 we see that the resulting mean errors are all very small. More interesting is the fact that three of the RMSE values are practically unchanged,

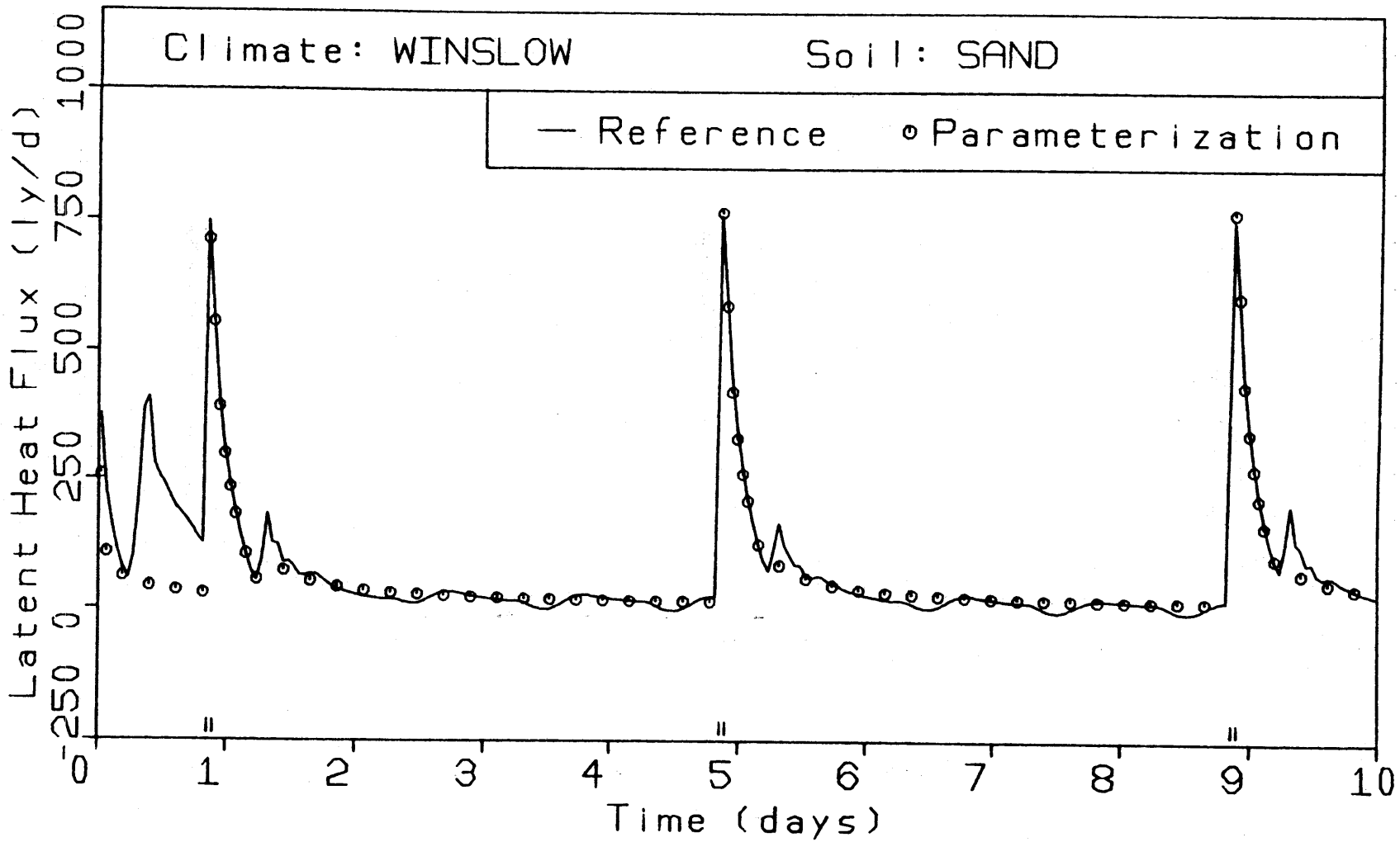

Figure 6.3

COMPARISON OF LATENT HEAT FLUXES COMPUTED BY THE REFERENCE MODEL AND BY THE PARAMETERIZATION. SAND, PERIODIC WINSLOW SCENARIO, R = 8.

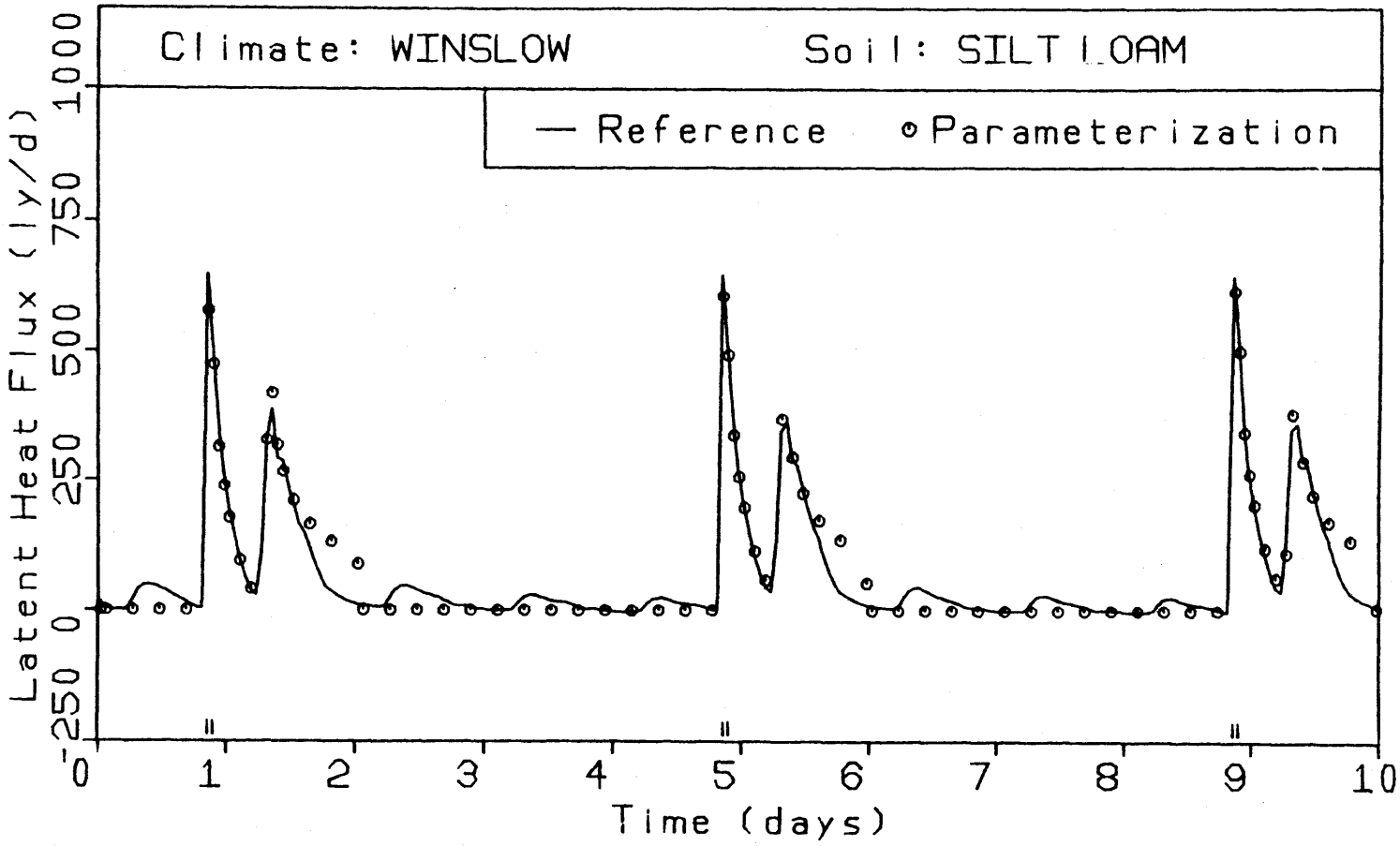

Figure 6.4

COMPARISON OF LATENT HEAT FLUXES COMPUTED BY THE REFERENCE MODEL AND BY THE PARAMETERIZATION. SILT LOAM, PERIODIC WINSLOW SCENARIO, R = 45.

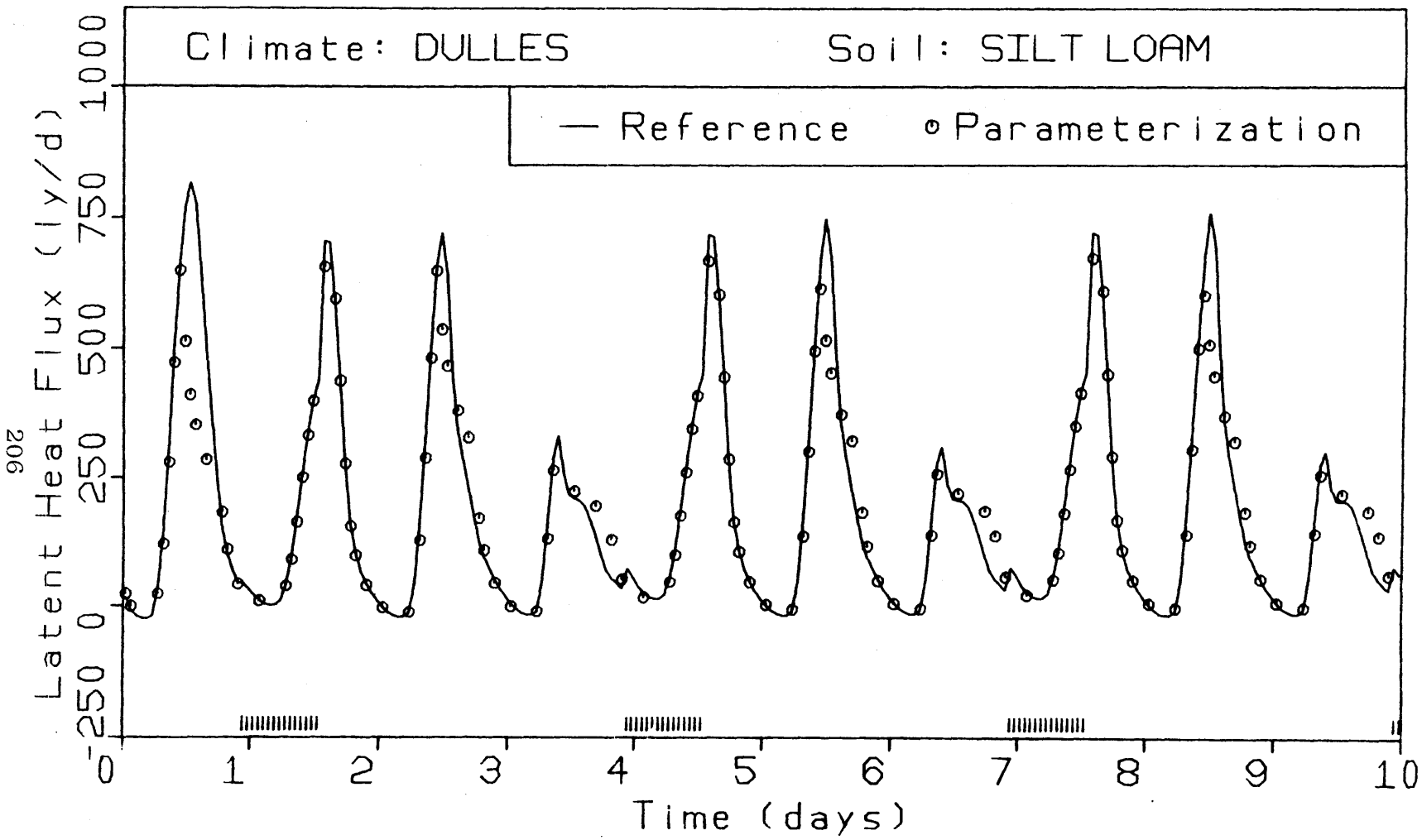

Figure 6.5

COMPARISON OF LATENT HEAT FLUXES COMPUTED BY THE REFERENCE MODEL AND BY THE PARAMETERIZATION. SILT LOAM, PERIODIC DULLES SCENARIO, R = 2.

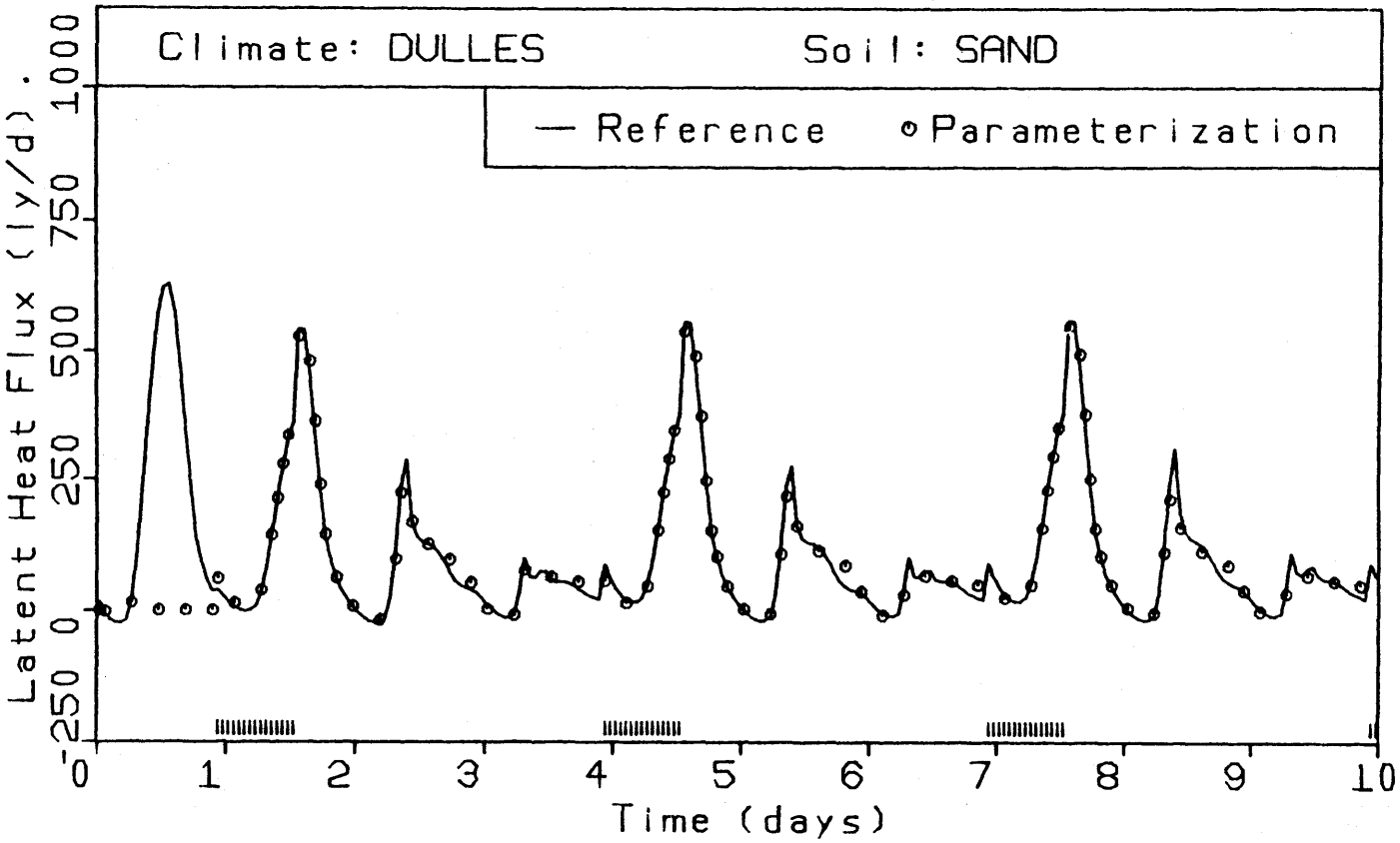

Figure 6.6

COMPARISON OF LATENT HEAT FLUXES COMPUTED BY THE REFERENCE MODEL AND BY THE PARAMETERIZATION. SAND, PERIODIC DULLES SCENARIO, R = 1.6.

indicating that the time distribution of evaporation is still predicted very well. The exception is the silt loam at Winslow, for which the RMSE rises from 32 to 80 ly/day. The corresponding evaporation series is plotted in Figure 6.7. The decrease of R from 45 to 2 clearly causes an underestimate of the extent of redistribution in this heavy, dry soil, resulting in excessively rapid evaporation.

Despite its failure to capture the time distribution of evaporation in one example, the redistribution sub-parameterization, with constant R, is successful overall in allowing predictions of the mean evaporation. The ability of this parameterization to calculate a cell depth internally is a significant advantage.

One final step in this analysis is to apply the parameterization, with R = 2, to predict evaporation during the month-long sequences of actual random weather data. The errors are summarized in Table 6.2, and are much lower, on average, than the corresponding statistics for both the two-node and the GFDL parameterization. The predictions are also as good as those of the nonlinear diffusion model with fixed cell depths that had been optimized individually. Mean errors at precipitation-limited Winslow are negligible. At Dulles, evaporation from the silt loam is underpredicted by 14%, and from the sand it is overpredicted by 9%.

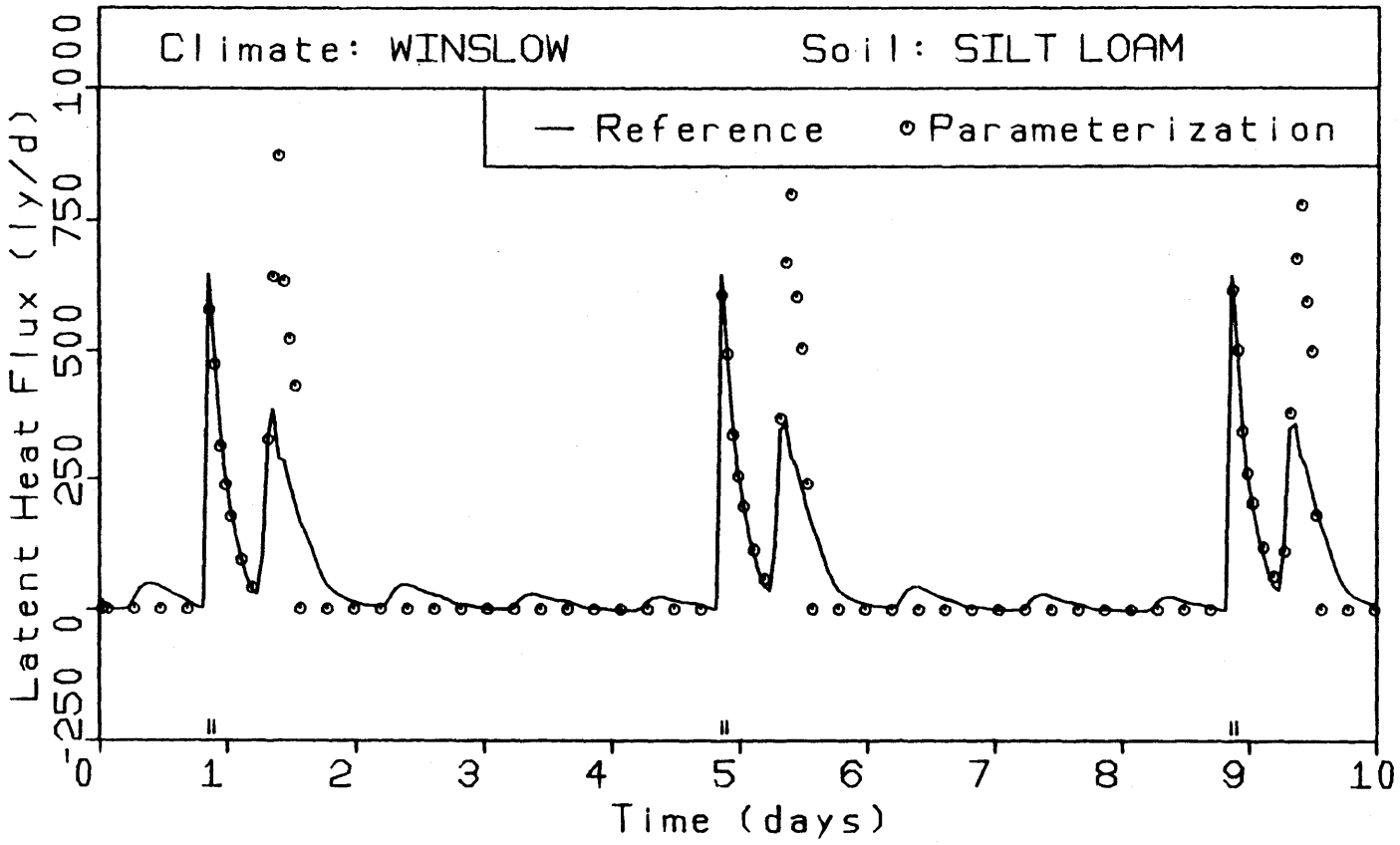

Figure 6.7

COMPARISON OF LATENT HEAT FLUXES COMPUTED BY THE REFERENCE MODEL AND BY THE PARAMETERIZATION. SILT LOAM, WINSLOW SCENARIO, R = 2.

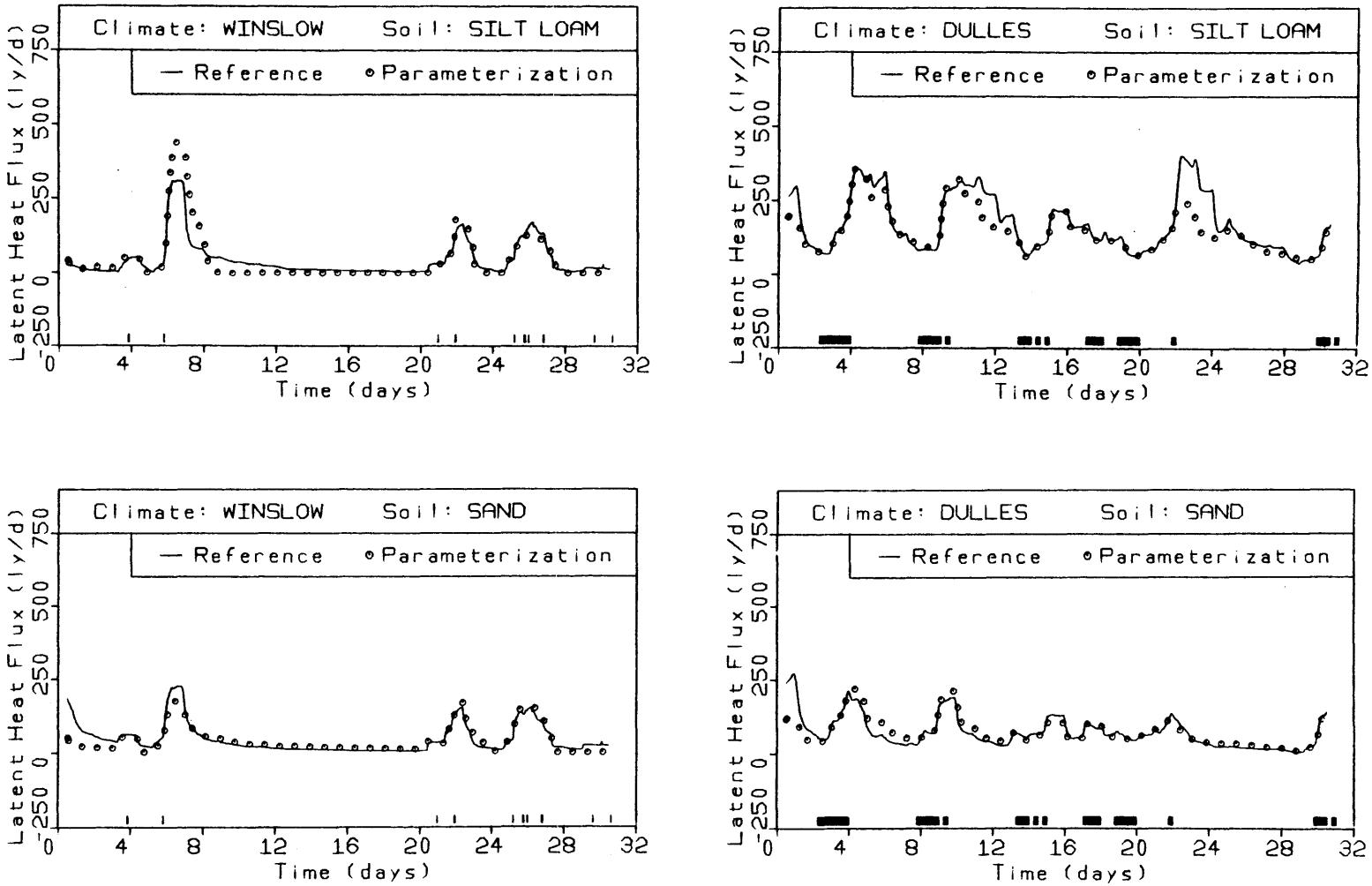

Figure 6.8

COMPARISONS OF LATENT HEAT FLUXES COMPUTED BY THE REFERENCE MODEL AND BY THE PARAMETERIZATION. ACTUAL WEATHER DATA AS INPUT. THE VALUE OF R IS FIXED AT 2 FOR ALL SCENARIOS.

The time distributions of the evaporative heat flux are plotted in Figure 6.8 for all four scenarios. For both soils, there is some failure to capture the shape of the curve following the second storm at Winslow, but the overall behavior is predicted well. Predictions at Dulles are also good, although there appears to be insufficient evaporation following two of the storms. On the whole, the set of predictions in Figure 6.8 is superior to the sets in Figures 5.5, 5.9, and 5.13.

6.4 Summary

The physically-based one-cell diffusion parameterization of Chapter 4 has been extended to allow automatic calculation of the cell size, Z, following each storm. Furthermore, a conceptual model of redistribution has been added to account for the progressive lengthening of Z that follows a storm. The redistribution rate is scaled by the hydraulic conductivity, with a constant of proportionality R, the redistribution parameter, being introduced.

The new parameterization compares favorably with the other parameterizations, even when the value of R is taken as a contant (R = 2) for both soils and for both climates. In particular, the problem noted with regard to the earlier diffusion model - incorrect decay of the exfiltration capacity - has been ameliorated. The idiosyncracy of the earlier model that allowed two distinct cell sizes to

fit the mean evaporation is avoided by the new model, which automatically calculates the correct one using a physically-based algorithm.

Two areas of research could lead to further improvement of this model. The first involves the redistribution parameterization. A more physically oriented approach, explicitly including capillary diffusion, could be used to calculate the redistribution rate or to arrive at a new expression for R in terms of the soil type and the initial moisture content. A second problem would be to account for carryover storage of water from one evaporation period to the next by formalizing one of the three approaches suggested in Section 6.2.

Chapter 7

SUMMARY AND CONCLUSIONS

7.1 Summary

We have developed a simple, physically-based parameterization of moisture and heat storage in soil. It is capable of faithfully reproducing the time variations of evaporation, sensible heat flux, and longwave radiation to the atmosphere. The development of the parameterization has been facilitated through the use of a complex simulation model as an experimental apparatus. This reference model served both to isolate the critical physical mechanisms to be parameterized and to provide data against which to test the parameterization.

In its final form, the proposed parameterization consists of a simplified square-wave model of the vertical moisture distribution, coupled to the force-restore procedure for determination of soil temperature at the surface. In the following paragraphs, the parameterization is briefly summarized. Equations presented previously are given their original numbers.

During a rain event, infiltration is calculated continuously according to

$$f_i = \min(P - E_p, f_i^*) \qquad (7.1)$$

where f_i is the actual rate of infiltration and f_i^* is the infiltration capacity. P and E_p are the precipitation and

potential evapotranspiration rates. The infiltration capacity is given as a function of cumulative infiltration, F_i, by

$$f_i^* = A_o\left\{1 + \left[-1 + \left(1 + \frac{4A_oF_i}{S_i^2}\right)^{1/2}\right]^{-1}\right\} \qquad (4.35)$$

where A_o and S_i are constant infiltration parameters, given by (4.44) and (4.45).

Following a rain event, the moisture content near the surface, $\bar{\theta}$, is estimated by solving the implicit equation

$$F_i(t_r) = A_o(0,\bar{\theta})\ t_r + S_i(0,\bar{\theta})\ t_r^{1/2} \qquad (6.2)$$

in which t_r is the total storm duration. A_o and S_i are now evaluated using (4.44) and (4.45), with θ_u replaced by $\bar{\theta}$ and with the upper limit of the integral in (4.45) replaced by the value of ψ for which θ_w equals $\bar{\theta}$.

The moisture distribution following the storm is conceptualized as a square wave (Figure 6.1) of magnitude $\bar{\theta}$ and depth Z, where

$$Z = F_i/\bar{\theta} \qquad (6.3)$$

The process of moisture redistribution following a storm is parameterized as an attenuation of the magnitude ($\bar{\theta}$) and a deepening of the length (Z) of the square wave (Figure 6.1) according to

$$\frac{d\bar{\theta}}{dt} = -\frac{R\bar{\theta}K(\bar{\theta})}{F_i} \tag{6.6}$$

where R is a constant called the redistribution parameter.

During the interstorm period, evaporation is calculated according to

$$E = \begin{cases} \min\left[E_p,\ f_e^*\right] & F_e < F_i \\ 0 & F_e = F_i \end{cases} \tag{7.2}$$

in which F_e is the cumulative exfiltration. The exfiltration capacity, f_e^*, is given as a function of F_e', the apparent cumulative exfiltration, by

$$f_e^* = S_e^2/2F_e' \tag{6.7}$$

The desorptivity, S_e, which is a function of $\bar{\theta}$, is calculated using (4.46), (4.48), (4.49), and (4.50). Since $\bar{\theta}$ is changing with time, we re-evaluate S_e each time step (i.e., hourly), and then correct F_e' according to

$$(F_e')_{new} = \left[(S_e)_{new}/(S_e)_{old}\right]^2 (F_e')_{old} \tag{6.8}$$

in order to assure continuity of f_e^* as given by (6.7). During a step, F_e' is predicted by

$$\frac{dF'_e}{dt} = E \tag{6.9}$$

The potential evaporation rate appears in (7.2). It is calculated using the surface temperature, T_1, and the assumption of a wet surface. The force-restore method is used to predict the soil surface temperature according to

$$\frac{dT_1}{dt} = c_1 G - c_2(T_1 - T_2) \tag{4.57}$$

where c_1 and c_2 are given by (4.58), (4.59), (4.68), and (4.69). G is the heat flux into the ground, given by a balance equation of the form

$$G = f_1(T_1, \theta_1, E) \tag{4.61}$$

The deep soil temperature, T_2, is predicted using

$$\frac{dT_2}{dt} = (\lambda C N_d \tau)^{-1/2} G \tag{4.62}$$

7.2 Conclusions

Our conclusions fall into two major categories. The first is concerned with the importance or negligibility of various physical effects in the prediction of surface evaporation and heat fluxes. The second set pertains to mathematical parameterization of the important physical effects in simplified models.

The complex system of equations governing coupled water and heat flow in soil can be simplified considerably without significant loss of accuracy in the calculation of fluxes across the land surface (Section 3.3). The influence of temperature on moisture retention (e.g., through the temperature dependence of surface tension) is unimportant to surface flux predictions, even though the thermally-induced liquid flow may be of the same order of magnitude as the isothermal diffusive liquid flow (Section 3.3.3). The heat of wetting is also negligible (Section 3.3.2). The variations of hydraulic conductivity that results from wide diurnal fluctuations of temperature near the soil surface can be ignored, but the temperature factor should be evaluated at the maximum air temperature (or at some other surrogate for the average daytime soil surface temperature) in order to obtain the best predictions (Section 3.3.4).

Water in the vapor phase below the surface provides an essential mechanism for moisture transport (Section 3.3.5). When water vapor is neglected, evaporation is underpredicted by as much as 36% in our scenarios. If the water vapor is re-introduced into the governing equations only in the term corresponding to isothermal vapor diffusion, then the evaporation errors become negligible. We conclude that the other vapor terms, including the thermal diffusion term, can be neglected.

Moisture retention hysteresis, in our scenarios, was not negligible in the sand, though it was negligible in the silt loam (Section 3.3.6).

The consequence of the physical simplifications mentioned above is the validation of considerably simpler conservation equations for soil moisture and heat. Soil moisture flow can be modelled using the isothermal flow equation (Section 4.2), with all parameters evaluated at constant characteristic temperatures. The flow of heat is governed by a simple diffusion equation. The only significant coupling remaining between moisture and heat fields beneath the soil surface is the dependence of the soil thermal parameters on moisture content. Even this connection can be parameterized simply, as we did successfully in the force-restore procedure (Sections 4.4.2 and 5.2).

Three moisture parameterizations requiring the specification of a storage cell size were proposed and evaluated. The best fits to the data from the reference model were achieved using a model in which the exfiltration and infiltration capacities are computed using idealized nonlinear diffusion solutions in conjunction with the time compression assumption (Section 5.3). With this parameterization, the larger of two distinct cell sizes that reproduce the mean evaporation correctly yields a desorptivity limitation on evaporation.

The nonlinear diffusion model required the speci-

fication of a soil- and event-dependent cell size. In order to compute this depth automatically in the parameterization, the model was extended. The nonlinear diffusion theory can be used to estimate the cell depth and average moisture content following a storm (Section 6.2), and a conceptual model of redistribution correctly accounts for the rate of decline of evaporation under soil control by updating those values periodically (Section 6.3). With the automatic cell depth calculations, this parameterization predicts evaporation well and requires only the physical properties of the soil; no conceptual parameters are needed. Improved results could be achieved by employing a more physically-based subparameterization of redistribution.

The force-restore method of ground surface temperature prediction performs very well (Section 5.2). This justifies a focus of attention on the hydrology, whose nonlinear physics require a more sophisticated model in order to achieve the same level of accuracy.

7.3 Recommendations for Future Research

Worthwhile improvement of the proposed parameterization could possibly result from two areas of work:

1. Incorporation of more memory into the model through one of the steps suggested in Section 6.2.

2. Improvement in the representation of redistribution, either through a different equation than (6.5) or through a physically-based definition of R dependent upon soil type and initial moisture content.

It appears that the proposed parameterization could easily be extended to include vegetation by coupling it to an existing vegetal canopy model.

Another extension would be to account for the immobilization of soil moisture brought on by freezing. Coupling with a snowpack parameterization is feasible, but would require a reassessment of the applicability of the force-restore procedure, which assumes strong diurnal forcing at the soil surface.

The simplified parameterization developed here can be applied to model the land surface in an atmospheric GCM. A reasonable first experiment would be designed to test the sensitivity of the GCM to this parameterization in comparison with current methods. Beyond that, this more physically-based parameterization might be more easily coupled to models of biomass production, etc., to study various land surface processes (e.g., CO_2 consumption, desertification, drought, deforestation) in the context of a GCM.

There is potential to estimate the effective soil properties for use in this model by application of the ecological optimality theory of Eagleson (1982), which

requires observation only of the climate characteristics and an estimate of the effective porosity. Conversely, this parameterization, in conjunction with a vegetation model, could provide a means for testing Eagleson's theory in the framework of a dynamic simulation model of an actual basin.

The simplicity and physical basis of this parameterization make it an excellent candidate for use in conjunction with remote sensing of surface soil moisture and temperature in a real-time soil moisture monitoring scheme. Applications for such a scheme can be found in agriculture, hydrology, and weather prediction.

The problem of spatial variability of hydrologic processes is one that often requires simplified models of point processes, since large batteries of simple models can be linked easily. The parameterization proposed here is such a model.

REFERENCES

Anderson, E. A., A point energy and mass balance model of a snow cover, NOAA T. R. NWS 19, 1976.

Buckman, H. O. and N. C. Brady, The Nature and Properties of Soils, MacMillan Company, New York, 1969.

Budyko, M. I., Teplovoi Balans Zemnoi Poverkhnosti, Gidrometeorologicheskoe Izadatel'stvo, Leningrad, 1956 (English translation by N. A. Stepanova, 1958, Office of Technical Services, U. S. Department of Commerce, Washington, 1958).

Budyko, M. I., N. A. Efimova, L. I. Zebenok, and L. A. Strokina, The heat balance of the earth's surface, Akad. Nauk SSSR, Izv. Ser. Georgr., No. 1, pp. 6-16, 1962 (Translation No. 153M, available from U. S. Department of Commerce, Office of Technical Services, Document No. 63-19851).

Charney, J. G., Dynamics of deserts and droughts in the Sahel, Quart. J. R. Met. Soc., 101, 193-202, 1975.

Charney, J. G., W. J. Quirk, S.-H. Chow, and J. Kornfield, A comparative study of the effects of albedo change on drought in semi-arid regions, J. Atmos. Sci., 34(9), 1366-1385, 1977.

Crank, J., The Mathematics of Diffusion, Oxford University Press, New York, 1956.

Curtis, D. C., Constrained stochastic climate simulation. Tech. Rep. 276, R. M. Parsons Laboratory, Department of Civil Engineering, M.I.T., Cambridge, Massachusetts, 1982.

Deardorff, J. W., Dependence of Air-Sea Transfer Coefficients on Bulk Stability, J. Geophys. Res., 73(8), 2549-2557, 1968.

Deardorff, J. W., Efficient prediction of ground surface temperature and moisture, with inclusion of a layer of vegetation, J. Geophys. Res., 83(C4), 1889-1903, 1978.

Eagleson, P. S., Dynamic Hydrology, McGraw-Hill, New York, 1970.

Eagleson, P. S., Climate, soil, and vegetation (7 parts), Water Resour. Res., 14(5), 705-776, 1978.

Eagleson, P. S., Ecological optimality in water-limited natural soil-vegetation systems, 1. Theory and hypothesis, Water Resour. Res., 18(2), 325-340, 1982.

Eagleson, P. S. and W. J. Shack, Some criteria for the measurement of rainfall and runoff, Water Resour. Res., 2(3), 427-436, 1966.

Edlefsen, N. A. and A. B. C. Anderson, Thermodynamics of soil moisture, Hilgardia, 15(2), 1943.

Gates, W. L., Numerical modeling of climatic change: A review of problems and prospects, Report No. P-547, The Rand Corporation, Santa Monica, California, 1975.

Global Atmospheric Research Program, The Physical Basis of Climate and Climate Modelling, GARP Publication No. 16, 1975.

Groenevelt, P. H. and B. D. Kay, On the interaction of water and heat transport in frozen and unfrozen soils: II. The liquid phase, Soil Sci. Soc. Am. Proc., 38(3), 400-404, 1974.

Hanks, R. J. and S. A. Bowers, Numerical solution of the moisture flow equation for infiltration into layered soils, Soil Sci. Soc. Am. Proc., 26(6), 530-534, 1962.

Haverkamp, R., M. Vauclin, J. Touma, P. J. Wierenga, and G. Vachuad, A comparison of numerical simulation models for one-dimensional infiltration, Soil Sci. Soc. Am. Proc., 41(2), 285-294, 1977.

Idso, S. B., R. D. Jackson, R. J. Reginato, D. A. Kimball, and F. S. Nakayama, The dependence of bare soil albedo on soil water content, J. Appl. Met., 14, 109-113, 1975.

Jury, W. A. and E. E. Miller, Measurement of the transport coefficients for coupled flow of heat and moisture in a medium sand, Soil Sci. Soc. Am. Proc., 38(4), 551-557, 1974.

Kimball, B. A., R. D. Jackson, R. J. Reginato, F. S. Nakayama, and S. B. Idso, Comparison of field-measured and calculated soil-heat fluxes, Soil Sci. Soc. Am. Proc., 40(1), 18-25, 1976.

Lai, S., J. M. Tiedje, and A. E. Erickson, In situ measurement of gas diffusion coefficient in soils, Soil Sci. Soc. Am. Proc., 40(1), 3-6, 1976.

Manabe, S., Climate and the ocean circulation, 1. The atmospheric circulation and the hydrology of the earth's surface, Monthly Weather Review, 97, 739-774, 1969.

Milly, P. C. D. and P. S. Eagleson, The coupled transport of water and heat in a vertical soil column under atmospheric excitation, Tech. Rep. 258, R. M. Parsons Laboratory, Department of Civil Engineering, M.I.T., Cambridge, Massachusetts, 1980.

Milly, P. C. D., Moisture and heat transport in hysteretic, inhomogeneous proous media: A matric head-based formulation and a numerical model, Water Resour. Res., 1982, in press.

Monin, A. S., Weather Forecasting as a Problem in Physics (translated by P. Superak), MIT Press, Cambridge, Massachusetts, 1972.

Monin, A. S. and A. M. Obukhov, Osnovnye zakonomernosti turbulentnogo peremeshivaniya v prizemnom sloye atmosfery, Akad. Nauk SSSR, Trudy Geofiz. Inst. No. 24(151), 163-187, 1954.

Mualem, Y., A conceptual model of hysteresis, Water Resour. Res., 10(3), 514-520, 1974.

Mualem, Y., A new model for predicting the hydraulic conductivity of unsaturated porous media, Water Resour. Res., 12(3), 513-522, 1976.

Mualem, Y., Extension of the similarity hypothesis used for modeling the soil water characteristics, Water Resour. Res., 13(4), 773-780, 1977.

Oke, T. R., Boundary Layer Climates, Halsted Press, 1978.

Philip, J. R. and D. A. de Vries, Moisture movement in porous materials under temperature gradients, Trans. Amer. Geophys. Union, 38(2), 222-232, 1957.

Reck, R. A., Global temperature changes: Relative importance of different parameters as calculated with a radiative-convective model, in Carbon Dioxide, Climate and Society, Ed. J. Williams, Pergamon Press, 1978.

Reeves, M. and E. E. Miller, Estimating infiltration for erratic rainfall, Water Resour. Res., 11(1), 102-110, 1975.

Rose, D. A., Water movement in porous materials: Part 2 - The separation of the components of water movement, Brit. J. Appl. Phys., 14, 491-496, 1963.

Sellers, W. D., Physical Climatology, University of Chicago Press, 1965.

Shukla, J. and Y. Mintz, Influences of land-surface evapotranspiration on the earth's climate, Science, 215, 1498-1501, 1982.

de Vries, D. A., Simultaneous transfer of heat and moisture in porous media, Trans. Amer. Geophys. Union, 39(5), 909-916, 1958.

de Vries, D. A., Thermal properties of soils, in Physics of Plant Environment, ed. W. R. Van Wijk, North Holland Publ. Company, Amsterdam, 1966.

Wierenga, P. J., D. R. Nielsen, and R. M. Hagan, Thermal properties of a soil based upon field and laboratory measurements, Soil Sci. Soc. Am. Proc., 33(3), 354-360, 1969.